Exchange Currents in Baryons[1]

Alfons J. Buchmann

Institute for Theoretical Physics, University of Tübingen,
Auf der Morgenstelle 14, D-72076 Tübingen, Germany

Z. Naturforsch. **52 a,** 877–940 (1997); received November 26, 1997

This paper reviews calculations of the electromagnetic properties of baryons using the constituent quark model. We start with a short discussion of spontaneous chiral symmetry breaking, which is essential in understanding the transition from QCD to the constituent quark model. We then discuss a chiral version of the constituent quark model, which simulates the symmetries and dynamical content of the underlying field theory in terms of gluon, pion and sigma exchange between constituent quarks. We show that the electromagnetic current charge and current operators, usually approximated by one-body operators (impulse approximation), must be supplemented by appropriate two-body terms (exchange currents). The latter represent the gluon and pion exchange degrees of freedom in the electromagnetic current operator. These exchange currents must be included for reasons of completeness and consistency. Most importantly, however, they are needed in order for the electromagnetic current to be conserved. We also study the effect of scalar exchange currents connected with the confinement and sigma exchange potentials. By including these two-body exchange currents we go beyond the single-quark impulse approximation, which has mainly been used up to now. The inclusion of gluon- pion-, and scalar-exchange currents in the quark potential model is the new point of the present work. We show that for some observables, such as the magnetic moments, charge, and magnetic radii of the proton and charged $\Delta(1232)$ states, exchange currents contribute at the level of some 10%. The same holds true for the magnetic moments of the entire baryon octet, with the exception of the Ξ^- magnetic moment. On the other hand, the neutron charge radius, the quadrupole moments of the Δ, and the $N \rightarrow \Delta$ transition quadrupole moment, are dominated by pion and gluon exchange contributions to the charge density operator. The inclusion of the pion and gluon exchange currents leads to a neutron charge radius of the correct size and sign. Based on the gluon and pion exchange current diagrams, we derive parameter-free relations between the neutron charge radius, the quadrupole moment of the Δ, and the $N \rightarrow \Delta$ transition quadrupole moment. Neglecting configuration mixing, we find that the neutron charge radius and the $N \rightarrow \Delta$ transition quadrupole moment are simply related as $Q_{N\rightarrow\Delta} = r_n^2/\sqrt{2}$. The implications of Siegert's theorem for the calculation of the E2 form factor in the $N \rightarrow \Delta$ transition are studied. Finally, we discuss the axial coupling constant of the nucleon. We show that the inclusion of axial pair exchange currents does not significantly alter the NRQM prediction.

Contents

[1] In partial fulfillment of the Habilitation requirements of the University of Tübingen.

Reprint requests to A. J. Buchmann, Fax: +49 7071 296400, E-mail: alfons.buchmann@uni-tuebingen.de.

0932-0784 / 97 / 1200-0877 $ 06.00

1. Introduction

The nucleon has a complicated internal structure. This is reflected, for example, by its anomalous magnetic moment, finite electromagnetic radius, and its excitation spectrum. These properties as well as the detailed interrelations among them are not very well understood. In fact, at energies of the order of the nucleon mass, the fundamental theory of strong interactions, quantum chromodynamics (QCD), cannot be rigorously applied. It is only at very high energies and momentum transfers ($\gg 1$ GeV) between quarks that the theory becomes amenable to a perturbation theoretical treatment and that its predictions can be tested.

Because it is not possible to calculate the properties of the nucleon at low and intermediate energies directly from first principles, it is necessary to devise models of baryon structure [1]. These models should incorporate the symmetries and dynamical content of QCD, in order to also test the theory in this energy regime. In recent years, it has become clear that the chiral symmetry of QCD and its spontaneous breaking play a crucial role in the formulation of a successful low-energy model of QCD. The cloudy bag model (CBM) [2], the Nambu-Jona-Lasinio model (NJL) [3], and the constituent quark model (CQM) [4] are frequently used. Each of these models emphasizes different degrees of freedom and properties of QCD. A better theoretical understanding of the nucleon structure on the confinement scale is closely related to the problem of the relevant degrees of freedom that best describe the low-energy properties of the nucleon.

Although the transition from the nearly massless quarks in the QCD-Lagrangian to the massive quarks of the constitutent quark model has not been understood in all its details, it is almost certain that the CQM is a viable low-energy realization of QCD. Among the different versions of the CQM, the nonrelativistic quark potential model (NRQM), which describes the nucleon as a bound state of three massive valence quarks interacting via various quark-quark potentials, has been remarkably successful in explaining a vast body of experimental results. Even in its simplest form, excluding any residual interaction between the quarks, it gives fairly accurate results for nucleon magnetic moments [5, 6] and some of the photoexcitation amplitudes of the nucleon [7, 8].

On the other hand, we know from high-energy electron-proton scattering that, in addition to the valence quarks, there are also gluons and quark-antiquark pairs (sea-quarks) inside the nucleon. It is generally assumed that these gluon and sea-quark degrees of freedom are to a large extent incorporated in the concept of constituent quarks and that the symmetries of QCD can be modelled by appropriate residual interactions between the constituent quarks. In fact, a number of recent theoretical works have shown that the many successes of the NRQM are not accidental [9] - [13]. It has been argued that

(i) constituent quarks are quasi-particles formed out of the bare "current" quarks of QCD and a cloud of quark-antiquark pairs [3], and that (ii) the NRQM, with appropriately chosen residual interactions, can be considered as a possible low-energy representation of QCD. The optimal choice of the NRQM Hamiltonian has still to be found. The present discussion centers around the question of whether the dynamics of the valence quarks is governed by one-gluon exchange forces [14, 15], instanton-induced interactions [16], or one-pion exchange forces [17]. This problem is far from being solved.

Electromagnetic properties of baryons and few-nucleon systems are quantities of fundamental importance. They provide valuable information on the degrees of freedom which are relevant in hadron physics and which should be incorporated in an effective potential model description of QCD. While quite general arguments (see Chap. 2) indicate the presence of residual gluon and pion degrees of freedom in such a potential model, the relative importance of gluon and pion exchange forces in the NRQM Hamiltonian is an open problem. Furthermore, flavor-dependent instanton-induced quark-quark interactions may play an important role at low-energies. These problems cannot be solved by considering strong interaction mass splittings alone. The *simultaneous* description of baryon mass splittings and electromagnetic properties is a more powerful test of the detailed form of the quark-quark potential.

A better understanding of the inner structure of the nucleon and of the relevant degrees of freedom which determine its low-energy properties is also the focus of major experimental efforts [18]. New continuous electron beam facilities, such as CEBAF (Newport-News), ELSA (Bonn), and MAMI (Mainz) have recently begun operation. Electron-nucleon scattering is a very powerful method to investigate the structure of the nucleon and the dynamics of its constituents. Because the electromagnetic interaction is well known and because the electron is pointlike, the measured cross-sections are directly related to the structure of the target. With the help of polarization or coincidence experiments, the measurement of individual electromagnetic multipole transitions to excited states of the nucleon become feasible. These experiments will provide detailed information about the spin structure of the transition and on the contribution of individual terms in the effective quark-quark interaction (spin-spin force, tensor force, spin-orbit force). For example, the recent determination of the C2/M1 ratio in the electroexcitation of the Δ-resonance provides important information on the tensor forces between quarks and on the related question of the deformation of the nucleon [19].

On the other hand, it is generally difficult to obtain quantitative information about the effective forces from electromagnetic observables. Consider, for example, the deuteron magnetic moment μ_d [20]:

$$\mu_d = \mu_p + \mu_n - \frac{3}{2} P_D \left(\mu_p + \mu_n - \frac{1}{2} \right) + \mu_{MEC}, \quad (1.1)$$

where μ_p and μ_n are the free proton and neutron magnetic moments. The term proportional to the deuteron D-state probability P_D comes from the orbital motion of the proton. Equation (1.1) shows that one cannot uniquely determine the D-state probability P_D in the deuteron wave function from the measured deuteron, proton, and neutron magnetic moments nor, therefore, the strength of the tensor force in the nucleon-nucleon interaction. The reason is intuitively clear. The continuous emission and absorption of charged mesons by the interacting nucleons leads to additional electromagnetic meson currents between the two nucleons. This gives rise to the meson exchange current (MEC) term μ_{MEC} in (1.1). Already, in 1937 Siegert [21] showed that in a theory where charged mesons are exchanged between the nucleons additional currents, called *exchange currents* have to be introduced in order to satisfy the continuity equation for the electromagnetic current. The effect of these exchange currents must be reliably known in order to extract information about the nucleon-nucleon interaction itself. The same argument applies to the quarks inside baryons. We must have some knowledge of the effect of exchange currents before we can learn something about inter-quark forces from experimentally measured electromagnetic properties of baryons.

One should recall that the study of exchange currents has led in the 70's and 80's to a quantitative understanding of the electromagnetic structure of light nuclei. By coupling the photon to the exchanged pion degrees of freedom one "sees" the pions in the nucleus. The existence of pion degrees of freedom inside the nucleus has thereby been proven beyond all doubt. The inclusion of pion exchange currents has removed many discrepancies between theory and experiment. The most famous example is the electrodisintegration of the deuteron near threshold and at

backward angles, where exchange currents change the impulse prediction by more than an order of magnitude in agreement with experiment [22]. At the same time it has become clear that the quark strucure of the nucleon has to be taken into account in order to formulate a more reliable theory of exchange currents between nucleons [23 - 28].

It is not unreasonable to expect that, as in nuclear few-body systems, some properties of the nucleon and its excited states will be very sensitive to such exchange degrees of freedom. However, there are no systematic studies of the effect of exchange currents on baryonic electromagnetic properties. In fact, most calculations of electromagnetic properties of baryons in the NRQM have been performed in the so-called impulse approximation, which assumes that the total electromagnetic current of the quarks is given by a sum of three *free* quark currents. This would be justified if the quark Hamiltonian would include only the kinetic energy and a momentum independent mean field (confining potential). Yet, modern versions of the NRQM include various momentum or isospin-dependent residual interactions between quarks, such as gluon [14, 15] and pion exchange [29, 30], in order to simulate the symmetries and dynamical features of QCD. These residual interactions clearly manifest themselves in the excitation spectrum of hadrons and are expected to influence their electromagnetic properties as well. Therefore, a model built on free quark currents is incomplete because it contradicts the basic requirement of electromagnetic current conservation. Current conservation demands that the total electromagnetic current operator of bound quarks necessarily consist of two pieces: the kinetic one-body quark currents and the two-body exchange currents associated with the dynamical processes that bind the quarks together.

The situation in this field before our investigation can be summarized as follows. Although there were a few calculations in the NRQM dealing with gluon or pion exchange currents [31 - 36] separately, there was no calculation in which gluon *and* pion exchange currents have been evaluated consistently with the gluon and pion exchange potentials used in the Hamiltonian as required by gauge invariance. Moreover, there were no studies of the effect of exchange currents on charge properties, such as charge radii, quadrupole moments, $N \rightarrow \Delta$ charge quadrupole transition, etc. In several works [37 - 43] we have studied the effect of two-body exchange currents on the electromagnetic properties of the $N-\Delta$ system, and of the strange octet and decuplet hyperons in the NRQM. The present review draws on these published results but also includes new results, for example, the $N \rightarrow \Delta$ electromagnetic transition form factors at finite momentum transfers, the quadrupole moment of the Ω^- hyperon, the use of Siegert's theorem in the quadrupole excitation of the Δ, and the axial coupling constant of the nucleon. Instead of focusing on a single observable such as the C2/M1 ratio, we give results for numerous low-energy observables, such as charge radii, quadrupole moments, magnetic moments, and magnetic radii of both the nucleon and the Δ using a *single* set of parameters previously determined by the empirical nucleon and Δ masses. This will provide further insight as to why the naive NRQM gives such good results for the magnetic moments but fails for the charge and magnetic radii. We will show to what extent the inclusion of gluon and pion two-body exchange currents, and of a finite electromagnetic size of the constituent quarks, resolves the problem with the electromagnetic radii. We also study how the gluon, pion, and scalar exchange currents affect the properties of the octet baryons. An extension to the weak decay of the neutron is briefly discussed. The latter analysis provides some new insights into an old problem of the NRQM.

Before introducing the model (Chapt. 3) and going on to specific applications in the single-baryon sector (Chapt. 4 - 8), we review the basic concepts that constitute the theoretical foundation of the nonrelativistic quark potential model.

2. From QCD to the Constituent Quark Model

In this chapter we state in brief the key ideas that have recently been discussed in connection with the theoretical foundations of the NRQM.

2.1. QCD

QCD, which is considered as the fundamental theory of strong interactions, is a non-Abelian gauge field theory. It has its roots in the application of the Yang-Mills idea [44] of local gauge invariance under a non-Abelian gauge group to the group $SU(3)_{color}$. As in quantum electrodynamics (QED), the requirement of invariance of the Lagrangian under local gauge transformations uniquely determines the form of the interaction between the fermions and the gauge field.

The strong interaction of quarks with color i and gluons is described by the Lagrangian [45] [2]

$$\mathcal{L}_{\mathrm{QCD}} = \sum_{i,j=1}^{3} \sum_{f=1}^{n_f} \overline{\Psi}_f^i (i\gamma_\mu (D^\mu)_{ij} - m_f \delta_{ij}) \Psi_f^j - \frac{1}{4} F_{\mu\nu}^a F^{a\mu\nu}, \tag{2.1}$$

where f indicates the flavor of the quark fields. In this work we need only the three lightest flavors, up, down, and strange i. e. $n_f = 3$. In (2.1) m_f is the *current* quark mass of flavor f (the constituent quark mass is introduced in Sect. 2.2). Furthermore,

$$(D_\mu)_{ij} = \partial_\mu \delta_{ij} - ig \frac{\lambda_{ij}^a}{2} G_\mu^a \tag{2.2}$$

is the covariant derivative, and

$$F_{\mu\nu}^a = \partial_\mu G_\nu^a - \partial_\nu G_\mu^a + g f_{abc} G_\mu^b G_\nu^c \tag{2.3}$$

the gluon field strength tensor, where G_μ^a is the gluon gauge field with color charge index $a = 1, \cdots, 8$. The coupling strength g appearing in D_μ and $F_{\mu\nu}^a$ is respectively the quark-gluon and gluon-gluon coupling constant. The 8 generators λ^a of $\mathrm{SU(3)_{color}}$, called Gell-Mann matrices, satisfy the following Lie-Algebra

$$\left[\lambda^a, \lambda^b\right] = 2i f_{abc} \lambda^c, \tag{2.4}$$

where the f_{abc} are the structure constants of $\mathrm{SU(3)_{color}}$. The non-Abelian character of QCD with all its important consequences derives from the non-commutativity of the generators λ^a.

The Lagrangian (2.1) is by construction invariant under the following local gauge transformations

$$\begin{aligned} \Psi'^i_f(x) &= \exp\left(-ig\alpha^a(x)(\lambda^a)_{ij}/2\right) \Psi_f^j(x), \\ G'^b_\mu(x) &= \exp\left(-g\alpha^a(x) f_{abc}\right) G_\mu^c(x) - \partial_\mu \alpha^b(x), \end{aligned} \tag{2.5}$$

where $\alpha(x)$ is a local phase. If (2.2) and (2.3) are inserted into (2.1), one gets in a symbolic notation the terms in Figure 2.1. The first two terms in Fig. 2.1 represent the kinetic energies of the free quark and gluon fields. The third term stands for the interaction of quark and gluon fields, whereas the fourth and fifth

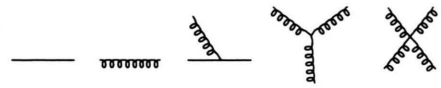

Fig. 2.1. Symbolic representation of individual terms of the QCD Lagrangian.

term represent gauge field self-interactions. The last two terms in Fig. 2.1 do not exist in an Abelian gauge theory like QED and are typical for a non-Abelian gauge theory such as QCD. They arise because gluons carry a color charge unlike the photon which is electrically neutral. In the following we discuss in brief the most important properties of the QCD Lagrangian (2.1).

Asymptotic freedom. QCD is an asymptotically free theory. This property of QCD is closely related to its non-Abelian structure, i. e. the presence of the last two terms in Fig. 2.1 [46]. "Asymptotic freedom" means that the strong coupling constant $g^2/4\pi = \alpha_s(Q^2)$ goes to zero for large momentum transfers (short distances) between the quarks. In a perturbative expansion the running coupling constant has the following form [47]

$$\alpha_s(Q^2) = \frac{12\pi}{(33 - 2n_f) \ln(Q^2/\Lambda_{\mathrm{QCD}}^2)}, \tag{2.6}$$

where Λ_{QCD} is the QCD mass scale[3]. Consequently, the quarks are essentially noninteracting or asymptotically free at very short distances. "Asymptotic freedom" is the basic assumption of the parton model, which explains the deep inelastic electron-proton scattering data in terms of elastic electron scattering on three *free* point-like partons inside the nucleon. It describes the experimentally measured inelastic structure functions of the nucleon as an *incoherent* superposition of individual quark momentum distribution functions $q_f(x)$. For example, for the inelastic structure function $F_2^{\mathrm{p}}(\nu, q^2)$ of the proton, one finds at large momentum transfer q^2 and large energy transfer ν of the virtual photon that $F_2^{\mathrm{p}}(\nu, q^2)$ no longer depends on q^2 and ν separately but only on the dimensionless Bjorken scaling variable $x = q^2/2M\nu$

$$F_2^{\mathrm{p}}(x) = \sum_f e_f^2 x q_f(x). \tag{2.7}$$

[2] Because our focus is on the symmetries and dynamical features that are relevant to low-energy QCD, we neglect ghost fields and gauge fixing terms in $\mathcal{L}_{\mathrm{QCD}}$.

[3] Λ_{QCD} is a free parameter of the theory and must be determined by experiment. An analysis of electron-proton scattering data suggests the value $\Lambda_{\mathrm{QCD}} \approx 250$ MeV [48].

This phenomenon is called Bjorken scaling. It indicates the absence of any mass- or length scale and is characteristic for electron-scattering on non-interacting structureless point-particles. Here, $q_f(x)$ is the probability of finding a parton, with flavor f and momentum fraction x of the total proton momentum, inside the proton. Of course, this is an idealistic picture. In reality, there are deviations from Bjorken scaling but for high energies and momentum transfers these can be calculated using perturbation theory in α_S. For small momentum transfers, quark-antiquark pairs (sea-quarks), i. e. the last two terms in the quark distribution function $q_f(x) = q_{f,v}(x)+q_{f,s}(x)+\bar{q}_{f,s}(x)$ dominate. In this regime, also pion degrees of freedom become increasingly important. In fact, the experimentally observed flavor asymmetry of the sea-quark distribution functions (more antidown than antiup-quarks in the sea of the nucleon) can be explained as a result of the coupling of pions to constituent quarks [49].

Chiral symmetry. Aside from asymptotic freedom, QCD has another important property, which is essential for its low-energy structure. In the limit of vanishing quark masses $\mathcal{L}_{\mathrm{QCD}}$ is invariant under *global* chiral symmetry transformations, i. e.

$$\Psi'(x) = \exp\left(\frac{i}{2}\boldsymbol{\tau}\cdot\boldsymbol{\alpha}\gamma_5\right)\Psi(x), \tag{2.8}$$

where $\boldsymbol{\tau}$ indicates the three SU(2) generators of rotations in isospin space (Pauli matrices) and $\boldsymbol{\alpha}$ stands for an arbitrary angle in that space. The Dirac matrix γ_5 produces a spinor of opposite parity. Chiral SU(2) symmetry takes into account the fact that strong interactions are invariant with respect to, both, isospin rotations and parity transformations of the fields [50]. But chiral symmetry is even more. Consider, for example, the mass term of the current quark fields $m_f\overline{\Psi}\Psi$ in $\mathcal{L}_{\mathrm{QCD}}$. Although such a term is invariant under parity transformations and isospin rotations (for equal masses of up and down quarks) separately, it is not invariant under the chiral transformation (2.8). Finite mass terms break chiral symmetry *explicitly*. On the other hand, for hypothetical 'massless' quarks, chirality or handedness is a good quantum number. In this case, there are only left-handed (spin antiparallel to the momentum) and right-handed (spin parallel to the momentum) quarks, and the above chiral transformations do not mix quarks with opposite handedness. The chiral symmetry of the QCD-Lagrangian is quite well satisfied due to the smallness of the current quark masses (5 - 10 MeV for up and down quarks) compared to the lightest hadron masses (140 MeV for the pion). This symmetry is spontaneously broken in the real world. Our major concern is the spontaneous breaking of chiral symmetry and not the small explicit breaking through finite current quark mass terms. For a more detailed discussion of chiral symmetry and its implications the reviews by Vogl and Weise [3] and Kirchbach [50] are recommended.

Confinement. With decreasing momentum transfer or increasing distance between the quarks the running coupling constant increases. (It would go to infinity for $Q^2 \to \Lambda^2_{\mathrm{QCD}}$, if (2.6) were valid for such small Q^2.) Consequently, the interaction between valence quarks themselves and between the valence quarks and the sea-quarks in the QCD vacuum becomes stronger. In addition, the nonlinear terms in the QCD Lagrangian become important. In this situation we would have to deal with an infinite sea of quark-antiquark excitations on top of complicated nonlinear gluon field configurations. These features of QCD at larger distances presumably lead to the experimentally established color confinement, i. e. the fact that all hadrons are *colorless* bound states of quarks (baryons) or quarks and antiquarks (mesons), although this has not been rigorously derived from QCD. In any case, it is clear that a perturbative solution of the QCD equations of motion for problems of medium energy hadron and nuclear physics is out of question. On the other hand, there is sufficient phenomenological support that these complicated low-energy features of QCD are adequately described by the NRQM.

2.2. *Spontaneous Breaking of Chiral Symmetry (SBCS)*

The term "spontaneously broken symmetry" describes a situation where the Lagrangian is invariant under a symmetry transformation but the ground state (vacuum) of the system is not. A familiar physical system which displays a spontaneously broken symmetry is the ferromagnet. Although the Lagrangian describing this system is rotationally invariant, the ground state of the ferromagnet has all its spins aligned in one direction if the temperature is below the critical Curie temperature T_{C}. This results in a macroscopic magnetization $\mathcal{M}$ pointing in a certain direction. In an external magnetic field different directions of the ferromagnet have different energies and the system

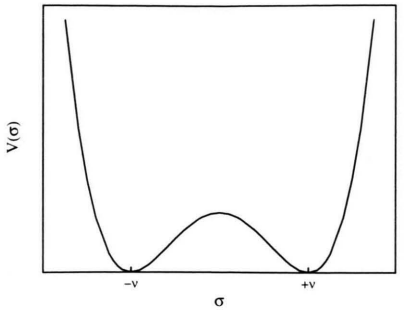

Fig. 2.2. The potential term $V(\pi = 0, \sigma) = \lambda^2(\sigma^2 - \nu^2)^2/4$ of $\mathcal{L}_\sigma$ with its two degenerate minima.

is not rotationally invariant. The spontaneously broken symmetry is characterized by a nonzero vacuum expectation value of the magnetization density:

$$\langle 0|\mathcal{M}|0\rangle \neq 0, \tag{2.9}$$

which depends on the temperature of the system. A similar phenomenon occurs in QCD.

The chiral symmetry of QCD and its spontaneous breaking is best explained with the help of the linear σ-model. The linear sigma model is the prototype of a chirally symmetric Lagrangian [2, 47]. The σ-model Lagrangian describes the interaction of massless fermions with massless scalar and pseudoscalar fields, the bosons being subject to some potential:

$$\begin{aligned}\mathcal{L}_\sigma = {} & i\overline{\Psi}\gamma_\mu\partial^\mu\Psi + g\overline{\Psi}(\sigma + i\boldsymbol{\tau}\cdot\boldsymbol{\pi}\gamma_5)\Psi + \frac{1}{2}(\partial_\mu\sigma)^2 \\ & + \frac{1}{2}(\partial_\mu\boldsymbol{\pi})^2 - \frac{1}{4}\lambda^2\left[\sigma^2 + \boldsymbol{\pi}^2 - \nu^2\right]^2,\end{aligned} \tag{2.10}$$

where σ is an isoscalar-scalar and $\boldsymbol{\pi}$ an isovector-pseudoscalar field in addition to the *a priori* massless fermion field Ψ (current quarks). For $\nu^2 > 0$, the potential term in the Lagrangian has a minimum on the circle $\boldsymbol{\pi}^2+\sigma^2 = \nu^2$. A nonzero vacuum expectation value for the $\boldsymbol{\pi}$ field would violate the symmetry of the vacuum under parity transformations. Therefore, it is natural to expand $V(\sigma, \boldsymbol{\pi} = 0)$ (see Fig. 2.2) around either one of the two degenerate minima at $\sigma = \pm\nu$. If we make the transformation

$$\sigma' = \sigma + \nu \qquad \boldsymbol{\pi}' = \boldsymbol{\pi} \tag{2.11}$$

we get

$$\begin{aligned}\mathcal{L}'_\sigma = {} & \overline{\Psi}(i\gamma_\mu\partial^\mu - g\nu)\Psi + g\overline{\Psi}(\sigma' + i\boldsymbol{\tau}\cdot\boldsymbol{\pi}'\gamma_5)\Psi \\ & + \frac{1}{2}(\partial_\mu\sigma')^2 - \frac{1}{2}(2\lambda^2\nu^2)\sigma'^2 + \frac{1}{2}(\partial_\mu\boldsymbol{\pi}')^2 \\ & + \lambda^2\nu\sigma'(\sigma'^2 + \boldsymbol{\pi}'^2) - \frac{1}{4}\lambda^2(\sigma'^2 + \boldsymbol{\pi}'^2)^2.\end{aligned} \tag{2.12}$$

The new field σ' measures the deviation of the orginal field σ from the stable minimum position at $\sigma = -\nu$. Note that the two Lagrangians $\mathcal{L}_\sigma$ and $\mathcal{L}'_\sigma$ are completely equivalent. In particular, $\mathcal{L}'_\sigma$ is still invariant under chiral transformations and some authors [2] prefer to speak of a "hidden symmetry" instead of a spontaneously broken symmetry.

Although the two Lagrangians (2.10) and (2.12) are equivalent, in practice we must use $\mathcal{L}'_\sigma$ and expand around $\sigma' = 0$, $\boldsymbol{\pi}' = 0$ if we want to derive and solve the equations of motion for the $\boldsymbol{\pi}$ and σ fields perturbatively. The use of $\mathcal{L}_\sigma$ with its unstable expansion point $\sigma = 0$ would not lead to convergent results. By choosing one of the two minimum positions (here: $\sigma = -\nu$) as the new origin for our perturbative expansion, we have spontaneously broken the reflection symmetry of the potential term in $\mathcal{L}_\sigma$ with respect to the transformation $\sigma \to -\sigma$. As a consequence, we observe that the fermion field has now a mass term $-g\nu\overline{\Psi}\Psi$. The fermion mass, $m = g\nu$, arises because the originally massless fermion moves through a complicated vacuum with a nonzero expectation value $\langle\sigma\rangle = -\nu \neq 0$. Similarly, the scalar field σ' acquires a mass term $m_\sigma^2 = 2\lambda^2\nu^2$ while the pseudoscalar field $\boldsymbol{\pi}'$ remains massless.

The latter property is a consequence of the Goldstone theorem which says that, whenever a global symmetry of the Lagrangian is spontaneously broken, there are accompanying massless bosons (Goldstone bosons) with the quantum numbers of the generators of the symmetry. In the present context of the spontaneously broken chiral symmetry of QCD these are the pseudoscalar pions. The σ-model clearly shows that: (a) one can preserve the chiral symmetry of the Lagrangian and the ensuing PCAC relation [50] even for massive fermions and that (b) one has in this case massive scalar and massless pseudoscalar fields coupling to the massive fermions. It also suggests that the spontaneous breaking of chiral symmetry by the physical QCD vacuum is responsible for the generation of massive constituent quarks. However, it does

not explain SBCS in terms of the fundamental gluon and quark degrees of freedom.

2.3. *Quasi-particle Interpretation of Constituent Quarks*

Further insight into the mechanism causing the transition from massless current quarks to massive finite sized constituent quarks can be gained from the Nambu-Jona-Lasino (NJL) model [51]. For recent reviews concerning the quasiparticle nature of constituent quarks and the NJL model see [3, 50]. The NJL Lagrangian describes massless and point-like spin 1/2 fermions interacting via a four-fermion interaction:

$$\begin{aligned}\mathcal{L}_{\mathrm{NJL}} &= \mathcal{L}_0 + \mathcal{L}_{\mathrm{int}} \\ &= i\overline{\Psi}\gamma_\mu\partial^\mu\Psi + g_0\left[(\overline{\Psi}\Psi)^2 - (\overline{\Psi}\boldsymbol{\tau}\gamma_5\Psi)^2\right].\end{aligned} \tag{2.13}$$

This model incorporates all global symmetries of QCD. In particular, it remains invariant under global chiral transformations (2.8), and was shown to constitute a good approximation to QCD in the low-energy domain [52]. The NJL model illustrates the important concept of *dynamical* symmetry breaking which means that there is a phase transition from massless to constituent quarks if the coupling strength g_0 between the initially massless fermions increases beyond a certain critical value.

To see this consider the transformation

$$\mathcal{L}_0' = \mathcal{L}_0 + m\overline{\Psi}\Psi,\ \mathcal{L}_{\mathrm{int}}' = \mathcal{L}_{\mathrm{int}} - m\overline{\Psi}\Psi, \tag{2.14}$$

which preserves the chiral invariance of $\mathcal{L}_{\mathrm{NJL}}$ and the corresponding equations of motion. However, the ground state (vacuum) of the free field Lagrangian is changed from one, for massless (bare) fermions described by the ket $|\Phi(0)\rangle$, to a new ground state, for massive (dressed) fermions of mass m, described by the ket $|\Phi(m)\rangle$. This new vacuum is called quasi-particle vacuum. In a second quantized theory, the free fermion field operator for a massless ($\lambda = 0$) or massive ($\lambda = m$) fermion is given as a superposition of particle destruction a_λ and antiparticle creation operators $b_\lambda^\dagger$

$$\begin{aligned}\Psi^\lambda(x) = \frac{1}{\sqrt{V}}\sum_{\boldsymbol{p},s}\big[&u^\lambda(\boldsymbol{p},s)a_\lambda(\boldsymbol{p},s)e^{ipx} \\ &+ v^\lambda(\boldsymbol{p},s)b_\lambda^\dagger(\boldsymbol{p},s)e^{-ipx}\big],\end{aligned} \tag{2.15}$$

where $u^\lambda(\boldsymbol{p},s)$ and $v^\lambda(\boldsymbol{p},s)$ are respectively particle and antiparticle Dirac spinors with spin projection s onto the direction of the momentum $\boldsymbol{p}$. The creation and annihilation operators for dressed fermions, or quasi-particles, are connected to those of the massless fundamental fermions via a Bogolyubov transformation [50]

$$\begin{aligned}a_m(\boldsymbol{p},s) &= \xi_{\boldsymbol{p}}a_0(\boldsymbol{p},s) + \eta_{\boldsymbol{p}}b_0^\dagger(-\boldsymbol{p},s), \\ b_m(\boldsymbol{p},s) &= \xi_{\boldsymbol{p}}b_0(\boldsymbol{p},s) - \eta_{\boldsymbol{p}}a_0^\dagger(-\boldsymbol{p},s),\end{aligned} \tag{2.16}$$

with

$$\begin{aligned}|\,\xi_{\boldsymbol{p}}\,|^2 &= \frac{1}{2}\left(1 + \frac{|\,\boldsymbol{p}\,|}{\sqrt{\boldsymbol{p}^2 + m^2}}\right), \\ |\,\eta_{\boldsymbol{p}}\,|^2 &= \frac{1}{2}\left(1 - \frac{|\,\boldsymbol{p}\,|}{\sqrt{\boldsymbol{p}^2 + m^2}}\right).\end{aligned} \tag{2.17}$$

The Bogolyubov transformation (or quasi-particle transformation) is the most general linear transformation between fermion creation and destruction operators which preserves the anticommutation relations for fermions. This means that the quasi-particles are again fermions. The transformation coefficients $\xi_{\boldsymbol{p}}$ and $\eta_{\boldsymbol{p}}$ are the occupation amplitudes of the quasi-particle state with momentum $\boldsymbol{p}$.

In the NJL model, the quasi-particles with their dynamical mass m are generated by the interaction of initially massless quarks with the filled Dirac sea (vacuum). This interaction gives rise to self-energy contributions to the fermion mass $m(g_0, \Lambda, m)$ which can be calculated from the so-called gap equation [3]

$$m = -2g_0\langle\overline{\Psi}\Psi\rangle = \frac{2g_0m}{\pi^2}\int_0^\Lambda \mathrm{d}p\,\frac{\boldsymbol{p}^2}{\sqrt{\boldsymbol{p}^2 + m^2}}, \tag{2.18}$$

where Λ is some cut-off mass to regularize the otherwise divergent integral. Its inverse is proportional to the size of the quasi-particle (see Chapt. 3). It can be shown that (2.18) has a nontrivial solution with $m \neq 0$ only if the coupling strength g_0 is greater than some critical value $g_{\mathrm{crit}} = \pi/\Lambda$. From (2.18) it is evident that $m \neq 0$ goes together with a nonzero vacuum expectation value of the scalar density of quark-antiquark pairs in the vacuum: $\langle\Phi(m)\ |\ \overline{\Psi}\Psi\ |\ \Phi(m)\rangle \neq 0$. This nonzero vacuum expectation value is often called scalar quark *condensate*. The term condensate refers to the the existence of a certain long-range order in

the vacuum as in macroscopic condensed matter. Numerically, the vacuum expectation value in the QCD vacuum is quite big $\rho_S \approx 2$ fm^{-3} compared to the vector density of nucleons in nuclei $\rho_V \approx 0.17$ fm^{-3}. This means that the QCD vacuum is quite densely populated with quark-antiquark pairs. As shown in [51] the existence of a scalar condensate in turn gives rise to massless collective excitations of bound quasi-particle pairs with pseudoscalar quantum numbers (pions) and to massive collective states with scalar quantum numbers (sigma mesons) with mass $m_\sigma = 2m$.

In more physical terms, the NJL model describes how an initially massless quark dresses itself with a polarization cloud of quark-antiquark pairs as it moves through the densely populated QCD vacuum. The constituent quark is thus made of a bare quark and an infinite number of quark-antiquark pairs (sea-quarks) with momenta less than the cut-off momentum Λ that are continuously excited from the QCD vacuum. In low-energy QCD, it is therefore more appropriate to work with the constituent quarks (quasi-particles with mass and intrinsic structure) and a simple quasi-particle vacuum, instead of with the original massless current quarks appearing in $\mathcal{L}_{QCD}$ and the complicated QCD vacuum.

In summary, both models (the linear σ-model and the NJL-model) suggest that, the chiral symmetry of the original QCD Lagrangian and its spontaneous breaking by the physical vacuum is responsible for the constituent quark mass generation and the coupling of massive constituent quarks to a massless Goldstone boson and a massive scalar meson. On the other hand, the deeper dynamical reasons which lead to SBCS are not explained by these models. There are recent developments based on instanton solutions of classical Yang-Mills theories that connect SBCS more directly to the first principles of QCD. The interested reader is referred to [9] and the more recent review [10] for further details.

3. The Constituent Quark Potential Model

In the previous chapter we have argued that constituent quarks are quasi-particles, i. e. bare particles surrounded by a cloud of $q\bar{q}$ pairs. These $q\bar{q}$ pairs can have, for example, gluon, pion, or σ-meson quantum numbers. In this sense, the constituent quark model reduces the infinitely many degrees of freedom that are excited at low energies to a manageable number of three quasi-particle (valence quark) degrees of freedom with some residual interactions between them. It should be clear then that the constituent quarks are themselves complicated objects. They have a mass $m_q \approx M_N/3$ and a finite size of $r_q \approx 0.4$ fm. These basic properties of constituent quarks incorporate already much of the complexity of QCD in the low-energy domain of hadron physics. However, there are still some residual interactions between the constituent quarks. These simulate the symmetries and dynamical features of QCD that are not yet included in the free quasi-particle description. Quite generally, the strong interaction between two spin-1/2 fermions, can be parametrized in terms of five relativistic bilinear invariants, namely scalar, pseudoscalar, vector, pseudovector, and tensor combinations that can be formed out of the Dirac spinors and γ-matrices. The model used here emphasizes *effective* vector, pseudoscalar, and scalar exchange. Below we give some physical motivation for this choice.

3.1. Hamiltonian

In the NRQM a baryon is treated as a nonrelativistic three-quark system and in the simplest case of equal quark masses m_q described by the Hamiltonian [4]

$$H = \sum_{i=1}^{3}\left(m_q + \frac{\boldsymbol{p}_i^2}{2m_q}\right) - \frac{\boldsymbol{P}^2}{6m_q} + \sum_{i<j}^{3} V^{conf}(\boldsymbol{r}_i, \boldsymbol{r}_j) + \sum_{i<j}^{3} V^{res}(\boldsymbol{r}_i, \boldsymbol{r}_j), \tag{3.1}$$

where $\boldsymbol{r}_i$, $\boldsymbol{p}_i$ are the spatial and momentum coordinates of the i-th quark, respectively. The fact that the center of mass motion, i. e. the third term in (3.1)

[4] For recent reviews of the NRQM see [4].

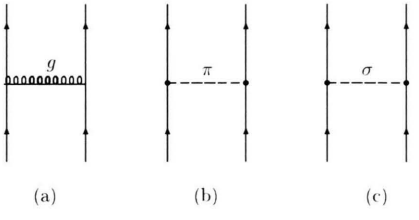

Fig. 3.1. Residual (a) one-gluon, (b) one-pion, and (c) one-sigma exchange potentials between constituent quarks.

can be exactly removed, is one of the main advantages of the NRQM. The SU(3) generalization to unequal quark masses is briefly discussed in Section 3.6. The Hamiltonian (3.1) consists of the standard nonrelativistic kinetic energy, a confinement potential, V^{conf}, and a residual interaction V^{res}. We point out that despite its nonrelativistic appearance the kinetic energy in (3.1) contains the bulk of relativistic corrections (see Sect. 5.3.5). The residual interaction (see Fig. 3.1) consists of various quark-quark potentials that reflect the symmetries and properties of QCD. These are: asymptotic freedom at short distances, chiral symmetry and its dynamical breaking which has important consequences for the form of the interaction at intermediate distances, and color confinement at large distances. In the following we discuss how these properties of QCD are incorporated into the potential model.

Asymptotic freedom is modelled in the NRQM by the one-gluon exchange potential, V^{OGEP}, which was first introduced by De Rujula, Glashow, and Georgi in 1975 [14]. Without retardation corrections and for equal quark masses it reads

$$V^{\text{OGEP}}(\boldsymbol{r}_i,\boldsymbol{r}_j) = \frac{\alpha_s}{4}\boldsymbol{\lambda}_i\cdot\boldsymbol{\lambda}_j\cdot\left\{\frac{1}{r}-\frac{\pi}{m_{\text{q}}^2}\left(1+\frac{2}{3}\boldsymbol{\sigma}_i\cdot\boldsymbol{\sigma}_j\right)\delta(\boldsymbol{r})-\frac{1}{4m_{\text{q}}^2}\frac{1}{r^3}\left(3\boldsymbol{\sigma}_i\cdot\hat{\boldsymbol{r}}\,\boldsymbol{\sigma}_j\cdot\hat{\boldsymbol{r}}-\boldsymbol{\sigma}_i\cdot\boldsymbol{\sigma}_j\right)\right.$$
$$\left.-\frac{1}{2m_{\text{q}}^2}\frac{1}{r^3}\left[3\left(\boldsymbol{r}\times\frac{1}{2}(\boldsymbol{p}_i-\boldsymbol{p}_j)\right)\cdot\frac{1}{2}(\boldsymbol{\sigma}_i+\boldsymbol{\sigma}_j)-\left(\boldsymbol{r}\times\frac{1}{2}(\boldsymbol{p}_i+\boldsymbol{p}_j)\right)\cdot\frac{1}{2}(\boldsymbol{\sigma}_i-\boldsymbol{\sigma}_j)\right]\right\}, \tag{3.2}$$

where $\boldsymbol{r}=\boldsymbol{r}_i-\boldsymbol{r}_j$; $\boldsymbol{\sigma}_i$ is the usual Pauli spin matrix, and $\boldsymbol{\lambda}_i$ is the color operator of the i-th quark. The latter is an 8-dimensional vector formed out of the 8 generators of $\text{SU(3)}_{\text{color}}$. This is in analogy to the spin operator of the i-th quark, $\boldsymbol{\sigma}_i$, which is a 3-dimensional vector formed out of the 3 generators of $\text{SU(2)}_{\text{spin}}$. Equation (3.2) contains a spin-independent part (color Coulomb), a spin-dependent part (color-magnetic interaction), a Galilean-invariant spin-orbit term, a Galilean-noninvariant spin-orbit term, and a tensor term. Because the gluon and the photon are both spin 1 gauge bosons, the one-gluon exchange potential V^{OGEP} is except for the color factor $\frac{1}{4}\boldsymbol{\lambda}_i\cdot\boldsymbol{\lambda}_j=\frac{1}{4}\sum_{a=1}^{8}\lambda_i^a\lambda_j^a$ and the replacement $\alpha_{\text{s}}\rightarrow\alpha$ identical to the well known Fermi-Breit interaction of QED [53]. However, unlike perturbative QCD, where the strong coupling constant α_{s} goes to zero at large inter-quark momenta as suggested by (2.6), the α_{s} of the NRQM is taken as an effective momentum independent constant in most applications. Consequently, constituent quarks are not free at short distances, but this should not be surprising because constituent quarks are quasi-particles with effective interactions that differ from the original interactions between the current quarks in $\mathcal{L}_{\text{QCD}}$. More importantly, the one-gluon exchange potential has the $\boldsymbol{\lambda}_i\cdot\boldsymbol{\lambda}_j\,\boldsymbol{\sigma}_i\cdot\boldsymbol{\sigma}_j$ spin-color structure of QCD at short distances. The color-magnetic interaction (CMI) is crucial for describing the experimentally observed mass spectrum of baryons and mesons. For example, it explains why the $\Delta(1232)$ with spin 3/2 is heavier than the $N(939)$ with spin 1/2. A $\boldsymbol{\sigma}_i\cdot\boldsymbol{\sigma}_j$ spin-dependence of the quark-quark interaction has already been anticipated on purely phenomenlogical grounds long before QCD [54].

Chiral symmetry is the other important property of QCD. In Chapt. 2 we have argued that the spontaneous breaking of this symmetry by the physical vacuum is responsible for the constituent quark mass generation, as well as for the appearence of pseudoscalar Goldstone bosons that couple to the constituent quarks. In the NRQM, this is modelled by introducing an effective quark-pion coupling and to lowest order by a one-pion exchange potential V^{OPEP} between constituent quarks [55 - 57]:

$$V^{\text{OPEP}}(\boldsymbol{r}_i,\boldsymbol{r}_j)=\frac{g_{\pi\text{q}}^2}{4\pi(4m_{\text{q}}^2)}\frac{\Lambda^2}{\Lambda^2-\mu^2}\boldsymbol{\tau}_i\cdot\boldsymbol{\tau}_j\,\boldsymbol{\sigma}_i\cdot\boldsymbol{\nabla}_r\,\boldsymbol{\sigma}_j\cdot\boldsymbol{\nabla}_r\left(\frac{e^{-\mu r}}{r}-\frac{e^{-\Lambda r}}{r}\right)=\frac{g_{\pi\text{q}}^2}{4\pi(4m_{\text{q}}^2)}\frac{1}{3}\frac{\Lambda^2}{\Lambda^2-\mu^2}\boldsymbol{\tau}_i\cdot\boldsymbol{\tau}_j$$
$$\cdot\left[\boldsymbol{\sigma}_i\cdot\boldsymbol{\sigma}_j\left(\mu^2\frac{e^{-\mu r}}{r}-4\pi\delta(\boldsymbol{r})\right)+\left(3\boldsymbol{\sigma}_i\cdot\hat{\boldsymbol{r}}\,\boldsymbol{\sigma}_j\cdot\hat{\boldsymbol{r}}-\boldsymbol{\sigma}_i\cdot\boldsymbol{\sigma}_j\right)\left(1+\frac{3}{\mu r}+\frac{3}{(\mu r)^2}\right)\mu^2\frac{e^{-\mu r}}{r}-(\mu\leftrightarrow\Lambda)\right], \tag{3.3}$$

where $r=|\boldsymbol{r}|$ and μ is the pion mass. Here, $\boldsymbol{\tau}_i$ denotes the isospin of the i-th quark. It should be noted that the pions are not treated here as $\text{q}\bar{\text{q}}$ composites but rather as fundamental Goldstone bosons connected with the

spontaneous breaking of chiral symmetry. The pion-quark coupling constant, $g^2_{\pi q}/(4\pi)$, is related to the well known πN coupling constant $f^2_{\pi N}/(4\pi)$ via

$$\frac{g^2_{\pi q}}{4\pi} = \left(\frac{3}{5}\right)^2 \frac{f^2_{\pi N}}{4\pi} \left(\frac{2m_q}{\mu}\right)^2 .$$

We use $f^2_{\pi N}/(4\pi) = 0.0749$ [58]. The factor $3/5$ at each vertex comes from a translation of the quark operator $\sum_i \boldsymbol{\tau}_i \boldsymbol{\sigma}_i$ to the corresponding operator $\boldsymbol{\tau}_N \boldsymbol{\sigma}_N$ in the space of nucleons [25]. The above form of the one-pion exchange potential results from the use of πq vertex function in momentum space of the form

$$F_{\pi q}(\boldsymbol{k}^2) = \left(\frac{\Lambda^2}{\Lambda^2 + \boldsymbol{k}^2}\right)^{1/2} , \tag{3.4}$$

where $\boldsymbol{k}$ is the three-momentum of the pion. Thus, the chiral symmetry breaking scale Λ is related to the hadronic size of the constituent quark via the usual definition

$$r^2_{\pi q} = -6 \frac{\mathrm{d}}{\mathrm{d}\boldsymbol{k}^2} F_{\pi q}(\boldsymbol{k}^2)|_{\boldsymbol{k}^2 \equiv 0} = \frac{3}{\Lambda^2} . \tag{3.5}$$

The larger Λ, the more point-like the constituent quark. For $\Lambda \to \infty$ the one-pion exchange potential (3.3) is unregularized and we recover a δ-function interaction between point-like constituent quarks.

In addition to the pion, its chiral partner, namely a massive scalar-isoscalar sigma-meson, is introduced into the NRQM [59, 60]. The parameters of this one-sigma exchange potential V^{OSEP} are fixed by the ones of the one-pion exchange potential and the constituent quark mass [59]:

$$V^{\mathrm{OSEP}}(\boldsymbol{r}_i, \boldsymbol{r}_j) = -\frac{g^2_{\sigma q}}{4\pi} \frac{\Lambda^2}{\Lambda^2 - m^2_\sigma} \left(\frac{e^{-m_\sigma r}}{r} - \frac{e^{-\Lambda r}}{r}\right) , \tag{3.6}$$

with

$$\begin{aligned} &\frac{g^2_{\sigma q}}{4\pi} = \frac{g^2_{\pi q}}{4\pi} = \frac{f^2_{\pi q}}{4\pi} \left(\frac{2m_q}{\mu}\right)^2 ; \\ &m^2_\sigma \approx (2m_q)^2 + \mu^2 , \\ &\Lambda_\pi = \Lambda_\sigma = \Lambda . \end{aligned} \tag{3.7}$$

Color confinement and spontaneous chiral symmetry breaking are related phenomena. Presumably, they can both be traced back to the existence of certain solutions of the classical QCD-Lagrangian called instantons [10]. According to Shuryak [9], the confinement scale is related to the scale of spontaneous chiral symmetry breaking as $\Lambda_{\mathrm{conf}} \approx \Lambda_{\mathrm{SBCS}}/3$. This means that the distances where confinement effects become important are somewhat larger than the distances where chiral symmetry is broken. In the NRQM, confinement is modelled by a linear or quadratic two-body quark-quark potential. Here, we take a two-body harmonic oscillator confinement potential

$$V^{\mathrm{conf}}(\boldsymbol{r}_i, \boldsymbol{r}_j) = -a_c \boldsymbol{\lambda}_i \cdot \boldsymbol{\lambda}_j (\boldsymbol{r}_i - \boldsymbol{r}_j)^2 , \tag{3.8}$$

where $\boldsymbol{\lambda}_i$ is again the color matrix of the i-th quark as in (3.2).

In summary, the potential model outlined above is an effective description that models the symmetries and main properties of the underlying quantum field theory in the simplest possible way. The phenomenological success of the potential model in baryon and nuclear few-body systems coupled with the scarcity of parameters employed indicates that constituent quarks interacting via two-body potentials is presumably a viable description of low-energy QCD.

3.2. *Baryon Ground State Wave Function*

We assume that the three valence quarks of equal mass m_q are in the lowest $(0s)^3$ harmonic oscillator state, denoted by $\varphi^{N(\Delta)}$

$$\begin{aligned} \varphi^{N(\Delta)}(\boldsymbol{r}_1, \boldsymbol{r}_2, \boldsymbol{r}_3) = &\left[\left(\frac{1}{\pi b^2}\right)^{3/4}\right]^3 \\ &\cdot \exp\left(-\frac{1}{2b^2}\left(\boldsymbol{r}_1^2 + \boldsymbol{r}_2^2 + \boldsymbol{r}_3^2\right)\right) . \end{aligned} \tag{3.9}$$

The harmonic oscillator constant b is defined as $b = 1/\sqrt{m_q \omega}$, where ω is the oscillator frequency. The relation between the oscillator frequency ω and the confinement strength a_c (3.8) is given by $a_c = m_q \omega^2/16$. The constant b determines the average hadronic size of the baryon and is usually called *quark core radius*.

$$\begin{aligned}
\boldsymbol{\rho} &= \boldsymbol{r}_1 - \boldsymbol{r}_2, \quad \boldsymbol{p}_\rho = \frac{m_2\boldsymbol{p}_1 - m_1\boldsymbol{p}_2}{m_1+m_2}, \\
\boldsymbol{\lambda} &= \boldsymbol{r}_3 - \frac{m_1\boldsymbol{r}_1 + m_2\boldsymbol{r}_2}{m_1+m_2}, \\
\boldsymbol{p}_\lambda &= \frac{(m_1+m_2)\boldsymbol{p}_3 - m_3(\boldsymbol{p}_1-\boldsymbol{p}_2)}{m_1+m_2+m_3}, \\
\boldsymbol{R} &= \frac{m_1\boldsymbol{r}_1 + m_2\boldsymbol{r}_2 + m_3\boldsymbol{r}_3}{m_1+m_2+m_3}, \quad \boldsymbol{P} = \boldsymbol{p}_1+\boldsymbol{p}_2+\boldsymbol{p}_3.
\end{aligned} \tag{3.10}$$

To separate the internal motion from the center of mass motion we introduce Jacobi coordinates (see Fig. 3.2). Using these coordinates, the kinetic and confinement parts of the Hamiltonian (3.1) separate into two independent internal oscillators with frequency ω:

$$H_0 = 3m_\mathrm{q} + \frac{\boldsymbol{p}_\rho^2}{m_\mathrm{q}} + \frac{1}{4}m_\mathrm{q}\omega^2\boldsymbol{\rho}^2 + \frac{3}{4}\frac{\boldsymbol{p}_\lambda^2}{m_\mathrm{q}} + \frac{1}{2}m_\mathrm{q}\omega^2\boldsymbol{\lambda}^2. \tag{3.11}$$

The fact that the center of mass motion (i. e. the 3rd term in (3.1)) can be exactly removed is one of the main advantages of the nonrelativistic quark model. The first four terms in (3.1) thus define the unperturbed Hamiltonian H_0. We take the eigenfunctions of H_0 as a convenient basis for expanding the baryon wave function.

The ground state eigenfunction of H_0 is then

$$\begin{aligned}
\varphi^{N(\Delta)}(\boldsymbol{\lambda},\boldsymbol{\rho}) = &\left(\frac{2}{4\pi b^2}\right)^{3/4}\left(\frac{2}{3\pi b^2}\right)^{3/4} \\
&\cdot \exp\left(-\frac{1}{4b^2}\boldsymbol{\rho}^2 - \frac{1}{3b^2}\boldsymbol{\lambda}^2\right).
\end{aligned} \tag{3.12}$$

Since the color part of the baryon wave function [1, 61]

$$\begin{aligned}
\left|\begin{array}{|c|c|}\hline & \\ \hline \\ \cline{1-1}\end{array}\right\rangle^{N(\Delta)}_{\text{color}} &= |[111]\rangle^{N(\Delta)}_{\text{color}} = \frac{1}{\sqrt{6}} \\
\cdot \Big(&r(1)b(2)y(3) + y(1)r(2)b(3) + b(1)y(2)r(3) \\
&- r(1)y(2)b(3) - y(1)b(2)r(3) - b(1)r(2)y(3)\Big)
\end{aligned} \tag{3.13}$$

is totally antisymmetric [5], and the spatial part of the lowest lying $(0s)^3$ state is completely symmetric, the spin and isospin part of the ground state wave functions is given by the symmetric combinations (we suppress the projection quantum numbers M_S and M_T)

$$|ST\rangle^{N(\Delta)} = \frac{1}{N}\sum_{s_{12}=0,1} |(s_{12}\tfrac{1}{2})S\rangle\,|(s_{12}\tfrac{1}{2})T\rangle, \tag{3.14}$$

where the normalization constant is $N = \sqrt{2}$ for the nucleon and $N = 1$ for the Δ-resonance. In the case of the Δ there is only one way to arrive at spin $S = 3/2$ and isospin $T = 3/2$ and the summation over the spin of the first two quarks is restricted to $s_{12} = 1$. The total wave function $\Phi_{N(\Delta)}$ is thus an inner product of the spatial wave function (3.12), the spin-isospin wave function (3.14), and the color wave function (3.13).

$$|\Phi_{N(\Delta)}\rangle = \varphi^{N(\Delta)}(\boldsymbol{\lambda},\boldsymbol{\rho}) \times |ST\rangle^{N(\Delta)} \times |[111]\rangle^{N(\Delta)}_{\text{color}}. \tag{3.15}$$

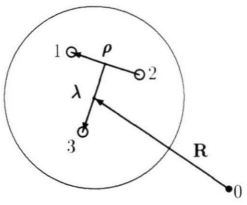

Fig. 3.2. Jacobi coordinates for the three-quark system.

3.3. Nucleon and Δ Mass Formulae

Equipped with the Hamiltonian (3.1) and the wave function (3.15) it is straightforward to calculate the nucleon and Δ masses. The masses of the N and Δ are given by the expectation values $\langle\Phi_N \mid H \mid \Phi_N\rangle$ and $\langle\Phi_\Delta \mid H \mid \Phi_\Delta\rangle$, respectively. We then get

$$\begin{aligned}
M_N(b) = &\,3m_\mathrm{q} + \frac{3}{2m_\mathrm{q}b^2} + 24a_\mathrm{c}b^2 - 2\alpha_\mathrm{s}\sqrt{\frac{2}{\pi}}\frac{1}{b} \\
&+ \frac{1}{3}\frac{\alpha_\mathrm{s}}{m_\mathrm{q}^2}\frac{1}{\sqrt{2\pi}}\frac{1}{b^3} - \frac{5}{4}\delta_\pi(b) + V^\sigma(b),
\end{aligned} \tag{3.16}$$

$$\begin{aligned}
M_\Delta(b) = &\,3m_\mathrm{q} + \frac{3}{2m_\mathrm{q}b^2} + 24a_\mathrm{c}b^2 - 2\alpha_\mathrm{s}\sqrt{\frac{2}{\pi}}\frac{1}{b} \\
&+ \frac{5}{3}\frac{\alpha_\mathrm{s}}{m_\mathrm{q}^2}\frac{1}{\sqrt{2\pi}}\frac{1}{b^3} - \frac{1}{4}\delta_\pi(b) + V^\sigma(b),
\end{aligned} \tag{3.17}$$

where the individual terms in (3.16, 3.17) are the kinetic, quadratic confinement, gluon, pion, and sigma

[5] This is denoted by a Young tableau with only one box in each row, i. e. [111]. For a good introduction into the relevant group theoretical concepts see the book by Close [61].

contributions, respectively. Subtracting (3.16) from (3.17) all spin-indpendent terms drop out and one gets

$$M_\Delta - M_N = \delta_g(b) + \delta_\pi(b), \tag{3.18}$$

where $\delta_\pi(b)$ and $\delta_g(b)$ are the *spin-dependent* pion and gluon contributions to the $\Delta - N$ mass splitting.

The explicit expressions for δ_g, δ_π, and V^σ are given as

$$\delta_g(b) = \frac{4\alpha_s}{3\sqrt{2\pi}m_q^2 b^3}, \tag{3.19}$$

$$\delta_\pi(b) = -4\frac{\Lambda^2}{\Lambda^2-\mu^2}\frac{f_{\pi q}^2}{4\pi\mu^2}\sqrt{\frac{2}{\pi}}\frac{1}{b}$$
$$\cdot\left\{\mu^2\left(1-\sqrt{\pi}(\frac{\mu b}{\sqrt{2}})e^{\mu^2 b^2/2}\mathrm{erfc}(\frac{\mu b}{\sqrt{2}})\right)-(\mu\leftrightarrow\Lambda)\right\},$$

$$V^\sigma(b) = -6\frac{\Lambda^2}{\Lambda^2-m_\sigma^2}\frac{g_{\sigma q}^2}{4\pi}\frac{1}{\sqrt{2\pi}}\frac{1}{b}$$
$$\cdot\left\{\left(1-\sqrt{\pi}(\frac{m_\sigma b}{\sqrt{2}})e^{m_\sigma^2 b^2/2}\mathrm{erfc}(\frac{m_\sigma b}{\sqrt{2}})\right)-(m_\sigma\leftrightarrow\Lambda)\right\}.$$

In order to indicate the two contributions to δ_π we write $\delta_\pi = \delta_{\pi_\mu} - \delta_{\pi_\Lambda}$ in the following.

3.4. *Determination of the Parameters*

The parameters of the NRQM are the quark-gluon coupling constant α_s, the confinement strength a_c, the harmonic oscillator parameter b, and the chiral cut-off mass Λ. In the presence of residual interactions the confinement strength a_c and size parameter b are not related via $a_c = 1/(16m_q b^4)$, as in the case of a pure harmonic oscillator potential but must be considered as independent parameters. In principle, the constituent quark mass m_q could also be varied. Here, we keep it fixed to $m_q = M_N/3 = 313$ MeV, in view of the many applications of the NRQM in hadron physics and nuclei [25, 62] where this value is the most natural. Choosing $m_q = M_N/3 = 313$ MeV allows to separate the center of mass motion of the system under consideration in a straightforward way. Furthermore, it has been shown that the momentum-dependent quark mass at the momentum scale of the nucleon mass is given by $m(p^2 = M_N^2) \approx M_N/3$ [12, 63, 64]. Hence, we use the constraint

$$M_N(b) = 3m_q. \tag{3.20}$$

Table 3.1. Quark model parameters.

b [fm]	α_s	a_c [MeV fm^{-2}]	m_σ [MeV]	$g_\sigma^2/(4\pi)$	Λ [fm^{-1}]
0.613	1.093	20.20	675	0.554	4.2

As in our previous calculation [37, 38], we take the value $\Lambda = 4.2$ fm^{-1}[57] which, according to (3.5) corresponds to a hadronic size of the constituent quark of $r_q = 0.4$ fm. This fixes the pion contribution, $\delta_\pi(b)$, to the $\Delta - N$ mass splitting. We then determine α_s from (3.18) and obtain

$$\alpha_s = \frac{3}{4}\sqrt{2\pi}m_q^2 b^3(M_\Delta - M_N - \delta_\pi(b)). \tag{3.21}$$

Next, we insert this expression for α_s into the formula for the nucleon mass M_N (3.16) and, using (3.20), obtain an expression for the confinement strength a_c as a function of b. Finally, we determine the oscillator parameter b from the variational condition, i. e. by partial differentiation of (3.16) with respect to b

$$\frac{\partial M_N(b)}{\partial b} = 0. \tag{3.22}$$

Using (3.22) to determine the variational parameter b amounts to approximately solving the Schrödinger equation for the Hamiltonian (3.1). If we exclude π- and σ-mesons (this is the standard one-gluon exchange Isgur-Karl model), (3.22) leads to a simple quadratic equation in b^2 where only $m_q = 313$ MeV and $M_\Delta - M_N = 293$ MeV enter.

The parameters used in this work are given in Table 3.1. The solution of (3.22) actually gives $b = 0.596$ fm. This is smaller but not very different from the value $b = 0.613$ fm without the σ-meson which was used in previous works [37, 38]. We continue to use our previous value $b = 0.613$ fm in anticipation of the value required by the neutron charge radius and our results for baryon magnetic moments which come out slightly better for $b = 0.613$ fm.

Previously [37, 38], we also studied the case without chiral π- and σ-interactions, i. e. employing only one-gluon exchange as residual interaction. This is the standard Isgur-Karl model. While it is possible to find a physical set of parameters for this case; we were unable to find a consistent set of parameters if gluons are switched off completely. In a model using only chiral interactions, one would have to increase the pion-quark coupling strength by a factor of two in

Table 3.2. Contribution of the kinetic energy (without the rest mass term) and individual potential terms in the Hamiltonian to the nucleon mass (3.16). We list the color-Coulomb (cc) and δ-function part (δ) of $V^{\rm OGEP}$ separately. The gluon ($\delta_{\rm g}$) and pion (δ_π) contributions to the $\Delta - N$ mass splitting (3.18) is also given. All entries are in [MeV].

Term	$T^{\rm kin}$	$V^{\rm conf}$	$V_{\rm cc}^{\rm OGEP}$	$V_\delta^{\rm OGEP}$	V^π	V^σ	Total	$\delta_{\rm g}$	δ_π
	496.6	182.2	–561.2	49.5	–118.9	–48.1	0.0	197.9	95.1

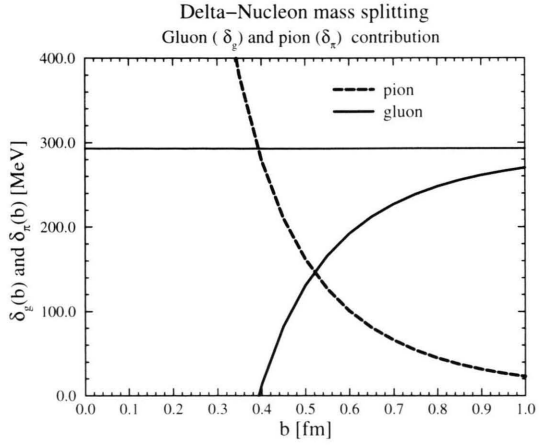

Fig. 3.3. Gluon contribution $\delta_{\rm g}$ (full line) and pion contribution δ_π (dashed line) to the $\Delta - N$ mass splitting as a function of the oscillator parameter b according to (3.18). The cut-off mass is $\Lambda_\pi = 4.2$ fm^{-1} corresponding to a hadronic constituent quark size of $r_{\pi{\rm q}} = 0.4$ fm. The horizontal line shows the experimental $\Delta - N$ mass splitting of $(M_\Delta - M_N)_{\rm exp} = 293$ MeV.

order to describe the $\Delta - N$ mass splitting. Because we want to apply the model without any modifications also to two-baryon systems, where the pion-quark coupling constant is directly connected with the empirical pion-nucleon coupling constant, we do not consider the case without gluons.

In order to appreciate the importance of the individual contributions to the nucleon mass M_N (3.16) we also show their numerical values, as well as the gluon ($\delta_{\rm g}$) and pion (δ_π) contributions to the $\Delta - N$ mass splitting in Table 3.2. We see that the kinetic and various potential contributions to the nucleon mass cancel each other exactly, so that the nucleon mass is simply the sum of the three constituent quark masses. This cancellation was achieved by adjusting the confinement strength $a_{\rm c}$ to give $M_N(b) = 3m_{\rm q}$. The authors of [12] suggest that this cancellation, the nearness of $m_{\rm q}$ to $M_N/3$, and the relative smallness of confinement effects are the reasons why the simple NRQM is so successful.

The quantities $\delta_{\rm g}$ and δ_π play a central role in this work. Their numerical values indicate the importance of the gluon-, and pion degrees of freedom in the mass spectrum. Furthermore, these quantities can also be used for describing gluon and pion cloud contributions to various electromagnetic properties as we will see in Chapt. 4. Note that the size of the pion contribution δ_π is completely determined by the value of the chiral symmetry breaking scale Λ and the quark core radius b. In Fig. 3.3 we show $\delta_{\rm g}(b)$ and $\delta_\pi(b)$ as functions of the quark core radius b for a fixed Λ_π. It is evident that, for small quark core radii $b < 0.5$ fm pion effects are dominant while the gluon cloud is more important for $b > 0.6$ fm.

3.5. *Configuration Mixing*

So far, the wave function for the N and Δ has been taken to be a pure $(0s)^3$ wave function. However, the residual interactions will admix higher excited states to the $(0s)^3$ ground state. If we restrict ourselves to $2\hbar\omega$ excitations, we have four excited states ($\Phi^N_{{\rm S}_{\rm S}'}, \Phi^N_{\rm S_M}$, $\Phi^N_{\rm D_M}, \Phi^N_{\rm P_A}$) for the N and three excited states ($\Phi^\Delta_{{\rm S}_{\rm S}'}, \Phi^\Delta_{\rm D_S}$, $\Phi^\Delta_{\rm D_M}$) for the Δ. The subscripts $L_{\rm sym}$ describe the orbital angular momentum (L) and the symmetry (sym) of the orbital wave function under particle exchange. Here, S denotes symmetric, M mixed symmetric and A antisymmetric orbital wave functions. A detailed description of these wave functions can be found in [65]. The N and Δ wave functions are then given by

$$\begin{aligned}\Phi_N &= a_{\rm S_S}\Phi^N_{\rm S_S} + a_{\rm S_S'}\Phi^N_{\rm S_S'} + a_{\rm S_M}\Phi^N_{\rm S_M} \\ &\quad + a_{\rm D_M}\Phi^N_{\rm D_M} + a_{\rm P_A}\Phi^N_{\rm P_A}, \qquad (3.23)\\ \Phi_\Delta &= b_{\rm S_S}\Phi^\Delta_{\rm S_S} + b_{\rm S_S'}\Phi^\Delta_{\rm S_S'} + b_{\rm D_S}\Phi^\Delta_{\rm D_S} + b_{\rm D_M}\Phi^\Delta_{\rm D_M}.\end{aligned}$$

One can now diagonalize the Hamiltonian (3.1) in a larger configuration space, including the excited ($2\hbar\omega$) harmonic oscillator configurations with nucleon or $\Delta(1232)$ quantum numbers. This improves the simple $(0s)^3$ wave functions (3.12) considerably and has been done in [37, 38] where a simultaneous calculation of the positive parity excitation spectrum and various electromagnetic properties of the nucleon has been performed. We emphasize that, one and the same parameter set with a relatively small quark core radius $b = 0.58$ fm has been used in the calculation

Table 3.3. Admixture coefficients for the four $2\hbar\omega$ excited states in the nucleon ground state wave function as defined in (3.23) and calculated in [37]. The corrected results of [30] which include the δ function of V^{OPEP} and the results of [65] using only V^{OGEP} are shown for comparison.

N	a_{S_S}	$a_{S'_S}$	a_{S_M}	a_{D_M}	a_{P_A}
[37]	0.934	–0.306	–0.178	–0.047	0.002
[30]	0.906	–0.383	–0.178	–0.045	0.003
[65]	0.931	–0.274	–0.233	–0.067	0.0
Δ	b_S	b_{S_S}	b_{D_S}	b_{D_M}	
[37]	0.990	0.083	–0.097	0.064	
[30]	0.994	0.024	–0.090	0.056	

Table 3.4. Nucleon (N) and Delta (Δ) spectrum with gluon and pion exchange between quarks (parameters from [37]). The results of [30] for a smeared out pion-quark vertex are shown for comparison. Experimental numbers from [48]. All entries in [MeV].

N [37]	N [30]	Exp.	Δ [37]	Δ [30]	Exp.
939	936	939 ± 0.7	1232	1235	1232 ± 2
1455	1465	1440 ± 30	1673	1701	$1600 \pm 50^{**}$
1706	1753	1710 ± 30	1840	1908	1920 ± 60
1890	1962	$2100 \pm 200^{*}$	1903	1974	2100 ± 200
1991	2062				

of the positive parity excitation spectrum and in the calculation of the electromagnetic properties of the nucleon.

In Table 3.3 we show the corresponding admixture coefficients obtained in [37] and compare them to other recent calculations. Note the relatively small D-state admixture which results in a tiny D-state probability of less than 0.5%. Table 3.4 shows the numerical results for the masses of the excited nucleon and Δ states. We point out that for the parameters used in this work, the negative parity states $N^*(1535)$ and $N^*(1520)$ would come out too low by some 200 MeV. Recently, a simultaneous description of the $N^*(1440)$ and the $N^*(1520)$, P-wave excitations has been obtained in the NRQM [17]. This simultaneous description of positive and negative parity nucleon resonances has been achieved by fitting potential matrix elements, with an unspecified radial form of the pseudoscalar meson exchange potential to *both* the mass of the $N^*(1440)$ and the mass of the $N^*(1520)$. A simultaneous description of the negative and positive parity excited states in the present framework is a challenge for the future.

In the present work, for sake of simplicity, we use the wave function (3.12). This approximation leads to analytic results for many observables and some interesting relations between them. It is, therefore, quite useful to highlight the contribution of exchange current effects to electromagnetic observables. In each case, we discuss how our qualitative results will be modified by configuration mixing effects.

3.6. *Masses of Octet Baryons*

In the previous section, we have used baryon wave functions specialized to three equal masses. The generalization to three quark flavors with different masses has been carried out in [39]. If we consider strange quarks with a mass different from the nearly degenerate up and down quark masses, it is crucial to use the original expressions for the Jacobi coordinates. This will lead to generalized orbital wave functions. The harmonic oscillator constants $b_{\boldsymbol{\rho}}$ and $b_{\boldsymbol{\lambda}}$ in the directions of the internal Jacobi-coordinates $\boldsymbol{\rho} = (\boldsymbol{r}_1 - \boldsymbol{r}_2)$ and $\boldsymbol{\lambda} = \boldsymbol{r}_3 - (m_1\boldsymbol{r}_1 + m_2\boldsymbol{r}_2)/(m_1 + m_2)$ can be expressed in terms of quark mass ratios and the oscillator parameter b used for the nucleon and the Δ. The orbital part of the wave function $\Phi_{3q}(f_1 f_2 f_3, \boldsymbol{\rho}, \boldsymbol{\lambda})$ depends now on three quark flavors f_1, f_2, f_3, and the full wave function can be written as

$$|B\rangle = \frac{1}{\sqrt{2}} \sum_{S_{12}=0,1} \left(\sum_{f_1 f_2 f_3} {}^{B}C^{S_{12}}(f_1 f_2 f_3) \times \Phi_{3q}(f_1 f_2 f_3, \boldsymbol{\rho}, \boldsymbol{\lambda}) \times |f_1 f_2 f_3\rangle \right) \times |S, S_z; S_{12}\rangle |[111]_{\mathrm{color}}\rangle. \tag{3.24}$$

$|f_1 f_2 f_3\rangle$ is the flavor part of the wave function. As in (3.15) the antisymmetry lies in the color space and is denoted by a Young tableau [111] (see (3.13)). The coefficients ${}^{B}C^{S_{12}}(f_1 f_2 f_3)$ are $\mathrm{SU}(3)_{\mathrm{flavor}}$ Clebsch-Gordan coefficients. These wave functions can be found for example in [61]. Note, however, that we use a different overall sign for the mixed symmetric states.

In addition to the changes in the wave function, the Hamiltonian must also be generalized to the case of unequal masses [39]. As before, the parameters for the present calculation are fitted to the N and Δ masses. In addition, we fix the ratio between light and

Table 3.5. The contributions of the various terms in the Hamiltonian (3.1) to the baryon masses [39]. All quantities are given in [MeV]. The experimental values represent averages over particles with different charge.

	$\sum_i m_i$	E_{kin}	V_{conf}	V_{gluon}	V_π	V_σ	m_{B}	m_{exp} [48]
p, n	939	497	189	–512	–119	–54	939	939
Δ	939	497	189	–314	–24	–54	1232	1232
Σ	1148	497	163	–540	–8	–63	1197	1193
Λ	1148	497	163	–561	–71	–63	1112	1116
Ξ	1356	497	138	–613	0	–74	1304	1318

strange quark masses to

$$m_{\text{u}}/m_{\text{s}} = 0.6.$$

The baryon masses m_{B} are determined as the expectation values of the Hamiltonian [39] between the wave functions (3.24). The result is shown in Table 3.5.

4. Electromagnetic Currents and Gauge Invariance

The interaction of the external electromagnetic field $A^\mu(x) = (\Phi(x), \boldsymbol{A}(x))$ with a hadronic system is described by the Hamilton operator

$$H_{\text{em}} = \int \mathrm{d}^4x \; J_\mu(x) A^\mu(x), \tag{4.1}$$

where $J_\mu(x) = (\rho(x), -\boldsymbol{J}(x))$ is the four-vector current density of the hadronic system. Thus, in a quark model description of baryons we must know the total quark charge and current operators in order to describe their electromagnetic properties.

4.1. One-body Currents

First, we consider the standard nonrelativistic one-body quark charge and current operators of point-like constituent quarks (see Fig. 4.1)

$$\begin{aligned}\rho^{(0)}_{[1]}(\boldsymbol{r}_i, \boldsymbol{x}) &= e_i \delta(\boldsymbol{r}_i - \boldsymbol{x}),\\ \boldsymbol{J}^{(0)}_{[1]}(\boldsymbol{r}_i, \boldsymbol{x}) &= \frac{e_i}{2m_{\text{q}}} \big(i\big[\boldsymbol{\sigma}_i \times \boldsymbol{p}_i, \delta(\boldsymbol{r}_i - \boldsymbol{x})\big] \\ &\qquad + \{\boldsymbol{p}_i, \delta(\boldsymbol{r}_i - \boldsymbol{x})\} \big),\end{aligned} \tag{4.2}$$

where e_i is the quark charge operator

$$e_i = \frac{1}{6} e (1 + 3\tau_3^{(i)}). \tag{4.3}$$

Fig. 4.1. Single quark current. The shaded circle indicates the finite electromagnetic size of the constituent quarks.

The decomposition (4.2) into isoscalar (IS) or isovector (IV) currents is accomplished by taking only the first or second term of (4.3) into account.

The commutator term in (4.2) is for obvious reasons called spin-current. The anticommutator term is called convection current. It is the properly antisymmetrized quantum mechanical operator corresponding to the classical current density $\boldsymbol{J}_i = \rho_i \boldsymbol{p}_i / m_{\text{q}}$ for a point particle. These operators describe the coupling of the external photon with a single quark at a time at the position $\boldsymbol{x}$. This is usually called impulse approximation and the currents of (4.2) are often referred to as impulse currents. Note that we do not use any anomalous magnetic moments for the constituent quarks which is a reasonable first order approximation [66].

It is usually more convenient to work with the Fourier transforms with respect to $\boldsymbol{x}$:

$$\begin{aligned}\rho^{(0)}_{[1]}(\boldsymbol{r}_i, \boldsymbol{q}) &= e_i e^{i\boldsymbol{q}\cdot\boldsymbol{r}_i},\\ \boldsymbol{J}^{(0)}_{[1]}(\boldsymbol{r}_i, \boldsymbol{q}) &= \frac{e_i}{2m_{\text{q}}} \big(i\big[\boldsymbol{\sigma}_i \times \boldsymbol{p}_i, e^{i\boldsymbol{q}\cdot\boldsymbol{r}_i}\big] \\ &\qquad + \{\boldsymbol{p}_i, e^{i\boldsymbol{q}\cdot\boldsymbol{r}_i}\} \big).\end{aligned} \tag{4.4}$$

Here, and in the following the three-momentum transfer of the photon is denoted by $\boldsymbol{q}$.

4.2. Two-body Exchange Currents

In most applications of the NRQM the total current has been approximated by the sum of the single-quark currents (4.4)

$$J^\mu \approx \sum_{i=1}^{3} J^\mu_{\text{imp}}(i). \tag{4.5}$$

However, as mentioned in the introduction, (4.5) contradicts electromagnetic current conservation. In the

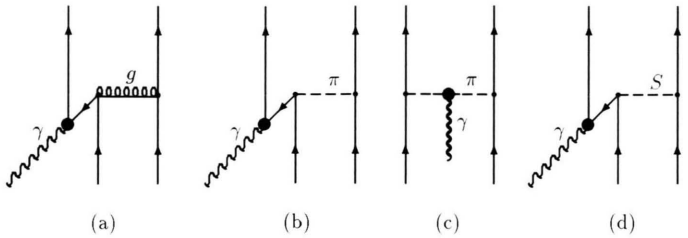

Fig. 4.2. Two-body exchange currents between quarks: (a) gluon-pair, (b) pion-pair, (c) pionic, (d) scalar pair. The large shaded circles indicate the finite electromagnetic size of the constituent quarks and the pion.

presence of various residual interactions between the quarks the total current operator of the hadron cannot simply be a sum of free quark currents but must be supplemented by various two-body currents. These two-body currents are closely related to the quark-quark potentials from which they can be derived by minimal substitution. Since the effect of the residual quark-quark potentials is clearly seen in the excited spectra of hadrons one expects the corresponding two-body currents to play an equally important role in various electromagnetic properties of hadrons.

The two-body exchange currents, considered in this work, provide an effective description of the residual gluon, pion, σ-meson and confinement degrees of freedom in various electromagnetic properties above and beyond those that are already contained in the constituent quark parameters (mass and size) and the quark wave function.

In the following, we list the two-body charge and current operators employed in this work. These operators have been derived by a nonrelativistic reduction of the Feynman diagrams of Fig. 4.2, keeping only the lowest nonvanishing order in a v/c expansion for each process [67] [6]. Nonlocal terms have been discarded as usual. The extent to which these operators are consistent with the Hamiltonian used in Chapt. 3 is discussed in Section 4.5.

We begin with the gluon-exchange current of Figure 4.2a,

$$\begin{aligned}
\rho^{\mathrm{IS/IV}}_{\mathrm{gq\bar{q}}}(\boldsymbol{r}_i,\boldsymbol{r}_j,\boldsymbol{q}) &= -i\frac{\alpha_\mathrm{s}}{16m_\mathrm{q}^3}\,\boldsymbol{\lambda}_i\cdot\boldsymbol{\lambda}_j\left\{e_i e^{i\boldsymbol{q}\cdot\boldsymbol{r}_i}\left[\boldsymbol{q}\cdot\boldsymbol{r}+(\boldsymbol{\sigma}_i\times\boldsymbol{q})\cdot(\boldsymbol{\sigma}_j\times\boldsymbol{r})\right]+(i\leftrightarrow j)\right\}\frac{1}{r^3},\\
\boldsymbol{J}^{\mathrm{IS/IV}}_{\mathrm{gq\bar{q}}}(\boldsymbol{r}_i,\boldsymbol{r}_j,\boldsymbol{q}) &= -\frac{\alpha_\mathrm{s}}{4m_\mathrm{q}^2}\,\boldsymbol{\lambda}_i\cdot\boldsymbol{\lambda}_j\left\{e_i e^{i\boldsymbol{q}\cdot\boldsymbol{r}_i}\frac{1}{2}(\boldsymbol{\sigma}_i+\boldsymbol{\sigma}_j)\times\boldsymbol{r}+(i\leftrightarrow j)\right\}\frac{1}{r^3},
\end{aligned}\tag{4.6}$$

where $\boldsymbol{r}=\boldsymbol{r}_i-\boldsymbol{r}_j$. The above coordinate space expressions for the gluon-exchange current have been derived using a nonrelativistic expansion of the Feynman diagram of Figure 4.2a. (for details see [28]). They describe a quark-antiquark pair creation process induced by the external photon with subsequent annihilation of the quark-antiquark pair into a gluon which is then absorbed at the site of another quark. Because the gluon does not carry any isospin the gluon-pair current has the same isospin structure as the one-body currents. These gluon-pair currents are of relativistic origin as reflected in the higher powers of $1/m_\mathrm{q}$ as compared to the nonrelativistic impulse current (4.4).

Pion-pair exchange currents (see Fig. 4.2b) resulting from pseudoscalar pion-quark coupling are discussed next. Because the pion is an isospin 1 particle the isospin structure of these operators is more complicated than that of the one-body or gluon exchange current. We list isoscalar and isovector current operators separately. We start with the isoscalar pion-pair current which is given as [27, 28]

$$\begin{aligned}
\rho^{\mathrm{IS}}_{\pi\mathrm{q\bar{q}}}(\boldsymbol{r}_i,\boldsymbol{r}_j,\boldsymbol{q}) &= \frac{ie}{6}\frac{g^2_{\pi\mathrm{q}}}{4\pi(4m_\mathrm{q}^2)}\frac{\Lambda^2}{\Lambda^2-\mu^2}\frac{1}{m_\mathrm{q}}\,\boldsymbol{\tau}_i\cdot\boldsymbol{\tau}_j\left\{e^{i\boldsymbol{q}\cdot\boldsymbol{r}_i}\boldsymbol{\sigma}_i\cdot\boldsymbol{q}\,\boldsymbol{\sigma}_j\cdot\nabla_{\mathbf{r}}+(i\leftrightarrow j)\right\}\left(\frac{e^{-\mu r}}{r}-\frac{e^{-\Lambda r}}{r}\right),\\
\boldsymbol{J}^{\mathrm{IS}}_{\pi\mathrm{q\bar{q}}}(\boldsymbol{r}_i,\boldsymbol{r}_j,\boldsymbol{q}) &= \frac{ie}{6}\frac{g^2_{\pi\mathrm{q}}}{4\pi(4m_\mathrm{q}^2)}\frac{\Lambda^2}{\Lambda^2-\mu^2}\frac{1}{2m_\mathrm{q}^2}\,\boldsymbol{\tau}_i\cdot\boldsymbol{\tau}_j\left\{e^{i\boldsymbol{q}\cdot\boldsymbol{r}_i}\boldsymbol{q}\times\nabla_{\mathbf{r}}\,\boldsymbol{\sigma}_j\cdot\nabla_{\mathbf{r}}+(i\leftrightarrow j)\right\}\left(\frac{e^{-\mu r}}{r}-\frac{e^{-\Lambda r}}{r}\right).
\end{aligned}\tag{4.7}$$

As is evident from (4.7), the isoscalar pion-pair current is of relativistic order in an $1/m_\mathrm{q}$ expansion. The isovector pion-pair current is given by

[6] Only for the spatial isovector pion pair current we keep the next-to-leading order term. This term is necessary in order to prove the proportionality of Δ magnetic moments to the charge of the Δ.

$$\rho^{\mathrm{IV}}_{\pi q\bar{q}}(\boldsymbol{r}_i,\boldsymbol{r}_j,\boldsymbol{q}) = \frac{ie}{2}\frac{g^2_{\pi q}}{4\pi(4m_q^2)}\frac{\Lambda^2}{\Lambda^2-\mu^2}\frac{1}{m_q}\left\{\tau_{i3}e^{i\boldsymbol{q}\cdot\boldsymbol{r}_i}\boldsymbol{\sigma}_i\cdot\boldsymbol{q}\,\boldsymbol{\sigma}_j\cdot\nabla_{\mathbf{r}}+(i\leftrightarrow j)\right\}\left(\frac{e^{-\mu r}}{r}-\frac{e^{-\Lambda r}}{r}\right),$$

$$\boldsymbol{J}^{\mathrm{IV}}_{\pi q\bar{q}}(\boldsymbol{r}_i,\boldsymbol{r}_j,\boldsymbol{q}) = e\frac{g^2_{\pi q}}{4\pi(2m_q)^2}\frac{\Lambda^2}{\Lambda^2-\mu^2}\left\{(\boldsymbol{\tau}_i\times\boldsymbol{\tau}_j)_3 e^{i\boldsymbol{q}\cdot\boldsymbol{r}_i}\boldsymbol{\sigma}_i\,\boldsymbol{\sigma}_j\cdot\nabla_{\mathbf{r}}+(i\leftrightarrow j)\right\}\left(\frac{e^{-\mu r}}{r}-\frac{e^{-\Lambda r}}{r}\right) \tag{4.8}$$

$$+\frac{i}{4m_q^2}\left\{\tau_{j3}e^{i\boldsymbol{q}\cdot\boldsymbol{r}_i}\boldsymbol{q}\times\nabla_{\mathbf{r}}\,\boldsymbol{\sigma}_j\cdot\nabla_{\mathbf{r}}+(i\leftrightarrow j)\right\}\left(\frac{e^{-\mu r}}{r}-\frac{e^{-\Lambda r}}{r}\right).$$

The two terms in the spatial current (4.8) are the leading order ($\mathcal{O}(m_q^{-1})$) pion pair-current proportional to $(\boldsymbol{\tau}_i\times\boldsymbol{\tau}_j)_3$ and its next-to-leading order ($\mathcal{O}(m_q^{-3})$) relativistic correction proportional to τ_{j3} shown in Figure 4.2b. Here, τ_{i3} denotes the third component of the isospin of the i-th particle.

The pionic current of Fig. 4.2c describes a process where the photon couples to the pion directly. It turns out that to order ($\mathcal{O}(m_q^{-2})$) the pionic exchange current does not contribute to the charge density but only to the spatial current

$$\rho^{\mathrm{IV}}_{\gamma\pi\pi}(\boldsymbol{r}_i,\boldsymbol{r}_j,\boldsymbol{q}) \approx 0,$$

$$\boldsymbol{J}^{\mathrm{IV}}_{\gamma\pi\pi}(\boldsymbol{r}_i,\boldsymbol{r}_j,\boldsymbol{q}) = e\frac{f^2_{\pi q}}{4\pi\mu^2}\frac{\Lambda^2}{\Lambda^2-\mu^2}(\boldsymbol{\tau}_i\times\boldsymbol{\tau}_j)_3\,\boldsymbol{\sigma}_i\cdot\nabla_i\,\boldsymbol{\sigma}_j\cdot\nabla_j\int_{-1/2}^{1/2}\mathrm{d}v\,e^{i\boldsymbol{q}\cdot(\boldsymbol{R}-\boldsymbol{r}v)}\left(z_\mu\frac{e^{-L_\mu r}}{L_\mu r}-z_\Lambda\frac{e^{-L_\Lambda r}}{L_\Lambda r}\right). \tag{4.9}$$

In the pionic exchange current we have used the following abbreviations: $\boldsymbol{R} = (\boldsymbol{r}_i+\boldsymbol{r}_j)/2$, $z_m(\boldsymbol{q},\boldsymbol{r}) = L_m\boldsymbol{r}+ivr\boldsymbol{q}$, and $L_m(q,v) = [\frac{1}{4}q^2(1-4v^2)+m^2]^{1/2}$.

Next, we construct scalar exchange currents from the generalized scalar σ-meson exchange and confinement potentials. If, as has been done in the one-gluon exchange potential, relativistic corrections up to order $\mathcal{O}(m_q^{-3})$ are included, both potentials become momentum dependent and lead to corresponding meson exchange currents. We use the classification scheme of Friar [68] where the leading order potential of each diagram in Fig. 3.1 is counted as being of order $\mathcal{O}(m_q^{-1})$. A derivation of the scalar exchange current from a general scalar-isoscalar exchange potential is given in Section 4.4. using minimal coupling in the scalar exchange potential. This result agrees with the local part of the relativistic scalar-isoscalar pair current derived from Feynman diagrams [69]. Note that the spatial part of the scalar exchange current has the same spin-isospin structure as the single-quark current:

$$\rho^{\mathrm{IS/IV}}_{\mathrm{S}}(\boldsymbol{r}_i,\boldsymbol{r}_j,\boldsymbol{q}) = \frac{1}{(2m_q)^3}\left\{e^{i\boldsymbol{q}\cdot\boldsymbol{r}_i}e_i\left(\frac{3}{2}\boldsymbol{q}^2-i\boldsymbol{q}\cdot\nabla_r+\frac{1}{2}\nabla_r^2\right)V^{\mathrm{S}}(\boldsymbol{r}_i,\boldsymbol{r}_j)+(i\leftrightarrow j)\right\},$$

$$\boldsymbol{J}^{\mathrm{IS/IV}}_{\mathrm{S}}(\boldsymbol{r}_i,\boldsymbol{r}_j,\boldsymbol{q}) = -\frac{1}{2m_q^2}\left\{e_ie^{i\boldsymbol{q}\cdot\boldsymbol{r}_i}\boldsymbol{\sigma}_i\times\boldsymbol{q}V^{\mathrm{S}}(\boldsymbol{r}_i,\boldsymbol{r}_j)+(i\leftrightarrow j)\right\}. \tag{4.10}$$

Equation (4.10) is used to calculate both the confinement- and σ-meson-exchange currents.

It is obvious that with the exception of the isovector pion-pair current (4.8) and the isovector pionic current (4.9), which are of the same relativistic order $\mathcal{O}(m_q^{-1})$ as the one-body current, all other two-body currents are relativistic corrections. This is shown in Table 4.1. We point out that some of these operators have a spin-isopin structure not present in the lowest order one-body or two-body currents. Thus, although being formally of higher order, they can induce, for example, spin-flip transitions to states not accessible by the lower order single-quark or two-body currents. This point will be examined in more detail below.

Finally, the total charge operator consists of the usual one-body charge and interaction dependent two-body charge operators

Table 4.1. Lowest relativistic order of each current operator according to the $(1/m_q)^n$ classification scheme [68].

	Imp	pion(IV)	pion(IS)	gluon	scalar
ρ	m_q^0	m_q^{-2}	m_q^{-2}	m_q^{-4}	m_q^{-4}
J	m_q^{-1}	m_q^{-1}	m_q^{-3}	m_q^{-3}	m_q^{-3}

$$\rho(\boldsymbol{q}) = \sum_{i=1}^{3} \rho_{[1]}(\boldsymbol{r}_i) + \sum_{i<j}^{3} \left(\rho_{\mathrm{gq\bar{q}}}(\boldsymbol{r}_i, \boldsymbol{r}_j) + \rho_{\pi \mathrm{q\bar{q}}}(\boldsymbol{r}_i, \boldsymbol{r}_j) + \rho_{\sigma \mathrm{q\bar{q}}}(\boldsymbol{r}_i, \boldsymbol{r}_j) + \rho_{\mathrm{conf}}(\boldsymbol{r}_i, \boldsymbol{r}_j) \right) . \tag{4.11}$$

Likewise the total current operator consists of the usual one-body operator and two-body exchange current operators tightly related to the different quark-quark interactions

$$\boldsymbol{J}(\boldsymbol{q}) = \sum_{i=1}^{3} \boldsymbol{J}_{[1]}(\boldsymbol{r}_i) + \sum_{i<j}^{3} \left(\boldsymbol{J}_{\mathrm{gq\bar{q}}}(\boldsymbol{r}_i, \boldsymbol{r}_j) + \boldsymbol{J}^{\mathrm{IV}}_{\pi}(\boldsymbol{r}_i, \boldsymbol{r}_j) + \boldsymbol{J}^{\mathrm{IS}}_{\pi \mathrm{q\bar{q}}}(\boldsymbol{r}_i, \boldsymbol{r}_j) + \boldsymbol{J}_{\sigma \mathrm{q\bar{q}}}(\boldsymbol{r}_i, \boldsymbol{r}_j) + \boldsymbol{J}_{\mathrm{conf}}(\boldsymbol{r}_i, \boldsymbol{r}_j) \right) , \tag{4.12}$$

where $\boldsymbol{J}^{\mathrm{IV}}_{\pi}(\boldsymbol{r}_i, \boldsymbol{r}_j) = \boldsymbol{J}^{\mathrm{IV}}_{\pi \mathrm{q\bar{q}}}(\boldsymbol{r}_i, \boldsymbol{r}_j) + \boldsymbol{J}^{\mathrm{IV}}_{\gamma \pi\pi}(\boldsymbol{r}_i, \boldsymbol{r}_j)$.

Before we discuss the important question of gauge invariance in Sect. 4.4 we show in the next section how the above expressions for pointlike quarks must be modified in order to include the finite electromagnetic size of the quarks and pions.

4.3. Electromagnetic Size of the Constituent Quarks

In Chapt. 3 we have seen that constituent quarks have a finite hadronic size which is given by the hadronic form factor (3.4). Similarly, the *electromagnetic* size of the constituent quarks is described by a monopole form factor

$$F_{\gamma \mathrm{q}}(\boldsymbol{q}^2) = \frac{1}{1 + \frac{1}{6}\boldsymbol{q}^2 r^2_{\gamma \mathrm{q}}} . \tag{4.13}$$

In order to take the internal electromagnetic structure of the constituent quarks into account, the charge and current operators of the previous section must simply be multiplied by the form factor (4.13). Both isoscalar and isovector parts of the single-quark charge operator are multiplied by the same quark form factor $F_{\gamma \mathrm{q}}(\boldsymbol{q}^2)$.

The finite electromagnetic radius $r_{\gamma \mathrm{q}}$ takes into account that constituent quarks are dressed particles, i.e. current quarks surrounded by a cloud of $\mathrm{q\bar{q}}$-pairs. The dominant contributions come from quark-antiquark pairs with pion quantum numbers. Vector meson dominance relates the electromagnetic radius of the constituent quarks to the ρ-meson pole according to Fig. 4.3. The notion of a finite electromagnetic size of the constituent quarks has been used before [3, 70, 71].

Although the mass and the electromagnetic radius of the constituent quarks are drastically change from their bare values, the magnetic moment of the quarks is basically not renormalized. Explicit calculation in the NJL model also shows that the anomalous magnetic moment of the constituent quarks is small

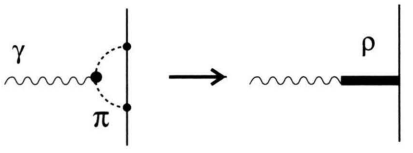

Fig. 4.3. Pion loop contribution to the electromagnetic form factor of the constituent quarks. Vector meson dominance relates the finite electromagnetic radius $r_{\gamma \mathrm{q}}$ of the constituent quarks to the vector meson mass m_ρ according to $r^2_{\gamma \mathrm{q}} \approx 6/m^2_\rho$ [3].

[3] as was previously anticipated on quite general grounds [66].

4.4. Conservation of the Electromagnetic Current

In this Section we discuss the extent to which the total electromagnetic quark current of an interacting quark system satisfies the continuity equation

$$\boldsymbol{q} \cdot \boldsymbol{J}(\boldsymbol{q}) = [H, \rho(\boldsymbol{q})] , \tag{4.14}$$

where $\rho(\boldsymbol{q})$ and $\boldsymbol{J}(\boldsymbol{q})$ are respectively the total charge density and current density for an interacting two-quark system.

We start with a decomposition of all operators in (4.14) into one- and two-body operators and denote them by subscript [1] and [2] respectively

$$\begin{aligned} \rho(\boldsymbol{q}) &= \rho_{[1]}(\boldsymbol{q}, \boldsymbol{r}_i) + \rho_{[1]}(\boldsymbol{q}, \boldsymbol{r}_j) + \rho_{[2]}(\boldsymbol{q}, \boldsymbol{r}_i, \boldsymbol{r}_j), \\ \boldsymbol{J}(\boldsymbol{q}) &= \boldsymbol{J}_{[1]}(\boldsymbol{q}, \boldsymbol{r}_i) + \boldsymbol{J}_{[1]}(\boldsymbol{q}, \boldsymbol{r}_j) + \boldsymbol{J}_{[2]}(\boldsymbol{q}, \boldsymbol{r}_i, \boldsymbol{r}_j), \\ H &= T_{[1]}(\boldsymbol{p}_i) + T_{[1]}(\boldsymbol{p}_j) + V_{[2]}(\boldsymbol{r}_i, \boldsymbol{r}_j, \boldsymbol{p}_i, \boldsymbol{p}_j). \end{aligned} \tag{4.15}$$

Proper symmetrization of the two-body operators is understood. In principle, this decomposition could be extended to three- and four-body operators. Furthermore, we perform a nonrelativistic reduction of each diagram in Fig. 4.1 and Fig. 4.2 and group terms of the same order $\mathcal{O}(m_q^{-n})$ with $n = 0, 1, 2, ..$ denoted by the superscripts in parentheses (n)

$$\begin{aligned}
\rho_{[1]}(\boldsymbol{q}, \boldsymbol{r}_i) &= \rho_{[1]}^{(0)}(\boldsymbol{q}, \boldsymbol{r}_i) + \rho_{[1]}^{(2)}(\boldsymbol{q}, \boldsymbol{r}_i), \\
\rho_{[2]}(\boldsymbol{q}, \boldsymbol{r}_i, \boldsymbol{r}_j) &= \rho_{[2]}^{(2)}(\boldsymbol{q}, \boldsymbol{r}_i, \boldsymbol{r}_j) + \rho_{[2]}^{(4)}(\boldsymbol{q}, \boldsymbol{r}_i, \boldsymbol{r}_j), \\
\boldsymbol{J}_{[1]}(\boldsymbol{q}, \boldsymbol{r}_i) &= \boldsymbol{J}_{[1]}^{(1)}(\boldsymbol{q}, \boldsymbol{r}_i) + \boldsymbol{J}_{[1]}^{(3)}(\boldsymbol{q}, \boldsymbol{r}_i), \\
\boldsymbol{J}_{[2]}(\boldsymbol{q}, \boldsymbol{r}_i, \boldsymbol{r}_j) &= \boldsymbol{J}_{[2]}^{(1)}(\boldsymbol{q}, \boldsymbol{r}_i, \boldsymbol{r}_j) + \boldsymbol{J}_{[2]}^{(3)}(\boldsymbol{q}, \boldsymbol{r}_i, \boldsymbol{r}_j).
\end{aligned} \tag{4.16}$$

In leading nonrelativistic order $\mathcal{O}(m_q^0)$, the charge density is not modified by exchange current effects, i. e. one has $\rho \approx \rho_{[1]}^{(0)}$. This can be seen from the explicit expressions for the two-body charge densities in Section 4.2. On the other hand, the spatial current density is already affected by exchange currents in leading nonrelativistic order $\mathcal{O}(m_q^{-1})$. Thus, one has in lowest nonrelativistic order $(n = 1)$

$$\begin{aligned}
&\boldsymbol{q} \cdot \left(\boldsymbol{J}_{[1]}(\boldsymbol{q}, \boldsymbol{r}_i) + \boldsymbol{J}_{[1]}(\boldsymbol{q}, \boldsymbol{r}_j) + \boldsymbol{J}_{[2]}(\boldsymbol{q}, \boldsymbol{r}_i, \boldsymbol{r}_j)\right) \\
&\quad = \left[H, \rho_{[1]}^{(0)}(\boldsymbol{q}, \boldsymbol{r}_i) + \rho_{[1]}^{(0)}(\boldsymbol{q}, \boldsymbol{r}_j)\right].
\end{aligned} \tag{4.17}$$

In this work, we ignore the higher relativistic orders in the kinetic energy and the one-body current density. For the two-body operators we keep in each case the lowest nonvanishing order. Equation (4.17) can be further decomposed. Let us first consider the standard nonrelativistic one-body current of the quarks (Fig. 4.1). It is a straightforward to show that the one-body current (4.4) and the kinetic energy term in (3.1) satisfy the following continuity equation

$$\boldsymbol{q} \cdot \boldsymbol{J}_{[1]}^{(1)}(\boldsymbol{q}, \boldsymbol{r}_i) = \left[\frac{\boldsymbol{p}_i^2}{2m_q}, \rho_{[1]}^{(0)}(\boldsymbol{q}, \boldsymbol{r}_i)\right], \tag{4.18}$$

where $\rho_{[1]}^{(0)}$ is the nonrelativistic one-body charge density of order $\mathcal{O}(m_q^0)$ in (4.4). Therefore, the two-body spatial current in (4.17) and the potential energy term in (3.1) satisfy the following continuity equation

$$\begin{aligned}
&\boldsymbol{q} \cdot \boldsymbol{J}_{[2]}(\boldsymbol{q}, \boldsymbol{r}_i, \boldsymbol{r}_j) \\
&\quad = \left[V_{[2]}(\boldsymbol{r}_i, \boldsymbol{r}_j, \boldsymbol{p}_i, \boldsymbol{p}_j), \rho_{[1]}^{(0)}(\boldsymbol{q}, \boldsymbol{r}_i) + \rho_{[1]}^{(0)}(\boldsymbol{q}, \boldsymbol{r}_j)\right].
\end{aligned} \tag{4.19}$$

Equation (4.19) is very important for this work. It provides a connection between the potentials used to calculate the excitation spectrum of the nucleon and the electromagnetic currents of bound quarks that are responsible for its electromagnetic properties. If the potential V is further decomposed into an isospin-independent part V^0 and an isospin-dependent part V^τ

$$V_{[2]} = V_{[2]}^0 + \boldsymbol{\tau}_i \cdot \boldsymbol{\tau}_j \, V_{[2]}^\tau \tag{4.20}$$

it becomes evident that there are two sources of contributions to the commutator on the right hand side: (i) the momentum-dependence and (ii) the isospin-dependence of the potential.

The gluon-pair current was already investigated in [28]. There it is shown that the gluon-pair current satisfies

$$\begin{aligned}
&\boldsymbol{q} \cdot \boldsymbol{J}_{\mathrm{gq\bar{q}}}(\boldsymbol{q}, \boldsymbol{r}_i, \boldsymbol{r}_j) \\
&\quad = \left[V^{\mathrm{OGEP}}(\boldsymbol{r}_i, \boldsymbol{r}_j), \rho_{[1]}(\boldsymbol{q}, \boldsymbol{r}_i) + \rho_{[1]}(\boldsymbol{q}, \boldsymbol{r}_j)\right],
\end{aligned} \tag{4.21}$$

where

$$\begin{aligned}
\rho_{[1]}(\boldsymbol{q}, \boldsymbol{r}_i) &= \rho_{[1]}^{(0)}(\boldsymbol{q}, \boldsymbol{r}_i) + \rho_{[1]}^{(2)}(\boldsymbol{q}, \boldsymbol{r}_i) \\
&= e_i e^{i\boldsymbol{q}\cdot\boldsymbol{r}_i}\left(1 - \frac{1}{4m_q^2}\left(\frac{1}{2}\boldsymbol{q}^2 - i\boldsymbol{\sigma}_i \cdot \boldsymbol{q} \times \boldsymbol{p}_i\right)\right)
\end{aligned} \tag{4.22}$$

is the one-body charge density including the relativistic Darwin-Foldy and spin-orbit corrections $\rho_{[1]}^{(2)}$ of order $\mathcal{O}(m_q^{-2})$. In other words, the spatial gluon-pair current density is consistent with the one-gluon exchange potential (3.2) provided that both spin-orbit terms in (3.2) and the relativistic corrections to the impulse charge density are taken into account. Thus, the origin of the gluon-pair current $\boldsymbol{J}_{\mathrm{gq\bar{q}}}$ can be traced back to the two spin-orbit terms and the color Coulomb term in the one-gluon exchange potential [28].

It is known [72] that the sum of the isovector pion-pair (4.8) and of the pionic currents (4.9) is connected with the one-pion exchange potential (3.3) via

$$\begin{aligned}
&\boldsymbol{q} \cdot \left(\boldsymbol{J}_{\pi \mathrm{q\bar{q}}}^{\mathrm{IV}}(\boldsymbol{q}, \boldsymbol{r}_i, \boldsymbol{r}_j) + \boldsymbol{J}_{\gamma\pi\pi}^{\mathrm{IV}}(\boldsymbol{q}, \boldsymbol{r}_i, \boldsymbol{r}_j)\right) \\
&\quad = \left[V^{\mathrm{OPEP}}(\boldsymbol{r}_i, \boldsymbol{r}_j), \rho_{[1]}^{(0)}(\boldsymbol{q}, \boldsymbol{r}_i) + \rho_{[1]}^{(0)}(\boldsymbol{q}, \boldsymbol{r}_j)\right]
\end{aligned} \tag{4.23}$$

and that these currents can be derived [22, 73, 74] by minimal substitution in (3.3).

In the following we discuss in some detail the continuity equation for the scalar exchange current. The scalar σ-exchange potential (3.6) and the confinement potential (3.8) do not require corresponding exchange currents because these leading order expressions are neither isospin nor momentum dependent. However, when these potentials are expanded to the same order $\mathcal{O}(m_q^{-3})$ as the one-gluon exchange potential, a more general momentum-dependent σ-exchange and confinement interaction emerges that will lead to an additional exchange current.

The motivation for going beyond the leading order in the scalar potential and current derives from the following considerations. Some time ago, Isgur and Karl [15] proposed that the spin-orbit term in the one-gluon exchange potential should be suppressed in order to obtain a reasonable agreement with experimental baryon spectra. They suggest that spin-dependent relativistic corrections to the scalar confinement potential, such as the Thomas term, could lead to the desired effect. It is therefore necessary to investigate the relativistic corrections to the confinement potential and the corresponding currents here in more detail.

The scalar-isoscalar potential, including relativistic corrections to order $\mathcal{O}(m_q^{-3})$ but without retardation corrections, is given by [72]

$$\begin{aligned} V^S &= V_0^S - \frac{1}{4m_q^2}\left(\frac{1}{2}\{(\boldsymbol{\sigma}_i\cdot\boldsymbol{p}_i)^2, V_0^S\} + \frac{1}{2}\{(\boldsymbol{\sigma}_j\cdot\boldsymbol{p}_j)^2, V_0^S\} + \boldsymbol{\sigma}_i\cdot\boldsymbol{p}_i V_0^S \boldsymbol{\sigma}_i\cdot\boldsymbol{p}_i + \boldsymbol{\sigma}_j\cdot\boldsymbol{p}_j V_0^S \boldsymbol{\sigma}_j\cdot\boldsymbol{p}_j\right) \\ &= V_0^S - \frac{1}{4m_q^2}\left(\{(\boldsymbol{\sigma}_i\cdot\boldsymbol{p}_i)^2, V_0^S\} + \{(\boldsymbol{\sigma}_j\cdot\boldsymbol{p}_j)^2, V_0^S\} + \frac{1}{2}(\nabla_1^2+\nabla_2^2)V_0^S\right. \\ &\qquad \left. + \frac{1}{r}\frac{\mathrm{d}V_0^S}{\mathrm{d}r}\left[\frac{1}{2}(\boldsymbol{\sigma}_1+\boldsymbol{\sigma}_2)\cdot\boldsymbol{r}\times(\boldsymbol{p}_1-\boldsymbol{p}_2) + \frac{1}{2}(\boldsymbol{\sigma}_1-\boldsymbol{\sigma}_2)\cdot\boldsymbol{r}\times(\boldsymbol{p}_1+\boldsymbol{p}_2)\right]\right). \end{aligned} \tag{4.24}$$

From V^S, after minimal substitution, we obtain,

$$\boldsymbol{J}^S_{\mathrm{min}}(\boldsymbol{r}_i,\boldsymbol{r}_j,\boldsymbol{q}) = -\frac{1}{2m_q^2}\left\{e_i e^{i\boldsymbol{q}\cdot\boldsymbol{r}_i}\left(V_0^S i\boldsymbol{\sigma}_i\times\boldsymbol{q} + \frac{1}{2}\left(\frac{1}{r}\frac{\mathrm{d}V_0^S}{\mathrm{d}r}\right)\boldsymbol{\sigma}_i\times\boldsymbol{r}\right) + (i\leftrightarrow j)\right\}, \tag{4.25}$$

where we have kept only the spin-dependent local terms. Adding the current defined by the commutator

$$\boldsymbol{q}\cdot\boldsymbol{J}^S_{\mathrm{rel}}(\boldsymbol{r}_i,\boldsymbol{r}_j,\boldsymbol{q}) = \left[V_0^S, \rho^{(2)}_{[1]}(\boldsymbol{q},\boldsymbol{r}_i) + \rho^{(2)}_{[1]}(\boldsymbol{q},\boldsymbol{r}_j)\right] \tag{4.26}$$

of the lowest order term V_0^S, and the relativistic correction ($\mathcal{O}(m_q^{-2})$) in the one-body charge density (4.22) cancels the spin-orbit type term in $\boldsymbol{J}^S_{\mathrm{min}}$ and we get

$$\boldsymbol{J}_S(\boldsymbol{r}_i,\boldsymbol{r}_j,\boldsymbol{q}) = \boldsymbol{J}^S_{\mathrm{min}} + \boldsymbol{J}^S_{\mathrm{rel}} = -\frac{1}{2m_q^2}\left\{e_i e^{i\boldsymbol{q}\cdot\boldsymbol{r}_i} i\boldsymbol{\sigma}_i\times\boldsymbol{q}V_0^S + (i\leftrightarrow j)\right\}. \tag{4.27}$$

Finally, the continuity equation for the scalar exchange current (confinement and σ-meson exchange) reads

$$\boldsymbol{q}\cdot\boldsymbol{J}_S(\boldsymbol{q},\boldsymbol{r}_i,\boldsymbol{r}_j) = \left[V^S(\boldsymbol{r}_i,\boldsymbol{r}_j),\ \rho_{[1]}(\boldsymbol{q},\boldsymbol{r}_i) + \rho_{[1]}(\boldsymbol{q},\boldsymbol{r}_j)\right], \tag{4.28}$$

where $\rho_{[1]}(\boldsymbol{q},\boldsymbol{r}_i)$ is the one-body charge density (4.22) and V^S the relativistically extended scalar exchange potential (4.24). Gauge invariance demands the use of the scalar exchange potential (4.24) that includes the relativistic corrections of order $\mathcal{O}(m_q^{-3})$ when determining the ground state parameters b and a_c. Our calculation of scalar exchange currents would be consistent only if the higher order corrections in the scalar potentials were included in the determination of these parameters. However, in this case (3.22) does not lead to an acceptable solution for b in the range $0.4-0.8$ fm. We have previously shown that, the inclusion of configuration mixed wave functions [38] leads again to a physical solution for $b = 0.606$ fm, that is very close to the value for $b = 0.596$ fm obtained from (3.22) without the relativistic corrections in V^S and without configuration mixing. We therefore continue

to use the parameters determined in Sect. 3.4, even though this is inconsistent from a formal point of view. We believe that this departure from consistency is negligible. We reiterate that we use one and the same parameter set to calculate baryon mass splittings and electromagnetic properties.

With respect to relativistic corrections, it is evident that although we formally satisfy the continuity equation for the spatial parts of the gluon, pion, and scalar exchange currents separately, complete consistency to order $\mathcal{O}(m_{\rm q}^{-3})$ for the total current is not established. In this order there are other terms in the Hamiltonian and current that need to be included, such as relativistic corrections to the kinetic energy and spatial one-body current (see Sect. 5.3.5). Furthermore, in this order there are also retardation corrections to the one-pion and one-gluon exchange potentials and corresponding exchange currents, which we have ignored. Finally, there are exchange currents corrections originating from forward propagating intermediate quark states [25, 75]. In principle, such corrections can be big as we will see in Sect. 5.3.5 for the case of relativistic corrections to the one-body current. We are also not completely consistent to order $\mathcal{O}(m_{\rm q}^{-2})$ because we do not include the relativistic corrections to the one-body charge density in the numerical calculation. Since we do not consider these terms, we violate the continuity equation formally already in this order. However, we satisfy the continuity equation (4.19) in lowest nonrelativistic order $\mathcal{O}(m_{\rm q}^{-1})$.

We do not include the relativistic corrections to the one-body currents, because (i) they are already next-to-leading order corrections, (ii) we believe that their use is somewhat against the spirit of the NRQM where the leading order one-body current already contains the bulk of relativistic corrections. An attempt to justify the second part of this statement is deferred to Section 5.3.5.

For the two-body currents, however, it turns out to be important to keep relativistic corrections; in many cases these *are* the lowest nonvanishing orders. For example, there is no modification of the charge density due to pion degrees of freedom in the extreme nonrelativistic limit; the lowest nonvanishing order is $\mathcal{O}(m_{\rm q}^{-2})$. It is important to keep these $\mathcal{O}(m_{\rm q}^{-2})$ corrections. They contribute new isospin, e. g. $\boldsymbol{\tau}_i \cdot \boldsymbol{\tau}_j$, and spin structures, $[\boldsymbol{\sigma}_i \times \boldsymbol{\sigma}_j]^2$ not present in the lowest one-body charge density and which, as we will show, are extremely important for some observables. The use of these higher order corrections is common practice in nuclear physics [24, 76 - 78].

One should keep in mind that a systematic v/c expansion does not converge for constituent quarks since the quark momenta and masses are of the same order. It seems that a proper choice of the various quark model parameters such as $m_{\rm q}$, b, and $r_{\gamma {\rm q}}$ in the Hamiltonian, wave function, and electromagnetic one-body current operator is a better way of including relativistic corrections [38] than insisting on formal consistency in a v/c expansion. We believe that by including the lowest order pion-, gluon-, and scalar-exchange currents, we obtain further information on the role of nonvalence quark degrees of freedom and deeper insight into which dynamical processes govern the electromagnetic properties of baryons than by ignoring two-body currents altogether.

5. Electromagnetic Form Factors of the $N - \Delta$ System

A hadron with spin J has, in general, $2J+1$ elastic electromagnetic form factors. This result can be deduced by writing the most general Lorentz-invariant expression for the electromagnetic current operator of a hadron with total angular momentum J. One then demands hermiticity, and that the diagonal matrix elements be invariant under time and parity transformations and satisfy the continuity equation for the electromagnetic current. This reduces the number of allowed form factors to $2J+1$. The $N(939)$ as a spin-1/2 particle has thus two elastic electromagnetic form factors; a charge monopole form factor and a magnetic dipole form factor. Likewise the spin-3/2 Δ-isobar has four elastic form factors [79] (and references therein): a charge monopole $F_{\rm C}^{\Delta}$, the charge quadrupole $F_{\rm Q}^{\Delta}$, the magnetic dipole $F_{\rm M1}^{\Delta}$, and the magnetic octupole F_{M3}^{Δ}. It turns out that the $M3$ form factor vanishes exactly for the ground state wave functions considered in this work. In order to describe the electromagnetic $N \rightarrow \Delta$ transition [80] one needs the transverse magnetic dipole $F_{\rm M1}^{N\rightarrow\Delta}$, the transverse electric quadrupole $F_{\rm E2}^{N\rightarrow\Delta}$ and the charge quadrupole (longitudinal) $F_{\rm C2}^{N\rightarrow\Delta}$ transition form factors. Thus, altogether there are nine on-shell form factors which characterize the electromagnetic properties of the $N - \Delta$ system.

5.1. Charge Monopole Form Factors

In the nonrelativistic quark model it is straightforward to calculate the charge form factor of a baryon. Quite generally the charge monopole form factor is defined as [81]:

$$F_{\mathrm{C}}(\boldsymbol{q}^2) = \sqrt{4\pi}\langle JM_J{=}JTM_{\mathrm{T}}| \qquad (5.1)$$
$$|\frac{1}{4\pi}\int \mathrm{d}\Omega_{\mathrm{q}}\rho(\boldsymbol{q})Y_0^0(\hat{\boldsymbol{q}})\,|\,JM_J{=}JTM_{\mathrm{T}}\rangle.$$

In impulse approximation and with pure $(0s)^3$ ground state wave functions the isoscalar and isovector charge form factors of the nucleon are:

$$F^{\mathrm{IS}}_{\mathrm{imp}}(\boldsymbol{q}^2) = F^{\mathrm{IV}}_{\mathrm{imp}}(\boldsymbol{q}^2) = \exp(-\boldsymbol{q}^2b^2/6). \qquad (5.2)$$

The two-body currents of Fig. 4.2 contribute as follows to the charge form factors

$$\begin{aligned}
F^{\mathrm{IS}}_{\mathrm{gq\bar{q}}}(\boldsymbol{q}^2) &= -\frac{\alpha_{\mathrm{s}}}{9m_{\mathrm{q}}^3}\,|\boldsymbol{q}|\,e^{-\boldsymbol{q}^2b^2/24}I_{\mathrm{gq\bar{q}}}(|\boldsymbol{q}|),\\
F^{\mathrm{IV}}_{\mathrm{gq\bar{q}}}(\boldsymbol{q}^2) &= 5F^{\mathrm{IS}}_{\mathrm{gq\bar{q}}}(\boldsymbol{q}^2),\\
F^{\mathrm{IS}}_{\pi\mathrm{q\bar{q}}}(\boldsymbol{q}^2) &= \frac{f^2_{\pi N}}{4\pi\mu^2}\frac{6}{5}\frac{1}{m_{\mathrm{q}}}\,|\boldsymbol{q}|\,e^{-\boldsymbol{q}^2b^2/24}I^{(11)}_{\pi q\bar{q}}(|\boldsymbol{q}|),\\
F^{\mathrm{IV}}_{\pi\mathrm{q\bar{q}}}(\boldsymbol{q}^2) &= \frac{1}{5}F^{\mathrm{IS}}_{\pi\mathrm{q\bar{q}}}(\boldsymbol{q}^2),\\
F^{\mathrm{IS}}_{\mathrm{S}}(\boldsymbol{q}^2) &= \frac{1}{3m_{\mathrm{q}}^2}e^{-\boldsymbol{q}^2b^2/24}I^{\mathrm{C}}_{\mathrm{S}}(|\boldsymbol{q}|),\\
F^{\mathrm{IV}}_{\mathrm{S}}(\boldsymbol{q}^2) &= F^{\mathrm{IS}}_{\mathrm{S}}(\boldsymbol{q}^2).
\end{aligned} \qquad (5.3)$$

Here, we have used the relation between the pion-quark and pion-nucleon coupling constants, namely $f^2_{\pi N}/(4\pi) = (5/3)^2 f^2_{\pi q}/(4\pi)$. The integrals $I_{\mathrm{gq\bar{q}}}(|\boldsymbol{q}|)$, $I^{(jj)}_{\pi\mathrm{q\bar{q}}}(|\boldsymbol{q}|)$, and $I^{\mathrm{C}}_{\mathrm{S}}(|\boldsymbol{q}|)$ in (5.3) are defined in the appendix. The total isoscalar/isovector charge form factor is given by the sum of all isoscalar/isovector contributions

$$F^{\mathrm{IS/IV}} = F^{\mathrm{IS/IV}}_{\mathrm{imp}} + F^{\mathrm{IS/IV}}_{\mathrm{gq\bar{q}}} + F^{\mathrm{IS/IV}}_{\pi\mathrm{q\bar{q}}} + F^{\mathrm{IS/IV}}_{\sigma\mathrm{q\bar{q}}} + F^{\mathrm{IS/IV}}_{\mathrm{conf}}. \qquad (5.4)$$

We also use the following definitions for the proton and neutron charge form factors:

$$F_{\mathrm{p}} = \frac{1}{2}(F^{\mathrm{IS}} + F^{\mathrm{IV}}),\ F_{\mathrm{n}} = \frac{1}{2}(F^{\mathrm{IS}} - F^{\mathrm{IV}}). \qquad (5.5)$$

As the difference between isoscalar and isovector charge form factors the neutron form factor receives no contribution from the one-body current in the present approximation which neglects configuration mixing.

In Fig. 5.1 we show our results for the charge form factor of the proton as a function of the four-momentum transfer q^2. Due to cancellations between various two-body terms of opposite signs the impulse approximation result is little affected by exchange currents. In order to highlight the effect of the exchange currents we also plot in Fig. 5.2 the deviation of both theory and experiment from the empirical dipole fit:

$$F_{\mathrm{dip}}(q^2) = \left(1 + q^2/18.23\mathrm{fm}^{-2}\right)^{-2}, \qquad (5.6)$$

where $q^2 = -q_\mu^2$. For momentum transfers $q^2 < 4$ fm $^{-2}$ the inclusion of the two-body charge densities slightly improves the pure gaussian behavior given by (5.2). The dashed line shows an impulse calculation using the improved proton wave functions of Giannini [65] for which an convenient parametrization in terms of the admixture coefficients exists. We observe a similar improvement over the unmixed impulse calculation. For higher momentum transfers the gaussian wave function inherent in all three curves decays too rapidly to describe the data. Note that $q = 2$ fm^{-1} is already beyond the limit of validity ($q \approx m_{\mathrm{q}}$) of the nonrelativistic approach.

The effect of the exchange currents is more pronounced in the neutron charge form factor of Figure 5.3. For the neutron charge form factor we obtain a very good agreement with the data at low momentum transfers only if exchange currents are included. Evidently, the neutron charge form factor is already at low energies almost completely dominated by the quark-antiquark pair currents. This conclusion also holds in a more complete calculation using improved wave functions in the evaluation of exchange currents [37]. For comparison we show the impulse calculation of [65] which badly fails to describe the data in this case. In the past, this problem of the impulse approximation has been repaired by increasing the harmonic oscillator constant b to about 1 fm. However, such a large value for b contradicts information from several other sources, which require values of $b \approx m_{\mathrm{q}}^{-1}$ or smaller. We will elaborate on this point in the next Section. A physically more consistent

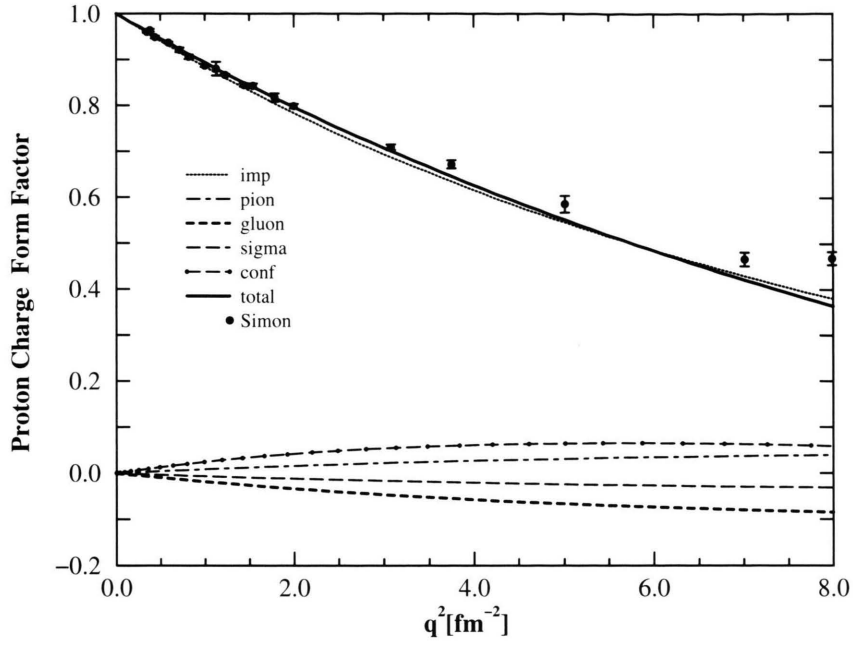

Fig. 5.1. Proton charge form factor as a function of the four momentum transfer $q^2 = -q_\mu^2$ [fm^{-2}]. The short dashed line shows the Gaussian form factor (5.2) for $b = 0.613$ fm. The full line shows the total form factor including exchange currents. The data are from [82].

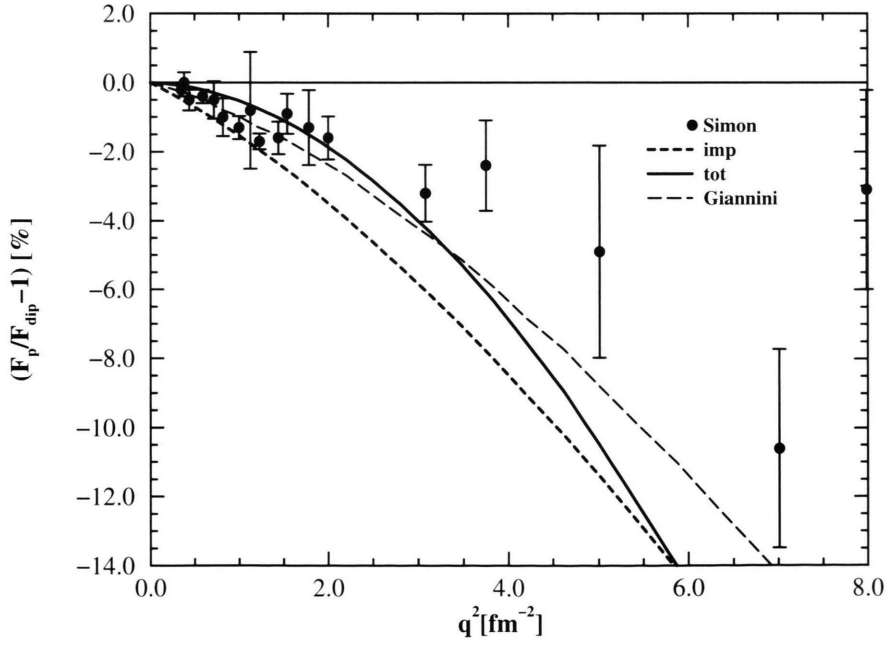

Fig. 5.2. Deviation of the proton charge form factor from the empirical dipole fit. The dashed line shows the impulse calculation of [65] for $b = 0.613$ fm multiplied by the quark form factor (4.13). The data are from [82].

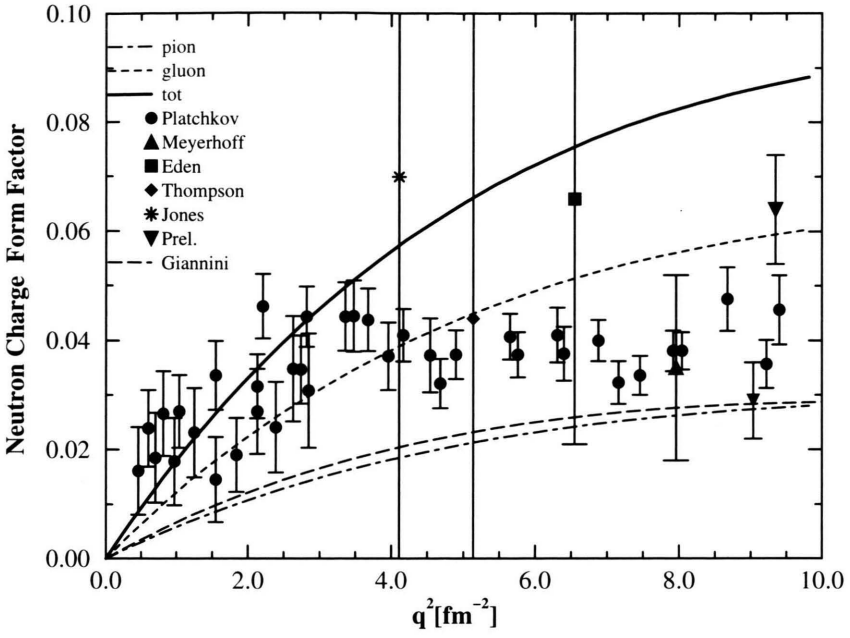

Fig. 5.3. Neutron charge form factor as a function of the four momentum transfer q^2 [fm^{-2}]. The dashed line shows the impulse calculation of [65] for $b = 0.613$ fm multiplied by the quark form factor (4.13). Data: The shaded circles [83] are based on elastic electron-deuteron data and the Paris potential. The shaded triangles are data from Mainz [84, 85]; the two inverted triangles are preliminary results [84]. The remaining data points have been taken at MIT-Bates [86 - 88].

picture is obtained if the exchange charge densities are included.

The nucleonic counterpart of the pion-pair charge operators (4.7) has first been used by Jackson et al. [76] in the deuteron and has become a standard correction for the charge properties of light nuclei [24, 78]; the application of (4.7) to the nucleon charge form factors appears to have been first done in [37].

5.1.1. Charge Radii of the Nucleon

The charge radii of baryons are important low-energy parameters. They measure the spatial extension of the charge distribution inside the baryon. They contain information about non-valence quark degrees of freedom and about the finite electromagnetic size of the valence quarks. In this section we concentrate on electromagnetic radii where the nonrelativistic quark model is expected to work best. Unlike the full form factors, the results for these static properties can be obtained in terms of analytic expressions, which makes the relation between the electromagnetic properties of the nucleon and Δ more transparent. In particular, the important role of non-valence quark degrees of freedom in various electromagnetic properties will become evident.

At low momentum transfers the form factor can be approximated as

$$F_{\mathrm{C}}(\boldsymbol{q}^2) = Z\left(1 - \frac{1}{6}\boldsymbol{q}^2 r_{\mathrm{C}}^2 + \cdots\right), \tag{5.7}$$

where the charge radius r_{C} is defined as the slope of the charge form factor at zero-momentum transfer

$$r_{\mathrm{C}}^2 = -\frac{6}{F_{\mathrm{C}}(0)}\frac{\mathrm{d}}{\mathrm{d}\boldsymbol{q}^2}F_{\mathrm{C}}(\boldsymbol{q}^2)|_{\boldsymbol{q}^2=0}. \tag{5.8}$$

In impulse approximation the proton and neutron mean square charge radii are according to (5.8,5.2)) given by

$$r_{\mathrm{p}}^{2\,\mathrm{imp}} = b^2,\ r_{\mathrm{n}}^{2\,\mathrm{imp}} = 0. \tag{5.9}$$

It is evident from (5.2) that with a quark core radius of $b \approx 0.5$ fm we would grossly underestimate the empirical charge radius of the proton. Using improved wave nucleon functions which contain admixtures of $2\hbar\omega$ excited states into the nucleon ground

state (configuration mixing) one obtains in impulse approximation the following expressions [65]:

$$r_{\rm p}^{2\,\rm imp} = b^2\left\{1+\frac{2}{3}\left[1-a_{\rm S}\left(a_{\rm S}-\sqrt{3}a_{\rm S_S}\right)\right.\right.$$
$$\left.\left.-a_{\rm S_M}\left(\sqrt{\frac{3}{2}}a_{\rm S}+\sqrt{2}a_{\rm S_S}\right)\right]\right\}, \quad (5.10)$$
$$r_{\rm n}^{2\,\rm imp} = b^2\left\{0+\frac{2}{3}a_{\rm S_M}\left(\sqrt{\frac{3}{2}}a_{\rm S}+\sqrt{2}a_{\rm S_S}\right)\right\}.$$

With standard admixture coefficients $a_{\rm S} = 0.90$, $a_{\rm S_S} = -0.34$ and $a_{\rm S_M} = -0.27$ [15] one obtains $r_{\rm p}^2 = 0.662\,b^2$ and $r_{\rm n}^2 = -0.112\,b^2$. Inserting the experimental charge radii we obtain in the case of the proton $b = 1.12$ fm and $b = 1.03$ fm in the case of the neutron. Similarly large radii are obtained with the admixture coefficients of other authors. Therefore, even with improved nucleon wave functions, which contain the effect of the residual interactions, one still needs a large quark core radius of $b \approx 1$ fm [15] to describe the experimental charge radii if only point-like single-quark electromagnetic currents are employed. However, such a large value for b is inconsistent with the value needed to describe the excitation spectrum of the nucleon [15]. Second, a quark core radius of $b \approx 1$ fm would contradict the traditional picture of the nucleus as a bound state of nucleons because the quark-exchange effects between individual nucleons would be intolerably large already in the deuteron [28] and would completely spoil the successful independent particle picture of the nuclear shell model [89]. Third, the use of pointlike constituent quarks quarks contradicts the results of the NJL-model where the mass and finite size of the constituent quarks appear as direct consequences of the spontaneous breaking of chiral symmetry.

These discrepancies can be resolved in the framework of the NRQM, by using a first finite electromagnetic radius $r_{\gamma \rm q}$ for the constituent quarks [3, 70], and by including two-body exchange currents. The finite electromagnetic size of constituent quarks finds a simple explanation in the fact that constituent quarks are dressed particles, i. e. current quarks surrounded by a cloud of sea-quarks. In addition, the two-body exchange currents describe degrees of freedom in the electromagnetic interaction not yet incorporated in the constituent quark mass and its finite electromagnetic size. We then get for the charge radii of proton and neutron [37, 38]

Table 5.1. Nucleon and $\Delta(1232)$ charge radii including two-body exchange currents with chiral interactions using $\Lambda = 4.2$ fm^{-1}. i: impulse; g: gluon; π: pion; σ: σ-meson; c: confinement; t: total; t = i + g + π + σ + c. A finite electromagnetic quark size $r_{\gamma \rm q}^2 = 0.36$ fm^2 is used. The experimental proton and neutron charge radii are $r_{\rm p} = 0.862 \pm 0.012$ fm and $\sqrt{|r_{\rm n}^2|} = 0.345 \pm 0.003$ fm, respectively [82]. The charge radius of the Δ^0 is zero in the present model. All entries are in [fm^2] except for the total result which is in [fm].

	$r_{\rm i}^2$	$r_{\rm g}^2$	r_π^2	r_σ^2	$r_{\rm c}^2$	$\sqrt{\lvert r_{\rm t}^2\rvert}$
p	0.736	0.119	−0.057	0.041	−0.174	0.815
n	0.000	−0.079	−0.038	0.000	0.000	0.342
Δ	0.736	0.198	−0.019	0.041	−0.174	0.884

$$r_{\rm p}^2 = b^2 + r_{\gamma \rm q}^2 + \frac{b^2}{2m_{\rm q}}\left(\delta_{\rm g}-\delta_\pi\right) + r_\sigma^2 + r_{\rm conf}^2, \quad (5.11)$$

$$r_{\rm n}^2 = -\frac{b^2}{3m_{\rm q}}\left(\delta_{\rm g}+\delta_\pi\right) = -b^2\frac{M_\Delta - M_N}{M_N}, \quad (5.12)$$

and the numerical results shown in Table 5.1. Explicit expression for $r_{\rm conf}^2$ and r_σ^2 can be obtained from (4.11) in [38].

Our result for the neutron is particularly simple. Because the neutron charge radius is given by the difference of isoscalar and isovector radii, the contributions of the one-body charge density, the finite size of the quarks, and the spin-independent scalar (confinement and sigma) exchange currents all cancel in $r_{\rm n}^2$. Only the spin-dependent pion and gluon exchange currents contribute to $r_{\rm n}^2$. The gluon and pion exchange currents can be expressed in terms of δ_π and $\delta_{\rm g}$, i. e. the pion and gluon contribution to the $N - \Delta$ mass splitting, because the exchange current operators have a structure similar to the corresponding two-body potentials. The particular combination of δ_π and $\delta_{\rm g}$ appearing in (5.12) makes it possible to express $r_{\rm n}^2$ via the experimental $\Delta - N$ mass splitting of (3.18). Equation (5.12) clearly shows that there is an intimate relation between: (i) the neutron charge radius, (ii) the spatial extension of the quark distribution inside the nucleon (the quark core radius b), and (iii) the excitation energy to the first excited state of the nucleon. From (5.12) we determine the quark core size as $b = 0.612$ fm, if the experimental numbers

for M_N, M_Δ, and r_n^2 are substituted. This independent determination of the quark core radius b is in agreement with the one obtained from the variational principle (3.22).

Exchange currents vs. configuration mixing

Let us try to give a physical interpretation of the result (5.12). In previous works, the nonvanishing charge radius of the neutron was attributed to the perturbing effect of the color-magnetic interaction on the ground state wave function [15, 90]. The color-magnetic interaction provides a repulsive force between any two quarks which are in a symmetric spin state ($S = 1$). This makes the Δ-isobar heavier than the nucleon, since the former contains more spin symmetric quark pairs. Similarly, the color-magnetic force repels the two down quarks in the neutron which are necessarily in an $S = 1$ state (Pauli principle). This leads to a negative tail in the neutron charge distribution and to a negative neutron charge radius.

We point out that this effect, which is usually described by a small admixture of the excited Φ_{S_M} state (3.23) into the nucleon ground state wave function, *is much too small*. It is around $r_n^2(\text{imp}) = -0.03$ fm^2 if a realistic quark core radius ($b \approx 0.6$ fm) is used (see the discussion below Fig.2 in [37]). The success of previous impulse calculations for the neutron charge is bought by tolerating a severe inconsistency: a value of $b \approx 0.5$ fm is typically used in the calculation of the excitation spectrum while a value $b \approx 1$ fm [65] is employed in the neutron charge radius calculation. This is inconsistent. In addition, a value for the quark core radius $b \approx 1$ fm is clearly unphysical.

The present explanation of the negative neutron charge radius is based on the spin-dependent two-body gluon- and pion *exchange charge operators*. This allows to get the correct size of the neutron charge radius for a reasonably small quark core radius $b \approx 0.6$ fm. The exchange currents discussed here are closely related to the spin-dependent terms in the potential that give rise to the Φ_{S_M} state. Yet, there is an important difference between these two mechanisms. We will explain this in more detail in Section 5.2.

Of course, in a fully consistent calculation both configuration mixing and exchange currents must be included and the question concerning their relative importance arises. In addition, the simple relation between the neutron charge radius and the $N - \Delta$ mass splitting will be modified in a more consistent calculation: b becomes slightly smaller to allow for the contribution of the impulse current. However, according to [37], (5.12) is satisfied to within 23% in a model with gluons only; in the model with gluons and pions it holds to within 12% even if configuration mixing is included. This indicates that the contribution of the one-body charge density is small. Therefore, we believe that (5.12) correctly describes the physics underlying the nonvanishing neutron charge radius and certain other observables, that are very sensitive to nonvalence quark degrees of freedom (gluons, pions, and sea-quarks).

In our previous calculation of the neutron charge form factor [37] including both configuration mixing and exchange currents we have seen that the neutron charge radius is clearly dominated by the gluon and pion quark-pair currents (see Fig. 4.2b - c) if a reasonably small quark core radius ($b = 0.5-0.6$ fm) is used. This finding gets support from other sources. For example, Christov et al. [91] find in their Nambu-Jona-Lasinio type quark model that the neutron charge radius is to a large extent determined by sea-quark and *not* by valence quark degrees of freedom. In the language of quark potential models, it is most natural to include these nonvalence quark degrees of freedom in electromagnetic observables in the form of *exchange currents*.

5.1.2. Charge Radii of the Δ

Similarly, we get for the charge radii of the charged Δ states [41]

$$r_\Delta^2 = b^2 + r_{\gamma q}^2 + \frac{b^2}{6m_q}\left(5\delta_g - \delta_\pi\right) + r_\sigma^2 + r_{\text{conf}}^2 \quad (5.13)$$

while we obtain

$$r_{\Delta^0}^2 = 0 \quad (5.14)$$

in the present model. From (5.11,5.13) we find for the charge radius of the charged Δ states the parameter-independent result

$$r_\Delta^2 = r_p^2 - r_n^2, \quad (5.15)$$

in which no quantity refers to the particular model used. Hence, the electromagnetic size of the Δ is somewhat larger than the size of the proton and the

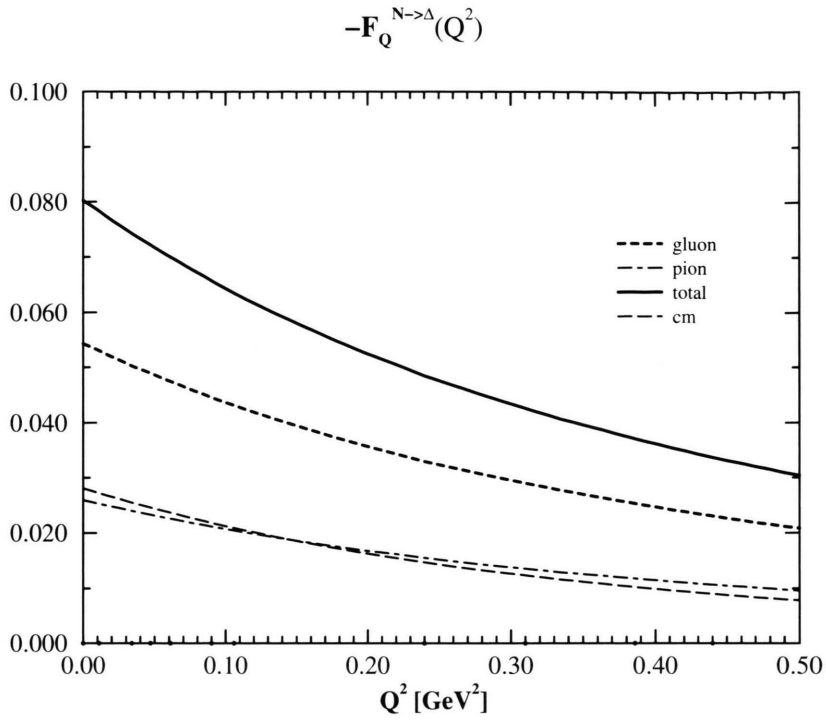

Fig. 5.4. The $N \rightarrow \Delta$ transition quadrupole form factor as a function of the four momentum transfer Q^2 [GeV^2]. The impulse calculation of [65] for b = 0.613 fm multiplied by the quark form factor (4.13) is shown for comparison (long-dashed line (cm)).

difference is given by the neutron charge radius. This is in agreement with other models of nucleon structure [92]. We point out that the charge radius of the Δ^0 is exactly zero in the present model, because all terms in (4.11) yield contributions to the Δ charge form factor that are proportional to the Δ charge

$$e_\Delta = \frac{1}{2}(1 + 2M_T), \tag{5.16}$$

where M_T is the third component of the isospin of the Δ. Therefore, the form factor (5.1) vanishes identically and the corresponding charge radius is zero. This can be understood because the Δ^0 wave function is symmetric in spin space and the spin-dependent forces do not introduce any asymmetry between ud and dd quark pairs.

5.2. *Charge Quadrupole Form Factors*

As a spin 3/2 particle the Δ has a quadrupole form factor that is usually defined as [81]

$$F_Q(\boldsymbol{q}^2) = -\frac{12\sqrt{5\pi}}{q^2}\langle J'M'_J{=}J'T'M'_T| \tag{5.17}$$
$$|\frac{1}{4\pi}\int d\Omega_q \rho(\boldsymbol{q}) Y_0^2(\hat{\boldsymbol{q}})\,|\,JM_J{=}JTM_T\rangle,$$

where $J' = J = 3/2$ and $T = T' = 3/2$ for the elastic quadrupole form factor and $J' = T' = 3/2$ and $J = T = 1/2$ for the $N \rightarrow \Delta$ transition form factor.

The electric quadrupole form factor of a composite system (nucleus, baryon, vector meson) is a measure for the deviation from spherical symmetry of the internal charge distribution. The low momentum transfer behavior of the quadrupole form factor is determined by the quadrupole moment Q and the quadrupole radius r_Q^2. The quadrupole moment is as usual defined by the $q \rightarrow 0$ limit of the quadrupole form factor (5.17). Our normalization for $F_Q(0)$ in (5.17) is in accord with the standard definition of the quadrupole moment:

$$F_Q(0) = Q = \int d^3\boldsymbol{x}\rho(\boldsymbol{x})(3z^2 - \boldsymbol{x}^2). \tag{5.18}$$

The quadrupole radius is the slope of the quadrupole form factor at $|\boldsymbol{q}| = 0$ divided by the quadrupole moment, i. e.

$$r_{\mathrm{Q}}^2 = \frac{-6}{Q} \frac{dF_{\mathrm{Q}}(\boldsymbol{q}^2)}{d\boldsymbol{q}^2}|_{\boldsymbol{q}=0}. \tag{5.19}$$

In Fig. 5.4 we show the $N \rightarrow \Delta$ quadrupole transition form factor, for which it is more likely that it can be extracted from the electro-pionproduction data.

5.2.1. Quadrupole Moment of the Δ

QCD predicts effective tensor forces between quarks. Consequently, baryons should be deformed. Experiments at all major electron laboratories are being devoted to measuring this deformation by photo/electro-excitation of the Δ-resonance [18]. From these measurements one hopes to extract the D-state probabilities a_{D}^2 and b_{D}^2 in (3.23) and from these further information about the tensor forces between quarks. However, even without an explicit D-state admixture in the wave function one can obtain a nonvanishing quadrupole moment coming from two-body exchange currents. This result, which seems at first surprising is actually to be expected.

We illustrate this first for the deuteron which is a more familiar example. The quadrupole moment of the deuteron is mainly due to the D-state admixture $u_2(r)$ in the relative wave function of the bound proton neutron system. The D-state admixture in the deuteron wave function is a consequence of the tensor forces between the nucleons. The quadrupole moment of the deuteron including the pion-pair current correction is given as

$$\begin{aligned} Q_{\mathrm{d}} = & \frac{1}{\sqrt{50}} \int_0^\infty \mathrm{d}r r^2 \, u_2(r) \left(u_0(r) - \frac{1}{\sqrt{8}} u_2(r) \right) \\ & + \frac{f_{\pi NN}^2}{4\pi} \frac{1}{M_N} \int_0^\infty \mathrm{d}r \, r \, Y_1(\mu r) \\ & \cdot \left(2u_0^2(r) - \sqrt{2} u_0(r) u_2(r) - \frac{1}{5} u_2^2(r) \right). \end{aligned} \tag{5.20}$$

The first term in (5.20) is due to the nonrelativistic one-body charge density $\rho_{[1]}^{(0)}$, while the second term is due to the isoscalar two-body pion pair charge density (4.7). The function $Y_1(x)$ is defined in the appendix. Evidently, the one-body contribution is only nonzero if there is a nonzero D-state wave function $u_2(r)$. On the other hand, even for a pure S-wave deuteron [7] one obtains a nonvanishing quadrupole moment due to the pion-pair exchange current term (the term u_0^2 in the integrand). This S-wave contribution provides actually the major part of the exchange current contribution to the quadrupole moment of the deuteron. Numerically, the exchange current contribution to the deuteron quadrupole moment is with 0.01 fm^2 rather small [28], compared to the contribution of the one-body charge density and the D-state in the deuteron, which is about 0.28 fm^2. We will see that this situtation is reversed in the case of the spin-3/2 Δ-isobar.

Table 5.2. $\Delta(1232)$ quadrupole moments including two-body exchange currents; i: impulse; g: gluon; π: pion; σ: σ-meson; c: confinement; t: total; t = i + g + π + σ + c. As in the neutron charge radius, spin-independent scalar exchange currents do not contribute to the Δ quadrupole moments. The quadrupole moment of the Δ^0 is zero in the present model. All entries are in [fm^2].

	Q_{i}	Q_{g}	Q_π	Q_σ	Q_{c}	Q_{t}
Δ^{++}	0.000	−0.158	−0.0761	0.000	0.000	−0.234
Δ^{+}	0.000	−0.079	−0.038	0.000	0.000	−0.117
Δ^{0}	0.000	0.000	0.000	0.000	0.000	0.000
Δ^{-}	0.000	0.079	0.038	0.000	0.000	0.117

With the two-body charge densities employed in this work we derive a parameter-independent relation between the neutron charge radius and the quadrupole moment of the Δ

$$\begin{aligned} Q_\Delta &= -b^2 \frac{(\delta_{\mathrm{g}} + \delta_\pi)}{3m_{\mathrm{q}}} e_\Delta \\ &= -b^2 \left(\frac{M_\Delta - M_N}{M_N} \right) e_\Delta = r_{\mathrm{n}}^2 e_\Delta, \end{aligned} \tag{5.21}$$

where $e_\Delta = (1 + 2M_{\mathrm{T}})/2$ is the charge of the Δ. Hence, for the Δ^{++} we predict a quadrupole moment of $Q_{\Delta^{++}} = -0.234$ fm^2. Numerical values for the other quadrupole moments are listed in Table 5.2. A similar relation between the neutron charge radius and the Δ quadrupole moment has been obtained on the basis of configuration mixing: $Q_\Delta = \frac{2}{5} r_{\mathrm{n}}^2 e_\Delta$, which gives e. g. for $Q_{\Delta^{++}} = -0.093$ fm^2 [94]. We will discuss the relation between exchange current and configuration mixing (tensor force) contributions to Q_Δ in more detail below. In contrast to our result (5.21),

[7] Also in a light-cone analysis one gets for an S-wave deuteron a nonvanishing quadrupole moment [93].

the derivation in [94] is based on the tensor force of the one-gluon exchange potential alone and does not contain the effect of two-body exchange currents.

We emphasize that even without an explicit D-state admixture in the Δ wave function, we have obtained a nonvanishing quadrupole moment. In the following, we give an explanation for this result. According to the definition of the quadrupole form factor (5.17), the charge density operator must contain a term $Y^{[2]}(\hat{\boldsymbol{q}})$, otherwise the quadrupole form factor vanishes, due to the orthogonality of the spherical harmonics. For example, after expanding the plane wave in (4.4), the one-body charge operator is proportional to

$$\rho_{[1]} \propto \left[Y^{[l]}(\hat{\boldsymbol{\rho}}) \times Y^{[l]}(\hat{\boldsymbol{q}})\right]^{[0]} . \tag{5.22}$$

For a pure S-state Δ wave function only the term $l = 0$ can contribute and consequently a $Y^{[2]}(\hat{\boldsymbol{q}})$ term is not allowed. On the other hand, the two-body gluon and pion charge densities contain a rank 2 tensor in spin space

$$\rho_{[2]} \propto \left[[\boldsymbol{\sigma}_i^{[1]} \times \boldsymbol{\sigma}_j^{[1]}]^{[2]} \times [Y^{[l]}(\hat{\boldsymbol{\rho}}) \times Y^{[2]}(\hat{\boldsymbol{q}})]^{[2]}\right]^{[0]} . \tag{5.23}$$

Therefore, it is possible to have a $Y^{[2]}(\hat{\boldsymbol{q}})$ part even if $l = 0$ and the quarks are all in S-states. That is why the two-body charge densities derived from Fig. 4.2b and Fig. 4.2d lead to a nonvanishing quadrupole moment. To state this in more physical terms we can say that due to the spin-dependent interaction currents between the quarks, the system can absorb a C2 or E2 photon.

As is evident from (5.21) these two-body charge densities describe the same gluon and pion degrees of freedom which are responsible for the tensor forces between quarks. The physical interpretation of both types of contributions (tensor force vs. two-body current) to the quadrupole moment is, however, quite different. This is illustrated in Figure 5.5a, b. The *two-body* pair-charge densities of Fig. 5.5b describe, as their name implies, the excitation of quark-antiquark pairs by the photon, or, stated differently, the absorption of a C2 photon on *two quarks*. On the other hand, in Fig. 5.5a the photon is absorbed by a *single quark*, which remains in a positive energy state between the absorption of the photon and the emission of the gluon or pion. There is no electromagnetic coupling of the photon to the quark-antiquark pairs inside the Δ in this case. In Fig. 5.5a, gluon and pion degrees of freedom show up as tensor force induced D-state admixtures to ground state wave functions (see (3.23)). In most applications of the CQM, the single-quark current of Fig. 5.5a has been used to estimate the effect of the one-gluon exchange potential on electromagnetic properties. Our results show that this is not a good approximation for the charge properties of the Δ which are appreciably affected by exchange currents. This is opposite to what one finds in light nuclei. For example, the deuteron quadrupole moment is mainly caused by the D-wave in the deuteron and exchange currents provide only a correction of a few percent [28] as we have already mentioned.

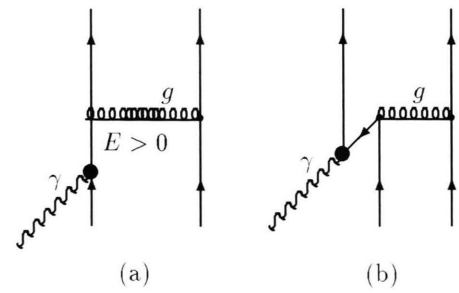

Fig. 5.5. One-body (a) and two-body (b) contributions to the quadrupole moment of the Δ and to the $N \rightarrow \Delta$ transition quadrupole moment. (a) *Single-quark* transition: The photon is absorbed on a single quark that propagates in a positive energy state. The diagram can be separated into a wave function part and a single-quark photon absorption amplitude. The dominant contribution of this reducible diagram is obtained by sandwiching the standard *one-body* current between wave functions containing D-state admixtures. (b) *Two-quark* transition: the photon couples to a quark-antiquark pair in the baryon. In the nonrelativistic limit the diagram reduces to a contact graph that *cannot* be separated into a wave function and a photon absorption amplitude. The system absorbs a C2 or E2 photon on *two quarks*, even if all quarks are in S-states. This contribution is effectively described by the *two-body* exchange charge operators. For some observables, it is numerically more important than diagram (a). Similar diagrams can be drawn for pion-exchange between quarks.

Obviously, a complete calculation comprises both D-waves in the nucleon and the exchange currents discussed in this work. Corrections due to D-waves will modify the simple result (5.21). However, according to our previous experience with the neutron charge radius we expect it to remain largely valid. Let us discuss this more quantitatively. Including configuration mixing but no exchange currents one obtains

neglecting the small b_D^2 contributions and with typical values for the admixture coefficients [65, 95]

$$Q_\Delta^{\text{imp}} = -b^2 \frac{4}{\sqrt{30}} \left(b_{S_S} b_{D_S} + \frac{2}{\sqrt{3}} b_{S'_S} b_{D_S} \right) e_\Delta = -0.087\, b^2 e_\Delta. \tag{5.24}$$

For $b = 0.61$ fm one obtains then $Q_\Delta^{\text{imp}} = -0.032$ fm^2 e_Δ. This has to be compared to our result $Q_\Delta^{\text{exc}} = -0.119$ fm^2 e_Δ. Thus in a complete calculation we expect the corrections to (5.21) coming from configuration mixing to be below some 30 %.

It is interesting that the ratio of the two single-quark current results for the quadrupole moment (5.24) and the neutron charge radius (5.12) takes the numerical value

$$\frac{Q_\Delta^{\text{imp}}}{r_n^{2\,\text{imp}}} = 0.734\, e_\Delta. \tag{5.25}$$

This ratio, which does not explicitly depend on b^2 differs from our prediction (5.21)

$$\frac{Q_\Delta}{r_n^2} = e_\Delta. \tag{5.26}$$

by some 30% which is the estimated accuracy of (5.21). Although the individual impulse results for the neutron charge radius and the Δ quadrupole moment amount to only 30% of the corresponding exchange current results, their ratio is again comparable to our parameter-independent result (5.21). Thus the ratio of the two observables, which is free of the not directly observable quark core radius b, is approximately given by (5.21). We consider this as another indication that (5.21) might have a more general validity.

Let us summarize this section. We have seen that it would be inappropriate to compare an eventual experimental number for Q_Δ with (5.24) or with a similar result in [96] and to infer from this a definite D-state admixture in the Δ wave function, or the strength of the tensor force as has been suggested [96]. Both effects, exchange currents and configuration mixing must be considered together before we can draw any conclusions about the details of the quark-quark forces from electromagnetic observables. In view of (5.21) it is likely that exchange currents are more important than mixed wave functions for this observable.

5.2.2. $N \to \Delta$ Transition Quadrupole Moment

We now turn to the $N \to \Delta$ quadrupole transition moment. This observable and the related E2/M1 ratio are exactly zero in the symmetric additive quark model. This is the content of the Becchi-Morpurgo selection rule, which is based on the single-quark transition model [97]. The inclusion of tensor forces due to one-gluon exchange between quarks leads to small D-state admixtures a_{D_M} (b_{D_S}, b_{D_M}) in the nucleon (Δ) ground states wave functions (3.23) and to non-zero C2 and E2 transition amplitudes as calculated from the one-body charge density operator [65]:

$$Q_{N\to\Delta}^{\text{imp}} = -b^2 \frac{M_N \omega}{\sqrt{45}} \frac{12}{\omega M_N \sqrt{6}} \Big(a_{S_S} b_{D_M} - a_{D_M} b_{S_S} + \frac{2}{\sqrt{3}} \left(a_{S'_S} b_{D_M} - a_{D_M} b_{S'_S} \right) + \frac{4}{\sqrt{6}} a_{S'_M} b_{D_M} + \frac{7}{\sqrt{30}} a_{D_M} b_{D_S} \Big). \tag{5.27}$$

Inserting standard mixing coefficients [65] one obtains

$$Q_{N\to\Delta}^{\text{imp}} = -0.079\, b^2. \tag{5.28}$$

The magnitude of this configuration mixing effect is, however, again too small, to explain the experimental result if a realistic quark core radius $b \approx 0.6$ fm is used. Using a realistic quark core radius $b = 0.613$ fm gives $Q_{N\to\Delta}^{\text{imp}} = -0.030$ fm^2 much smaller than the empirical $Q_{N\to\Delta}^{\text{exp}} = -0.075(13)$ fm^2 (see Sect. 6.4).

Here, we show that the major part of the small C2 transition amplitude is probably due to two-body pion and gluon exchange charge densities. This is analogous to the neutron charge radius and quadrupole moment discussed previously. Although all quarks in the N and the Δ are assumed to be in S-states the system can absorb a C2 or E2 photon by simultaneously flipping the spins of *two quarks* (see Figure 5.6). A glance at (5.23) shows that the two-body charge operators can indeed induce such a double spin-flip transition. Using the total charge density (4.11) and replacing the initial state by the nucleon wave function, we obtain from the $q \to 0$ limit of (5.17)

Table 5.3. $N \rightarrow \Delta$ transition quadrupole moments, including two-body exchange currents; i: impulse; g: gluon; π: pion; σ: σ-meson; c: confinement; t: total; t = i + g + π + σ + c. As in the neutron charge radius, spin-independent scalar exchange currents do not contribute to the Δ quadrupole moments. The experimental values for the transition quadrupole moment are: $Q_{N\rightarrow\Delta} = -(0.043 \pm 0.040)$ fm^2 using the empirical values for the helicity amplitudes [48]; $Q_{N\rightarrow\Delta} = -0.075(13)$ fm^2 using the phenomenological analysis of [98] and $\mu_{N\rightarrow\Delta} = 3.9 - 4.2\,\mu_N$ [80]; $Q_{N\rightarrow\Delta} = -0.085$ fm^2 using a recent Mainz analysis [99], and the recent LEGS measurement favors an even larger value $Q_{N\rightarrow\Delta} = -0.105(15)$ fm^2 [100]. All entries are in [fm^2].

	i	g	π	σ	c	t
$p \rightarrow \Delta^+$	0.000	−0.056	−0.027	0.000	0.000	−0.083
$n \rightarrow \Delta^0$	0.000	−0.056	−0.027	0.000	0.000	−0.083

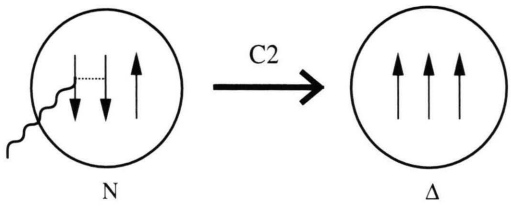

Fig. 5.6. Gluon and pion exchange current induced double spin flip contribution to the C2 transition form factor. The nonseparable contact diagram on the left results from a nonrelativistic reduction of diagram (b) in Figure 5.5. The dominant part of the C2 transition form factor is due to photon absorption on a correlated pair of quarks, interacting via gluon and pion exchange. The C2 photon simultaneously flips the spin of *two quarks* in the nucleon leading to the $\Delta(1232)$. This process is more important than the one where an C2 photon is absorbed on a single-quark (impulse approximation) moving in a D-wave (see Fig. 5.5a).

$$Q_{N\rightarrow\Delta} = -\frac{1}{\sqrt{2}} b^2 \frac{(\delta_g + \delta_\pi)}{3m_q} = -\frac{1}{\sqrt{2}} b^2 \left(\frac{M_\Delta - M_N}{M_N}\right) = \frac{1}{\sqrt{2}} r_n^2 . \tag{5.29}$$

The corresponding numerical results are listed in Table 5.3.

Equation (5.29) relates the transition quadrupole moment to the neutron charge radius. As in (5.21) no model parameter such as m_q or b appears in the final expression (5.29). Furthermore, the quadrupole moment of the excited Δ^+ state and the transition quadrupole moment of the $p \rightarrow \Delta^+$ transition are simply connected by a Clebsch-Gordan coefficient $(1/\sqrt{2})$.

It is interesting that the Skyrme model predicts for the pionic contribution a relation between the $N \rightarrow \Delta$ transition quadrupole moment and the isovector charge radius of the nucleon [101]

$$Q_{N\rightarrow\Delta}^{\text{Skyrme}} = -\frac{\sqrt{2}}{10}\left(r_p^2 - r_n^2\right). \tag{5.30}$$

Note the different definition of $Q_{N\rightarrow\Delta}$ here and in [101]. Including exchange currents into the NRQM shows that the NRQM leads to a similar conclusions as the Skyrme model concerning the important role of nonvalence quark degrees of freedom for some electromagnetic properties of the nucleon.

Exchange currents vs. configuration mixing

Is there any quantitative evidence for the correctness of the relations we derived aside from the qualitative connection with the Skyrme model result above? Let us first look at the single-quark transition NRQM result including configuration mixing. In the ratio of (5.28) and (5.10) the dependence on the oscillator parameter drops out and we obtain

$$\frac{Q_{N\rightarrow\Delta}^{\text{imp}}}{r_n^{2\,\text{imp}}} = 0.66. \tag{5.31}$$

This should be compared to our prediction

$$\frac{Q_{N\rightarrow\Delta}}{r_n^2} = \frac{1}{\sqrt{2}} = 0.71. \tag{5.32}$$

Therefore, in standard impulse approximation, the ratio between $Q_{N\rightarrow\Delta}^{\text{imp}}$ and $r_n^{2\,\text{imp}}$ which is free of the unphysically large harmonic oscillator value b typically used there, agrees remarkably well with our prediction.

It is almost needless to say that the simple result (5.29) will be modified in a more complete calculation including D-waves in the nucleon and Δ. Nevertheless, we expect that (5.29) captures the essential physics that makes both observables special and interesting: both r_n^2 and $Q_{N\rightarrow\Delta}$ are dominated by nonvalence quark degrees of freedom. Future experimental results must be carefully interpreted; the entire transition quadrupole moment *cannot* be attributed to the D-state admixtures in the N and Δ ground state wave functions. The effect of two-body exchange currents

must be taken into account, if one wants to isolate the effect of the quark-quark potential itself. To speak of deformed valence quark orbits emphasizes only one aspect of the $N \to \Delta$ quadrupole transition that may turn out to be of minor importance. If in a future experiment a $N \to \Delta$ transition quadrupole moment of the order $r_n^2/\sqrt{2}$ is confirmed it would most certainly be evidence for an important role of nonvalence quark degrees of freedom, i. e. in our language, pion and gluon exchange currents between quarks in this observable.

Transition quadrupole radius

In addition to the transition quadrupole moment, the transition quadrupole radius may possibly be extracted from the data. We obtain according to the definition (5.19)

$$r^2_{N\to\Delta} = \frac{1}{Q_{N\to\Delta}}\left(\frac{-\sqrt{2}}{8}b^2 r_n^2 + r^2_{\gamma q} Q_{N\to\Delta}\right) = \frac{b^2}{4} + r^2_{\gamma q}, \tag{5.33}$$

indicating a rather flat slope of the form factor at the origin. We see that the first term due to the gluon and pion exchange currents is suppressed in comparison to the contribution of the quark finite size $r^2_{\gamma q}$. We suggest to analyze the low-momentum transfer data in terms of the Taylor expansion of the quadrupole transition form factor

$$F_Q^{N\to\Delta}(\boldsymbol{q}^2) = Q_{N\to\Delta}\left(1 - \frac{1}{6}\boldsymbol{q}^2 r^2_{N\to\Delta}\right) \tag{5.34}$$

in order to extract the transition quadrupole radius and the electromagnetic radius of the constituent quark.

5.3. *Magnetic Dipole Form Factors*

In this Section we will be mainly concerned with the low-momentum transfer behavior of the magnetic form factors; in particular with the magnetic moments and radii for which analytic expressions can be derived. The magnetic dipole form factor is defined as [81]:

$$F_M(\boldsymbol{q}^2) = \frac{2\sqrt{6\pi}M_N}{iq}\langle JM_J{=}JTM_T| \; |\frac{-i}{4\pi}\int \mathrm{d}\Omega_q [Y^1(\hat{\boldsymbol{q}})\times \boldsymbol{J}(\boldsymbol{q})]^1 \; | JM_J{=}JTM_T\rangle, \tag{5.35}$$

where $\boldsymbol{J}$ is the total current operator (4.12). We calculate the magnetic dipole operator between the ground state wave function of the nucleon given by (3.15). The single quark current contribution to the isoscalar and isovector magnetic form factor of the nucleon is given by

$$F^{IS}_{imp}(\boldsymbol{q}^2) = e^{-\boldsymbol{q}^2 b^2/6}, \; F^{IV}_{imp}(\boldsymbol{q}^2) = 5e^{-\boldsymbol{q}^2 b^2/6}. \tag{5.36}$$

The two-body currents of Figs. 4.2 contribute as follows to the magnetic form factors

$$\begin{aligned}
F^{IS}_{gq\bar{q}}(\boldsymbol{q}^2) &= \alpha_s \frac{4}{9}\frac{M_N}{m_q^2}\frac{1}{q}e^{-\boldsymbol{q}^2 b^2/24} I_{gq\bar{q}}(|\boldsymbol{q}|),\\
F^{IV}_{gq\bar{q}}(\boldsymbol{q}^2) &= 2F^{IS}_{gq\bar{q}}(\boldsymbol{q}^2),\\
F^{IS}_{\pi q\bar{q}}(\boldsymbol{q}^2) &= -\frac{f^2_{\pi N}}{4\pi\mu^2}\frac{2}{25}\frac{M_N}{m_q^2}e^{-\boldsymbol{q}^2 b^2/24}\\
&\quad\cdot (I^{(00)}_{\pi q\bar{q}}(|\boldsymbol{q}|) + I^{(22)}_{\pi q\bar{q}}(|\boldsymbol{q}|)),\\
F^{IV}_{\pi q\bar{q}}(\boldsymbol{q}^2) &= -\frac{f^2_{\pi N}}{4\pi\mu^2}\frac{144}{25}M_N\frac{1}{|\boldsymbol{q}|}e^{-\boldsymbol{q}^2 b^2/24} I^{(11)}_{\pi q\bar{q}}(|\boldsymbol{q}|),\\
F^{IV}_{\gamma\pi\pi}(\boldsymbol{q}^2) &= -\frac{f^2_{\pi N}}{4\pi\mu^2}\frac{24}{25}M_N e^{-\boldsymbol{q}^2 b^2/24} I_{\gamma\pi\pi}(|\boldsymbol{q}|),\\
F^{IS}_S(\boldsymbol{q}^2) &= -2\frac{M_N}{3m_q^2}e^{-q^2 b^2/24} I^M_S(|\boldsymbol{q}|),\\
F^{IV}_S(\boldsymbol{q}^2) &= 5F^{IS}_S(\boldsymbol{q}^2).
\end{aligned} \tag{5.37}$$

The integrals $I_{gq\bar{q}}$, $I^{(jj)}_{\pi q\bar{q}}(q)$, $I_{\gamma\pi\pi}(q)$, and $I^M_S(q)$ in (5.37) are defined in the appendix. The total isoscalar/isovector magnetic form factor is thus given by the sum of all isoscalar/isovector contributions

$$\begin{aligned}
F^{IS/IV} &= F^{IS/IV}_{imp} + F^{IS/IV}_{gq\bar{q}} + F^{IS/IV}_{\pi q\bar{q}}\\
&\quad + F^{IV}_{\gamma\pi\pi} + F^{IS/IV}_{\sigma q\bar{q}} + F^{IS/IV}_{conf}.
\end{aligned} \tag{5.38}$$

We also use the following definitions for the proton and neutron magnetic form factors:

$$F_p = \frac{1}{2}(F^{IS} + F^{IV}), \; F_n = \frac{1}{2}(F^{IS} - F^{IV}). \tag{5.39}$$

In Fig. 5.7 we show our results for the magnetic form factor of the proton divided by the calculated magnetic moment. We observe that the inclusion of exchange currents leads for moderate momentum

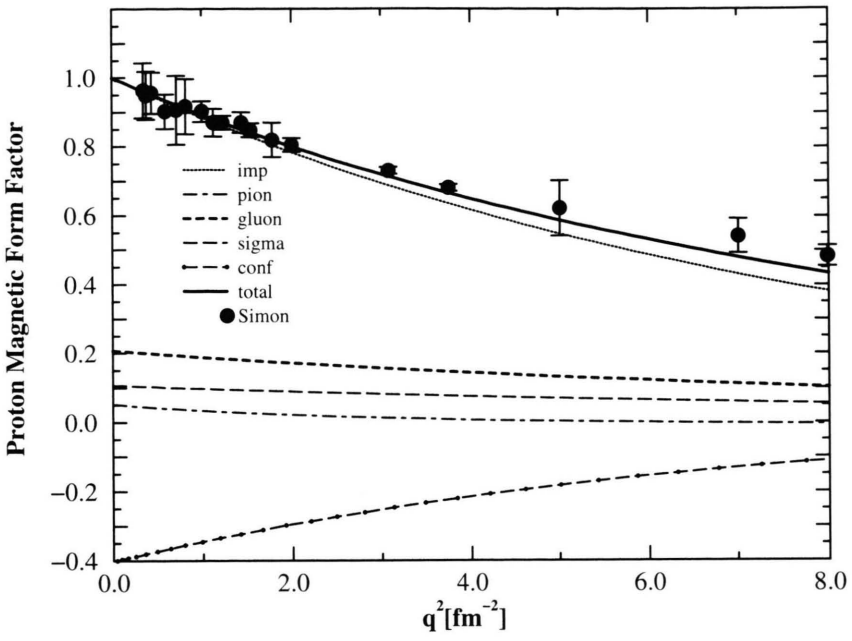

Fig. 5.7. Proton magnetic form factor divided by the calculated proton magnetic moment as a function of the four momentum transfer q^2 [fm^{-2}]. All data points [82] are divided by the experimental proton magnetic moment.

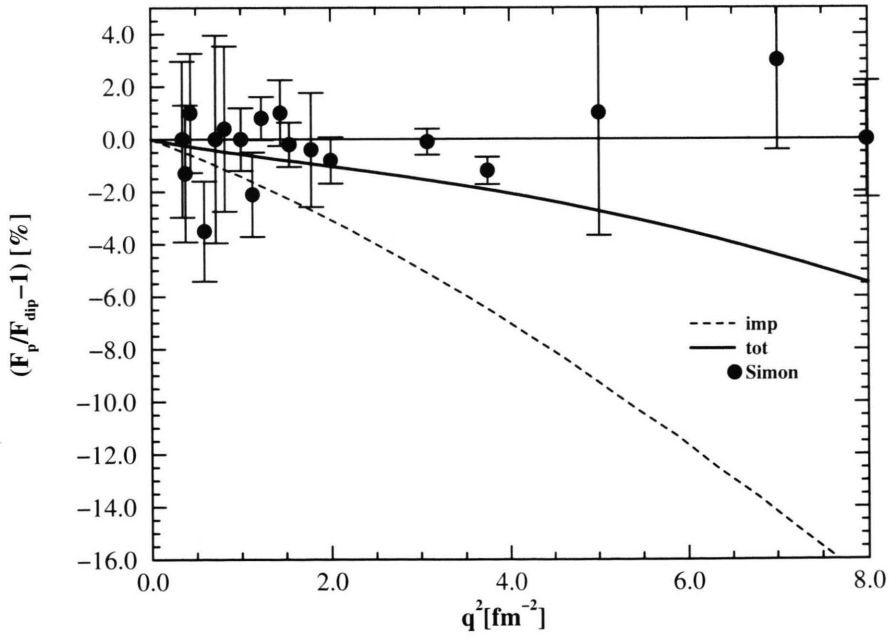

Fig. 5.8. Proton magnetic form factor as a function of the four momentum transfer q^2 [fm^{-2}]. Deviation from the empirical dipole form factor in percent. The data points are from [82].

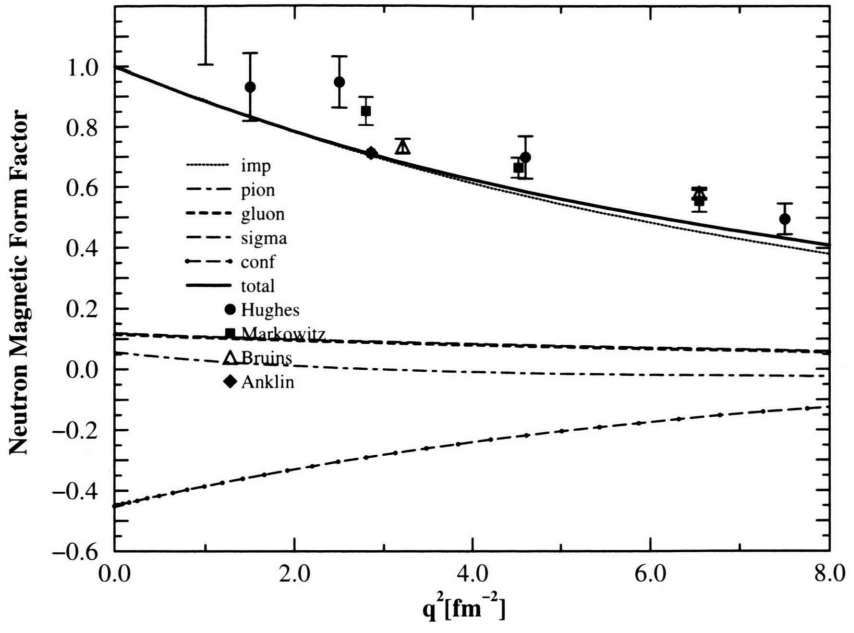

Fig. 5.9. Neutron magnetic form factor divided by the calculated neutron magnetic moment as a function of the four momentum transfer q^2 [fm^{-2}]. The experimental data points [102, 106 - 108] are divided by the experimental magnetic moment of the neutron.

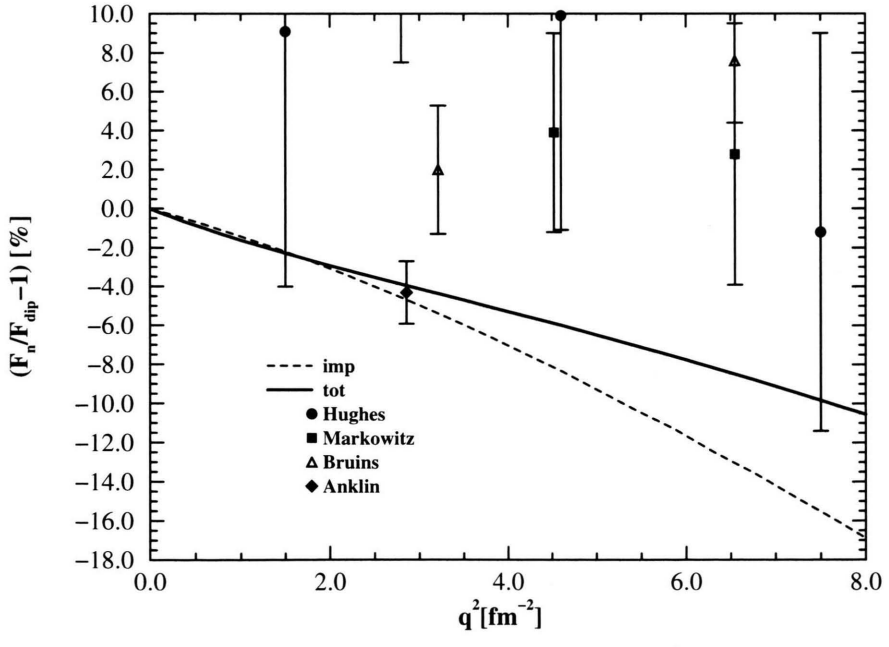

Fig. 5.10. Neutron magnetic form factor as a function of the four momentum transfer q^2 [fm^{-2}]. Deviation from the empirical dipole in percent. Same notation as in Figure 5.9.

transfers to some improvement of the theoretical description. This can be better appreciated by looking at Fig. 5.8 which shows the deviation of the calculated form factor from the empirical dipole fit in percent. Figures 5.9 and 5.10 show the corresponding results for the magnetic form factor of the neutron. In the case of the neutron, the data show systematic positive deviations from the empirical dipole fit that are not reproduced by our quark model calculation. Our calculation seems to be consistent only with the data point of Anklin et al. [102].

5.3.1. Magnetic Moments of the Nucleon

The magnetic moment of a composite system is defined as the $q \to 0$ limit of the magnetic dipole form factor (5.35). The NRQM in its simplest form employing only the single-quark spin current (4.4) and unmixed ground state wave functions predicts the baryon magnetic moments fairly accurately (see also Table 6.1). This is one of the original successes of the NRQM [5] which remains unsurpassed by more "sophisticated" low-energy models of QCD.

By simply adding the magnetic moments of three *free* quarks with $m_q = M_N/3$ one obtains

$$\mu_p = \frac{1}{3}(4\mu_u - \mu_d), \; \mu_n = \frac{1}{3}(4\mu_d - \mu_u) \quad (5.40)$$

in units of nuclear magnetons (μ_N). Assuming that quark magnetic moments are not renormalized [66] and given by their Dirac values and that there is perfect isospin symmetry on the quasiparticle level $m_u = m_d$ one gets $\mu_d = -\mu_u/2$. Choosing the canonical value $m_q = M_N/3$ for the constituent quark mass one has $\mu_u = 2\mu_N$. With (5.40) one obtains $\mu_p = 3$ and $\mu_n = -2$. These theoretical values deviate by less than 10% from the experimental ones and the theoretical ratio $-3/2$ [5] deviates by less than 3% from the experimental value -1.46 [48]. Furthermore, the additive quark model prediction for the magnetic moments of all other members of the spin 1/2 baryon octet agree with the experimental values within 10% with the exception of the Ξ^- magnetic moment. In this case, the exchange currents lead to a 40% decrease of the calculated magnetic moment, in agreement with experiment (see Chapt. 6) [103][8].

[8] By slightly modifying the quark mass and by introducing small anomalous magnetic moments for the quarks one could further improve the agreement with the experimental values.

Thus, it seems that we are dealing with a similar situation as in the deuteron. The deuteron magnetic moment $\mu_d^{exp} = 0.857406(1)$ n.m. is to a very good accuracy given by the sum of the free proton and neutron magnetic moments, i.e. $\mu_d \approx \mu_p + \mu_n = 0.88$ n.m. This can be qualitatively understood because the deuteron is a weakly interacting system in which the constituents spend most of the time outside of their mutual interaction region. Corrections coming from the deuteron wave function such as a small D-state admixture and explicit two-body currents only marginally affect the deuteron magnetic moment and simple addition of free particle magnetic moments is a very good approximation.

On the other hand, it is far from obvious why such an extreme idealization which neglects all binding effects should work in the low-energy regime of QCD. Constituent quarks are subject to strong forces[9] that confine them inside a region of about $r \simeq 0.6$ fm. Moreover, as we have previously argued, in addition to the three valence quarks, there are also effective gluon, pion and σ exchange interactions between the valence quarks. These residual degrees of freedom manifest themselves not only in the baryon wave function but also as explicit two-body exchange current operators. The latter have to be included for reasons of gauge invariance and are expected to strongly influence the electromagnetic properties of a baryon. For these reasons, it is a priori not clear why the simple additive quark model which neglects all interaction effects in wave functions and electromagnetic currents works so well for the baryon magnetic moments.

Let us first discuss the corrections coming from configuration mixing. The mixing of different harmonic oscillator shells due to the short-range nuclear forces and its effect on nuclear magnetic moments (Arima-Horie effect) has been systematically studied already forty years ago [104]. In nuclei, configuration mixing leads to characteristic deviations from the Schmidt lines that in most cases improve the agreement with experiment [105]. A similar effect occurs in the quark model. Using such improved quark model wave function which include the effect of the residual quark-quark interactions one derives in impulse approximation [65] in units of nuclear magnetons (μ_N)

$$\mu_p\left(1 - \frac{2}{3}a_{S_M}^2\right), \; \mu_n = -2\left(1 - a_{S_M}^2\right). \quad (5.41)$$

[9] The potential energies involved (see Table 3.2) are of the same order as the constituent quark masses.

With typical admixtures $a_{S_M} = -0.27$ [15] one obtains with $\mu_p = 2.85$ and $\mu_n = -1.85$ some improvement with respect to the additive result (5.40).

Next, we evaluate the two-body currents of Sect. 4.2 between nucleon wave functions. In the case of simple ground state wave functions (3.15) one can express the two-body current contributions to magnetic moments in terms of potential matrix elements. This is intuitively clear because of the close connection between two-body currents and potentials. We obtain [38]

$$\mu_p = 3 + \frac{b^2}{3} M_N \delta_g(b) + M_N \delta_\pi(b)\left(\frac{1}{4M_N^2} - \frac{b^2}{3}\right) - M_N\left((\frac{1}{\mu^2} + \frac{1}{3}b^2)\delta_{\pi_\mu}(b) - (\mu \leftrightarrow \Lambda)\right) - \frac{6}{M_N}\left(V^{\text{conf}}(b) + V^\sigma(b)\right), \quad (5.42)$$

$$\mu_n = -2 - \frac{b^2}{9} M_N \delta_g(b) + M_N \delta_\pi(b)\left(\frac{1}{4M_N^2} + \frac{b^2}{3}\right) + M_N\left((\frac{1}{\mu^2} + \frac{1}{3}b^2)\delta_{\pi_\mu}(b) - (\mu \leftrightarrow \Lambda)\right) + \frac{4}{M_N}\left(V^{\text{conf}}(b) + V^\sigma(b)\right).$$

The first term in (5.42) correspond to the well-known single quark current result $\mu_p = 3\mu_N$ and $\mu_n = -2\mu_N$. The other terms are the gluon-pair, pion-pair, pionic, and scalar exchange current contributions to the magnetic moments expressed through corresponding potential matrix elements. Exchange current corrections to baryon magnetic moments were calculated before [31 - 33, 35, 109]; the advantage of (5.42) is that their simple analytic form allows a comparison of, for example, the role of gluon and pion degrees of freedom in baryon mass formulae and magnetic moments.

Equation (5.42) clearly show that there is a close relation between the gluon and pion contributions to the $\Delta - N$ mass-splitting and the role of gluon and pion degrees of freedom in the magnetic moments. In the $(0s)^3$ model the relative importance of gluon and pion degrees of freedom is largely governed by the size of the pion-quark interaction region as discussed in Chap. 3. Furthermore, the gluon and pion exchange current contributions to the magnetic moments depend explicitly on the size of the quark core.

Table 5.4. Nucleon magnetic moments including two-body exchange currents; i: impulse; g: gluon; π: pion; σ: σ-meson; c: confinement; t: total; t = i + g + π + σ + c. The contribution of the pion pair ($\pi q\bar{q}$) and the pionic ($\gamma\pi\pi$) currents are separately listed. The experimental proton and neutron magnetic moments are $\mu_p = 2.792847386(63)\ \mu_N$ and $\mu_n = -1.91304275(45)\ \mu_N$, respectively [48]. All entries are in μ_N.

	μ_i	μ_g	$\mu_{\pi q\bar{q}}$	$\mu_{\gamma\pi\pi}$	μ_σ	μ_c	μ_t
p	3.000	0.598	−0.262	0.411	0.308	−1.164	2.890
n	−2.000	−0.199	0.313	−0.411	−0.205	0.776	−1.726

The magnetic moments of the nucleon are therefore quite sensitive to the model parameters Λ and b.

In Table 5.4 we list our numerical results which can be easily verified using the parameters of Table 3.1 and (5.42). We see that individual exchange magnetic moments are large. They can easily make up for 30% or more of the experimental nucleon magnetic moments. But there are substantial cancellations among the different terms. For example, there is a substantial cancellation between the pionic and pion-pair current contributions. This leads to a relatively small overall pion exchange magnetic moment. This has been first noted in [35] in a slightly different model. Note also the large gluon contribution $\mu^p_{gq\bar{q}} = b^2 M_N \delta_g/3$ to the proton magnetic moment. A large gluon contribution to the proton magnetic moment was also found by Hwang [109] in the bag model. For a Lorentz scalar confinement potential this gets cancelled by a similarly large scalar exchange current correction $\mu^p_S = -6(V^{\text{conf}}+V^\sigma)/M_N$ as was first realized in [38]. For a Lorentz vector type confinement one obtains an exchange current contribution that has the same sign as the the one-gluon exchange current and there is no cancellation. We point out that the confinement and σ-exchange contributions to the magnetic moments depend only on the expectation values $V^{\text{conf}}(b)$ and $V^\sigma(b)$ appearing in the nucleon mass formula (3.16), respectively. These were already fixed in Chapter 3.

This cancellation between gluon and scalar exchange currents occurs in both models (with and without π/σ) although it is more complete if chiral interactions are included. For this cancellation it is essential that the condition $M_N(b) = 3m_q = 939$ MeV is satisfied (see Table 3.2). The actual degree of cancellation depends sensitively on the quark core radius b. For an almost complete cancellation a value of $b \approx 0.6$ fm is required. This value of b is consistent with the one obtained from the neutron charge radius.

One may wonder why the vector- and scalar-exchange currents calculated here are much larger than their counterparts in nuclear physics. For example, vector and scalar exchange currents contribute only a few percent to the ^{3}He or ^{3}H magnetic moments whereas in the three-quark system they can easily account for 30% of the experimental value. This strong enhancement in the three-quark system can be qualtitatively understood. Orbital matrix elements of two-body vector and scalar exchange currents are of order $1/b^3$. Because of the smaller size of the nucleon ($b \approx 0.5$ fm) in comparison to the size of the three-nucleon system ($b \approx 1.5$ fm) the exchange currents are more important here.

Our main result is that the overall exchange current contribution is of the order of only 10% of the impulse approximation despite the fact that the contributions of individual two-body currents are substantially larger. Thus, we basically recover the additive quark model result. We emphasize that we use here the same values for all parameters as in Chapter 3. If we did not insist on the consistency between the values for b and a_c in Chap. 3 (where they determine the confinement contribution to the nucleon mass) and here (where they describe the size of the confinement exchange magnetic moment) our argument concerning the cancellations in Table 3.2 and Table 5.4 would be meaningless.

Effect of the δ-function in V^{OPEP}

We add some remarks concerning the important role of the δ-function in the one-pion exchange potential for the cancellation of the pion-pair and pionic currents. It was first observed in [38] that the δ-function in V^{OPEP} has important consequences for the nucleon magnetic moments; in particular with respect to the cancellation between the isovector pion-pair and pionic exchange current contributions. To see this let us study the two extreme cases: (i) inclusion of the full δ-function in V^{OPEP}, (ii) complete elimination of the δ-function in V^{OPEP}. The first choice corresponds to the limit $\Lambda \to \infty$ and is a special case of the formulae given in this work. However, in the second case *we must make corresponding changes in the one-pion exchange current* in order to preserve gauge invariance. We derive the matrix elements of V^{OPEP} between nucleon states corresponding to case (ii) by first letting Λ go to infinity in (3.16) and then removing the term

$$\delta_{\pi_\Lambda}(b, \Lambda \to \infty) = -\frac{f_{\pi N}^2}{4\pi\mu^2}\frac{72}{25}\frac{1}{\sqrt{2\pi}b^3}. \tag{5.43}$$

Equation (5.43) corresponds to the $(0s)^3$ matrix element of the δ-function term in (3.3). The remaining term, δ_{π_μ}, is also shown in Figure 3.3. For the magnetic moments we then obtain

$$\mu_p = 3 + \frac{b^2}{3}M_N(\delta_g - \delta_{\pi_\mu}) + \frac{\delta_{\pi_\mu}}{4M_N} - M_N\left(\frac{1}{\mu^2} + \frac{1}{3}b^2\right)\delta_{\pi_\mu} - 6\frac{(V^{\text{conf}}(b) + V^{\sigma}(b))}{M_N}, \tag{5.44}$$

$$\mu_n = -2 - \frac{b^2}{3}M_N\left(\frac{1}{3}\delta_g - \delta_{\pi_\mu}\right) + \frac{\delta_{\pi_\mu}}{4M_N} + M_N\left(\frac{1}{\mu^2} + \frac{1}{3}b^2\right)\delta_{\pi_\mu} + 4\frac{(V^{\text{conf}}(b) + V^{\sigma}(b))}{M_N}. \tag{5.45}$$

The presence of the (smeared-out) δ-function term in (3.3) results in a strong pion cloud contribution, δ_π, to mass splittings but in a relatively small contribution of the pion cloud to magnetic moments. If the δ-function piece is left out in (3.3) the situation is reversed. One obtains a small pion contribution to mass splittings but a very big pion cloud contribution to nucleon magnetic moments of around 1 (-1) μ_N to the proton(neutron) that by themselves would lead to inacceptable results for the nucleon magnetic moments. However, one must keep in mind that without the δ-function in (3.3) the one-gluon exchange potential is almost solely responsible for the $\Delta - N$ mass splitting. This leads to a much larger value for α_s and an substantially increased color Coulomb attraction. The latter must be compensated by an increased confinement contribution in (3.16). Without the δ-function in V^{OPEP} one finds for the proton magnetic moment according to (5.45) $\mu_p = 3 + 0.936 + 0.925 - 1.812 = 3.049\,\mu_N$ and $\mu_n = -2 - 0.312 - 0.934 + 1.208 = -2.038\,\mu_N$, where the numbers correspond to the impulse, gluon, pion and scalar exchange current contributions. We observe again an almost complete cancellation between various exchange currents.

5.3.2. Magnetic Moments of the Δ

In the additive quark model one obtains in units of nuclear magnetons $\mu_N = \frac{e}{2M_N}$:

$$\mu_\Delta = 3\,e_\Delta. \tag{5.46}$$

Table 5.5. $\Delta(1232)$ magnetic moments, and $N \rightarrow \Delta$ transition magnetic moments including two-body exchange currents; i: impulse; g: gluon; π: pion; σ: σ-meson; c: confinement; t: total; t = i + g + π + σ + c. The contribution of the pion pair ($\pi q\bar{q}$) and the pionic ($\gamma\pi\pi$) currents are separately listed. The experimental range for the Δ^{++} magnetic moment is $\mu_{\Delta^{++}} = 3.7 - 7.5\ \mu_N$ [48]. An older value is $\mu_{\Delta^{++}} = 5.7 \pm 1.0\ \mu_N$[112] while the most recent value is $\mu_{\Delta^{++}} = 4.52 \pm 0.50\,\mu_N$ [113]. The experimental range for the $N \rightarrow \Delta$ transition magnetic moment is $\mu_{p\rightarrow\Delta^+} \approx 3.4 - 4.2\mu_N$ [65, 114]. All entries are in μ_N.

	μ_i	μ_g	$\mu_{\pi q\bar{q}}$	$\mu_{\gamma\pi\pi}$	μ_σ	μ_c	μ_t
Δ^{++}	6.000	2.391	0.304	0.000	0.615	−2.328	6.981
Δ^{+}	3.000	1.195	0.152	0.000	0.308	−1.164	3.491
Δ^{0}	0.000	0.000	0.000	0.000	0.000	0.000	0.000
Δ^{-}	−3.000	−1.195	−0.152	0.000	−0.308	1.164	−3.491
$p \rightarrow \Delta^+$	2.828	0.282	−0.406	0.582	0.290	−1.098	2.477
$n \rightarrow \Delta^0$	2.828	0.282	−0.406	0.582	0.290	−1.098	2.477

Including two-body exchange currents, we have

$$\mu_\Delta = \Big(3 + \frac{2b^2}{3} M_N \delta_g(b) + \frac{3\delta\pi(b)}{2M_N} - \frac{6}{M_N}\left(V^{\text{conf}}(b) + V^{\sigma}(b)\right)\Big) e_\Delta . \tag{5.47}$$

The first term in (5.42) corresponds to the well-known single-quark current result $\mu_\Delta = \mu_p e_\Delta$. The remaining terms express the gluon, pion, and scalar exchange current contributions, through corresponding potential matrix elements. All contributions to the Δ magnetic moments are proportional to the charge of the Δ. Therefore, the Δ^0 magnetic moment is predicted to be zero. This is in agreement with the additive quark model as well as with a recent lattice calculation [110]. We list our numerical results in Table 5.5. Note the large gluon contribution to the Δ^{++} magnetic moment, which gets cancelled by a similarly large *scalar* exchange current correction. Again, we find that for this cancellation it is essential that the condition $M_N(b) = 3m_q = 939$ MeV be satisfied and that the harmonic oscillator parameter $b \approx 1/m_q \approx 0.6$ fm be consistent with the neutron charge radius (5.12). Note that in the case of the Δ elastic form factors, the dominant isovector pion pair and pionic exchange currents proportional to $(\tau_1 \times \tau_2)_3$ do not contribute. Therefore, we have to include the next-to-leading order isovector pion pair-current in (4.8), which is of the same order as the isoscalar pion pair-current. We then reproduce the general result [111] that the Δ magnetic moments and radii are proportional to the charge of the Δ given in (5.16). In [111] it has been argued that the pion contribution to the isoscalar nucleon magnetic moment used by Brown et al. [32] induces an intolerably large violation of this proportionality. Here, we show that if the isovector and isoscalar pion exchange currents are consistently calculated to the same nonrelativistic order, the proportionality of the Δ magnetic moments to the charge of the Δ holds even in the presence of pions.

Our result does not significantly deviate from the experimental value $\mu_{\Delta^{++}} = 5.7 \pm 1.0\ \mu_N$[112] and is within the experimental range $\mu_{\Delta^{++}} = 3.7 - 7.5\,\mu_N$ given by the Particle Data Group [48]. However, it is clearly larger than the most recent experimental value [113]. It should be mentioned that the determination of $\mu_{\Delta^{++}}$ from $\pi p \rightarrow \pi p\gamma$ bremsstrahlung experiments [113, 112] needs theoretical input from πN scattering models with Δ degrees of freedom. Therefore, the extraction of the "bare" Δ^{++} magnetic moment from the πp bremsstrahlung data has a certain model dependence that should not be underestimated. We also mention that quark model calculations, such as the one presented here, neglect the coupling of the Δ to the πN decay channel and thus predict "bare" electromagnetic moments. Our result for the Δ^{++} magnetic moment agrees reasonably well with a chiral bag model calculation by Krivoruchenko [115].

5.3.3. $N \rightarrow \Delta$ Transition Magnetic Moment

Early evidence for the existence of a close connection between the electromagnetic properties of the nucleon and the Δ-isobar was provided by the quark model prediction of the $N \rightarrow \Delta$ magnetic transition moment [5, 114]. The additive quark model predicts

$$\mu_{p\rightarrow\Delta^+} = \frac{2\sqrt{2}}{3}\mu_p \tag{5.48}$$

some 30 % lower than phenomenological estimates which range between $3.4 - 4.2\mu_N$. In contrast to the magnetic moments, where both isoscalar and isovector exchange currents contribute, only isovector currents contribute to the $N \rightarrow \Delta$ transition magnetic moment. Using (5.42), we can express our result for the transition moment as

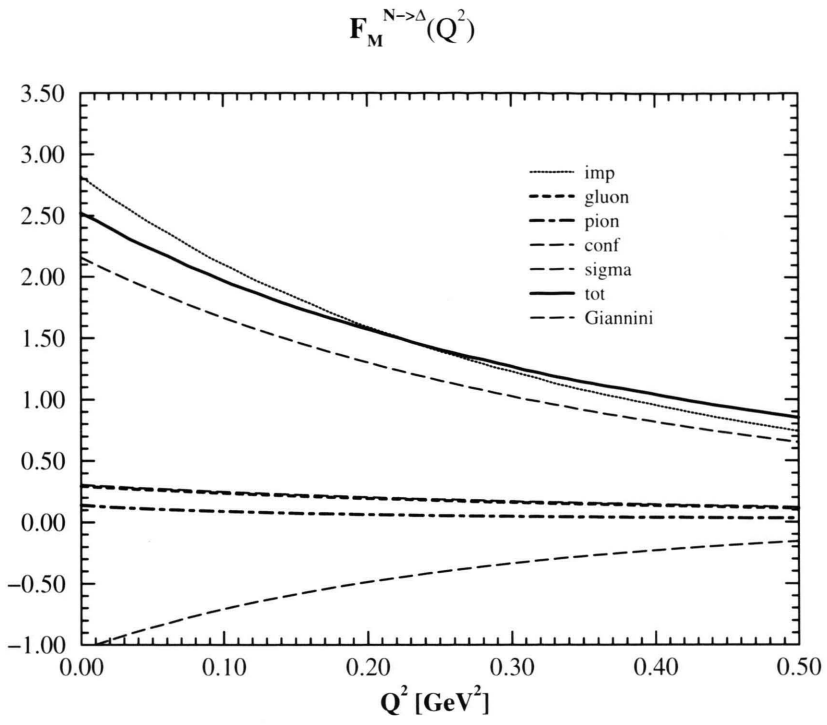

Fig. 5.11. The magnetic dipole $N \rightarrow \Delta$ transition form factor including exchange currents. An impulse calculation using the admixture coefficients of Giannini [65] is also shown.

$$\mu_{N\rightarrow\Delta} = \frac{2\sqrt{2}}{3}\left(\mu^{\mathrm{p}}_{\mathrm{imp}} + \frac{1}{2}\mu^{\mathrm{p}}_{\mathrm{gq\bar{q}}} + \frac{3}{2}\left(\mu^{\mathrm{IV\,p}}_{\gamma\pi\pi} + \mu^{\mathrm{IV\,p}}_{\pi\mathrm{q\bar{q}}}\right) + \mu^{\mathrm{p}}_{\sigma} + \mu^{\mathrm{p}}_{\mathrm{conf}}\right). \tag{5.49}$$

We point out that in contrast to the findings of Robson [36], the pionic contribution is very important for the $N \rightarrow \Delta$ transition magnetic moment. This can be seen from (5.49) which relates the pionic contribution to the $N \rightarrow \Delta$ transition magnetic moment to the corresponding contribution to the proton magnetic moment. We obtain the numbers in the last two rows of Table 5.5. We observe substantial cancellations among the different terms. For example, the pionic contribution $\mu_{\gamma\pi\pi} = 0.58\mu_N$ is nearly canceled by the pion pair contribution $\mu_{\pi q\bar{q}} = -0.41\mu_N$. As a result, the total transition moment is only about 13% lower than the impulse value. We point out that our analytic result for the total pion exchange current contribution to the transition magnetic moment, $\mu^{\pi}_{p\rightarrow\Delta^+} = 0.176\,\mu_N$, is somewhat larger than a recent phenomenological estimate, which gives $\mu^{\pi}_{p\rightarrow\Delta^+} \approx 0.074\,\mu_N$ [17].

Finally, we would like to point out that the dominant contribution to the $N \rightarrow \Delta$ transition magnetic moment comes from the single quark current, i. e. the first term in (5.49). One can show that the impulse contribution is proportional to the overlap of the orbital symmetric nucleon and Δ wave functions. This holds true even in the presence of configuration mixing provided that the D-state admixture is small. Therefore, any model in which this overlap is small, due to, for example, very different values of b in the nucleon and Δ wave functions will give a very small value of the $N \rightarrow \Delta$ transition moment.

We close this section by summarizing the main points. It has been known for some time that baryon magnetic moments are valence quark dominated. Our calculation explicitly shows that corrections coming from nonvalence quark degrees of freedom, such as exchange currents, are important but rarely exceed 15% of the additive quark model value. The problem with the underestimation of the $N \rightarrow \Delta$ transition magnetic moment persists also after inclusion of exchange currents.

5.3.4. Magnetic Radii

Magnetic radii of hadrons measure the extension of the spatial current distribution. As the charge radii, they are interesting quantities which are quite sensitive to various model assumptions. The magnetic radius is defined as the slope of the magnetic form factor at zero momentum transfer:

$$r_{\mathrm{M}}^2 = -\frac{6}{F_{\mathrm{M}}(0)}\frac{\mathrm{d}}{\mathrm{d}\boldsymbol{q}^2}F_{\mathrm{M}}(\boldsymbol{q}^2)|_{\boldsymbol{q}^2=0}. \tag{5.50}$$

Thus one obtains

$$r_{\mathrm{M}}^2 = r_{\mathrm{imp}}^2 + r_{\mathrm{gq\bar{q}}}^2 + r_{\pi\mathrm{q\bar{q}}}^2 + r_{\gamma\pi\pi}^2 + r_{\sigma\mathrm{q\bar{q}}}^2 + r_{\mathrm{conf}}^2. \tag{5.51}$$

In the SU(2) sector we define corresponding isoscalar and isovector radii:

$$r^{2\,\mathrm{IS/IV}} = -\frac{6}{F^{\mathrm{IS/IV}}(0)}\frac{\mathrm{d}}{\mathrm{d}q^2}F^{\mathrm{IS/IV}}(q^2)|_{q=0}, \tag{5.52}$$

where $F^{\mathrm{IS/IV}}(0)$ is the total isoscalar (IS) or isovector (IV) magnetic form factor (5.35) at $q = 0$, i. e. the *total* magnetic moment. Employing the ground state wave functions (3.15) we can derive analytic expressions for the isoscalar and isovector magnetic radii of the nucleon.

For the lowest order impulse approximation we get

$$r_{\mathrm{imp}}^{2\,\mathrm{IS}} = \frac{\mu_{\mathrm{imp}}^{\mathrm{IS}}}{F^{\mathrm{IS}}(0)}b^2,\; r_{\mathrm{imp}}^{2\,\mathrm{IV}} = \frac{\mu_{\mathrm{imp}}^{\mathrm{IV}}}{F^{\mathrm{IV}}(0)}b^2, \tag{5.53}$$

where $\mu_{imp}^{\mathrm{IS/IV}}$ is the impulse contribution to the magnetic moment and is given by (5.40).

For the gluon- and pion quark-antiquark pair currents and the pionic (pion-in-flight) contributions we obtain the following results:

$$\begin{aligned}
r_{\mathrm{gq\bar{q}}}^{2\,\mathrm{IS}} &= \frac{1}{F^{\mathrm{IS}}(0)}\frac{11}{90}M_N b^4\delta_{\mathrm{g}},\\
r_{\mathrm{gq\bar{q}}}^{2\,\mathrm{IV}} &= \frac{1}{F^{\mathrm{IV}}(0)}\frac{11}{45}M_N b^4\delta_{\mathrm{g}},\\
r_{\pi\mathrm{q\bar{q}}}^{2\,\mathrm{IS}} &= \frac{1}{F^{\mathrm{IS}}(0)}\frac{1}{180}\frac{M_N}{m_{\mathrm{q}}^2}b^2(10\delta_\pi + \frac{3}{2}b\delta'_\pi),\\
r_{\pi\mathrm{q\bar{q}}}^{2\,\mathrm{IV}} &= -\frac{1}{F^{\mathrm{IV}}(0)}\frac{1}{15}M_N b^4(10\delta_\pi + \frac{3}{2}b\delta'_\pi),
\end{aligned} \tag{5.54}$$

$$\begin{aligned}
r_{\gamma\pi\pi}^{2\,\mathrm{IV}} = -\frac{1}{F^{\mathrm{IV}}(0)}\frac{1}{6}M_N b^4\Big(&\delta_\pi + \frac{1}{5}b\delta'_\pi\\
&- [\frac{6}{\mu^4 b^4}(\delta_{\pi_\mu} + b\delta'_{\pi_\mu}) - \frac{6}{\Lambda^4 b^4}(\delta_{\pi_\Lambda} + b\delta'_{\pi_\Lambda})]\Big),
\end{aligned}$$

where $\delta'_\pi(b) = \partial\delta_\pi(b)/\partial b$. For the magnetic radii due to the scalar (confinement and σ-exchange) current we get

$$\begin{aligned}
r_{\mathrm{S}}^{2\,\mathrm{IS}} &= -\frac{1}{F^{\mathrm{IS}}(0)}\frac{M_N}{18m_{\mathrm{q}}^2}b^2(4\langle V^{\mathrm{S}}\rangle(b) + b\frac{\partial}{\partial b}\langle V^{\mathrm{S}}\rangle(b)),\\
r_{\mathrm{S}}^{2\,\mathrm{IV}} &= 5\frac{F^{\mathrm{IS}}(0)}{F^{\mathrm{IV}}(0)}r_{\mathrm{S}}^{2\,\mathrm{IS}}.
\end{aligned} \tag{5.55}$$

The total isoscalar/isovector magnetic radius $r^{2\,\mathrm{IS/IV}}$ is then given by the sum of all isoscalar/isovector terms in (5.54, 5.55) and the magnetic radii of the proton and neutron are given by

$$\begin{aligned}
r_{\mathrm{p}}^2 &= \frac{1}{F_{\mathrm{p}}(0)}(r^{2\,\mathrm{IS}}F^{\mathrm{IS}}(0) + r^{2\,\mathrm{IV}}F^{\mathrm{IV}}(0))/2\\
r_{\mathrm{n}}^2 &= \frac{1}{F_{\mathrm{n}}(0)}(r^{2\,\mathrm{IS}}F^{\mathrm{IS}}(0) - r^{2\,\mathrm{IV}}F^{\mathrm{IV}}(0))/2.
\end{aligned} \tag{5.56}$$

In contrast to the magnetic moments, the magnetic radii depend on the shape of the confinement potential, because the second term in (5.54,5.55) involves the partial derivative with respect to the size parameter b of the nucleon. This dependence may be helpful in discriminating between different confinement models recently proposed [116]. In the formulae below we have used the quadratic confinement (3.8) which allows to write the confinement contribution to the magnetic radii in a more compact form.

Next, we list the results for the Δ magnetic radii:

$$\begin{aligned}
r_\Delta^2 = \frac{e_\Delta}{\mu_\Delta}\Big\{&3b^2 + \frac{11}{30}M_N b^4\delta_{\mathrm{g}}(b)\\
&+ \frac{3}{20M_N}b^2\Big(10\delta_\pi(b) + \frac{3}{2}b\delta'_\pi(b)\Big)\\
&- \frac{9}{M_N}b^2V^{\mathrm{conf}}(b)\\
&- \frac{3}{2M_N}b^2\Big(4V^\sigma(b) + b\frac{\partial}{\partial b}V^\sigma(b)\Big)\Big\}\\
&+ r_{\gamma\mathrm{q}}^2.
\end{aligned} \tag{5.57}$$

Table 5.6. Magnetic radii of the nucleon and $\Delta(1232)$ including two-body exchange currents; i: impulse; g: gluon; π: pion; σ: σ-meson; c: confinement; t: total; t = i + g + π + σ + c. The contribution of the pion pair ($\pi q\bar{q}$) current and the pionic current ($\gamma\pi\pi$) are listed separately. The magnetic radius of the Δ^0 is zero. A finite electromagnetic quark size, $r^2_{\gamma q} = 0.36$ fm^2, is used. The experimental proton and neutron magnetic radii are $r^2_p = 0.858 \pm 0.056$ fm and $r^2_n = 0.876 \pm 0.070$ fm [82]. All entries are in [fm^2], except for total results which are in [fm].

	r^2_i	r^2_g	$r^2_{\pi q\bar{q}}$	$r^2_{\gamma\pi\pi}$	r^2_σ	r^2_c	$\sqrt{\lvert r^2_t\rvert}$
p	0.764	0.117	−0.053	0.185	0.058	−0.372	0.836
n	0.852	0.065	−0.105	0.309	0.065	−0.415	0.878
Δ	0.632	0.194	0.025	0.000	0.048	−0.308	0.769
$p \to \Delta^+$	0.840	0.064	−0.096	0.305	0.064	−0.409	0.876

Likewise, we obtain for $N \to \Delta$ magnetic transition radii:

$$
\begin{aligned}
r^2_{N\to\Delta} &= \frac{2\sqrt{2}}{\mu_{N\to\Delta}} \\
&\cdot \Big\{ b^2 + \frac{11}{360} M_N b^4 \delta_g(b) \\
&\quad - \frac{1}{60} M_N b^4 \Big(10\delta_\pi(b) + \frac{3}{2} b\delta'_\pi(b) \Big) \\
&\quad + \frac{1}{2} r^{2\,p}_{\gamma\pi\pi} \mu_p - \frac{3}{M_N} b^2 V^{\mathrm{conf}}(b) \\
&\quad - \frac{1}{2M_N} b^2 \Big(4V^\sigma(b) + b \frac{\partial}{\partial b} V^\sigma(b) \Big) \Big\} + r^2_{\gamma q}.
\end{aligned}
\tag{5.58}
$$

Here, $r^{2\,p}_{\gamma\pi\pi}$ is the pionic current contribution to the proton magnetic radius [38].

As is clearly seen in Table 5.6, the scalar exchange current cancels the effect of gluon and pion exchange currents to a large extent. We reiterate that a vector-type confinement potential would have the same sign as the gluon contribution and would completely spoil the agreement obtained.

5.3.5. Relativistic Corrections to the One-Body Current

In [37] it was suggested that the relativistic corrections to the single quark charge density operator, in particular the term proportional to $\boldsymbol{q}^2/(8m_q^2)$ (Darwin term) in $\rho_{[1]}$

$$
\rho_{[1]}(\boldsymbol{r}_i, \boldsymbol{q}) = e_i e^{i\boldsymbol{q}\cdot\boldsymbol{r}_i} \Big(1 + \frac{1}{4m_q^2} \Big(\frac{-\boldsymbol{q}^2}{2} + i\boldsymbol{\sigma}_i \cdot (\boldsymbol{q} \times \boldsymbol{p}_i) \Big) \Big),
\tag{5.59}
$$

brings the proton charge radius closer to its experimental value.

A similar effect is observed for the magnetic radii if one includes the relativistic correction to the spatial impulse current density. Up to order $\mathcal{O}(m_q^{-3})$, the spatial impulse current operator is given as

$$
\begin{aligned}
\boldsymbol{J}_{[1]}(\boldsymbol{r}_i, \boldsymbol{q}) = \frac{e_i}{2m_q} \Big(& \{\boldsymbol{p}_i, e^{i\boldsymbol{q}\cdot\boldsymbol{r}_i}\} + i \left[\boldsymbol{\sigma}_i \times \boldsymbol{p}_i, e^{i\boldsymbol{q}\cdot\boldsymbol{r}_i}\right] \\
& - \frac{1}{8m_q^2} \left[\boldsymbol{p}_i, \left[\boldsymbol{p}_i^2, e^{i\boldsymbol{q}\cdot\boldsymbol{r}_i}\right]\right] \\
& - \frac{i}{4m_q^2} \left[\boldsymbol{p}_i^2, \{\boldsymbol{\sigma}_i \times \boldsymbol{p}_i, e^{i\boldsymbol{q}\cdot\boldsymbol{r}_i}\}\right] \\
& - \frac{1}{4m_q^2} \{\boldsymbol{p}_i^2, \{\boldsymbol{p}_i, e^{i\boldsymbol{q}\cdot\boldsymbol{r}_i}\}\} \\
& - \frac{i}{4m_q^2} \left[\boldsymbol{\sigma}_i \times \boldsymbol{p}_i, \{\boldsymbol{p}_i^2, e^{i\boldsymbol{q}\cdot\boldsymbol{r}_i}\}\right] \Big).
\end{aligned}
\tag{5.60}
$$

These relativistically extended single-quark charge and current operators (5.59,5.60) satisfy the following continuity equation

$$
\boldsymbol{q} \cdot \boldsymbol{J}_{[1]} = \left[T, \rho_{[1]}(\boldsymbol{q}, \boldsymbol{r}_i)\right],
\tag{5.61}
$$

where

$$
T = m_q + \frac{\boldsymbol{p}_i^2}{2m_q} - \frac{\boldsymbol{p}_i^4}{8m_q^3}
$$

is the kinetic energy of a single quark expanded to order $\mathcal{O}(m_q^{-3})$.

Let us study the effect of these relativistic corrections of order $\mathcal{O}(m_q^{-3})$ on the magnetic properties of the nucleon. For the magnetic radii we obtain evaluating (5.60) between ground state wave functions

$$
r^2_p = \frac{3}{F_p(0)} \Big(b^2 + \frac{1}{4m_q^2} \Big), \; r^2_n = \frac{-2}{F_n(0)} \Big(b^2 + \frac{1}{4m_q^2} \Big).
\tag{5.62}
$$

For $m_q \approx 1/b$ one observes a 25% increase by the relativistic correction term $1/(4m_q^2)$. This appears to be a reasonable correction to the leading order b^2 term. However, the same relativistic correction will dramatically modify the impulse magnetic moments [38]

$$
\mu_p = 3\Big(1 - \frac{2}{3m_q^2 b^2} \Big), \; \mu_n = -2\Big(1 - \frac{2}{3m_q^2 b^2} \Big).
\tag{5.63}
$$

This results in a very small contribution of the valence quarks to the magnetic moments, namely $\mu_p = 0.885\ \mu_N$ and $\mu_n = -0.590\ \mu_N$ for the proton and neutron respectively. This is a 70% correction. If one takes this correction to the one-body current into account, most of the proton and neutron magnetic moments must come from nonvalence quark degrees of freedom. This is against the spirit of the nonrelativistic quark model where the main contribution to the magnetic moments is expected to come from the nonrelativistic single quark current, which by the choice of the effective quark mass already incorporates substantial relativistic corrections as one can see from the following plausibility argument.

A Plausibility Argument

Consider the nonrelativistic expansion of the relativistic kinetic energy of a single quark

$$\sqrt{m_q^2 + \boldsymbol{p}^2} = m_q + \frac{\boldsymbol{p}^2}{2m_q} + \cdots .$$

An estimate for p based on the uncertainty relation shows that $p \approx 1/b \approx m_q$, where b is the quark core radius. This means that the convergence radius of the series is practically zero and the series diverges. However, if we truncate the series after the $p^2/(2m_q)$ term and use the canonical value $p \approx m_q$, the numerical value for the relativistic kinetic energy is for the left hand side $\sqrt{2}\, m_q$ while for the right hand side it is $1.5\, m_q$; a six percent deviation (see also the review by Lucha et al. [4]). For the strange quark, the agreement between left and right hand side is within 3%. The inclusion of higher order terms, such as the $p^4/(8m_q^3)$ would only make the agreement worse. For example, with harmonic oscillator wave functions one obtains

$$\left\langle \frac{-p^4}{8m_q^3} \right\rangle = -\frac{5}{6}\frac{\langle T\rangle^2}{M_N},$$

where $\langle T\rangle$ can be read off Table 3.2. This amounts to 40% of the $\langle p^2/2m_q\rangle$ term.

Thus, despite its nonrelativistic appearance, the kinetic energy on the right hand side contains a considerable amount of relativistic corrections. This is due to the actual values of the constituent quark mass and the quark core radius. These arguments seem to be underlying the recent work of the Vienna group [117]. One should also recall that the lowest eigenenergy of a massless quark in the bag is (for bag radii that fit the magnetic moments) very close to the constituent quark mass [2]. It is conceivable that the lowest order terms in the kinetic energy, as well as in the one-body charge and current density are sufficient to account for perhaps the bulk of relativistic effects. Therefore, in the framework of the NRQM, it seems to be legitimate to ignore next-to-leading order corrections in all one-body operators (kinetic energy, one-body charge and current density) consistently. It is evident from (4.18) that one should not use next-to-leading order relativistic corrections in the one-body charge and current operator if one ignores them in the kinetic energy. We believe that these observations are mainly responsible for the many success of the NRQM, and constitute an important part of the NRQM paradigm.

We emphasize that these heuristic arguments are not completely satisfactory from a formal point of view. The neglect of relativistic corrections in the one-body operators formally destroys gauge and Lorentz invariance in any but the leading order $\mathcal{O}(m_q^{-1})$. This is the price we have to pay in order to avoid a drastic departure from the successful additive quark model where the bulk of the baryon magnetic moments comes from the leading order single-quark current without the $\mathcal{O}(m_q^{-3})$ terms.

Recently, the Helsinki group [118] has included the relativistic corrections to the one-body current operator and studied whether two-body exchange currents could explain the difference between the reduced impulse magnetic moments and the empirical values. One of their main findings is that the *phenomenological* exchange currents consistent with their phenomenological pseudoscalar Goldstone boson exchange interactions are small. This is in qualitative agreement with our findings [38] using analytic expressions for the exchange currents. Furthermore, they argue that about 50% of the proton and neutron magnetic moment is due to exchange currents associated with the phenomenological short-range part of the quark-quark interaction. While they are convinced that it *cannot be pseudoscalar meson exchange*, they state that the dynamical origin of the phenomenological short-range part of the quark-quark interaction is rather uncertain. They suggest a axial-vector short-range interaction leading to *axial vector* meson exchange currents that provide about 50% of the nucleon magnetic moments. In this way they obtain a simultaneous description of the axial properties and magnetic moments of the baryon octet.

This interpretation constitutes a radical departure from the successful additive NRQM, and is *inconsistent* with the NRQM paradigm that relativistic effects are implicitly taken into account by the choice of the effective quark mass, and effective quark core radius. Our calculation and interpretation of the axial coupling constant of the nucleon in the NRQM with axial exchange currents is given in Chapter 8.

6. Electromagnetic Properties of Hyperons

In this chapter we extend our investigation to the SU(3)-flavor sector and calculate some representative properties of strange hyperons. In the more general case that strange quarks are involved the charge operator for pointlike quarks is

$$e_i = \frac{e}{2}\left(B_i + S_i + \tau_z^{(i)}\right), \tag{6.1}$$

where B_i=1/3 is the baryon number and S_i is the strangeness of the i-th quark. This is the well-known Gell-Mann Nishijima relation applied to quarks. The expressions for the two-body current operators for different quark masses can be found in [39]. As in Chapt. 5, the generalized current operators have to be multiplied with the electromagnetic form factor of the constituent quark given in (4.13).

After having studied the low-energy electromagnetic properties of the nucleon and Δ in some detail, one should check whether the concepts developed in connection with the two-body exchange currents also work in the more general case of three quark flavors. As an isovector particle, the pion does not couple to the strange quark and the relative importance of pion, gluon and scalar exchange currents maybe considerably changed in comparison to the SU(2) case. In principle, this could tilt the subtle balance that led to the cancellations between different exchange current contributions in the nucleon magnetic moments. We will see that this is not the case. In what follows, the quadrupole moment of the Ω^-, the magnetic moments of the octet hyperons, and their magnetic radii are calculated.

6.1. *Quadrupole Moment of the Ω^-*

Experimentally, it is rather difficult to measure the quadrupole moment of the short-lived Δ-isobar with high precision. On the other hand, the Ω^--hyperon is stable with respect to strong interactions. Its mean life time is with $0.822(12)10^{-10}$ sec long enough to be captured into a Bohr-orbit of a heavy nucleus. The interaction of the electric quadrupole moment of the Ω^- with the nuclear electric field leads to a change of the binding energy of the Ω^- and a corresponding small level shift of the emitted X-rays compared to the case of a bound heavy particle without a quadrupole moment. The feasibility of such an experiment to measure the Ω^- quadrupole moment has been studied by Sternheimer and Goldhaber [119].

In the case of the Ω^- only the isoscalar part of the gluon exchange charge density survives. The isoscalar and isovector pion exchange charge density are both isospin-dependent and can thus not contribute. We then obtain

$$Q_{\Omega^-} = b^2 \frac{\delta_g(b)}{M_N}\left(\frac{m_u}{m_s}\right)^{5/2}, \tag{6.2}$$

where b is the oscillator parameter for the up and down quarks. The m_u/m_s mass ratios have been factored out in (6.2). In the SU(3) limit $m_u/m_s = 1$ and one has

$$Q_{\Omega^-} = Q_{\Delta^-}(\text{gluon}), \tag{6.3}$$

i.e. the quadrupole moment of the Ω^- is given by the gluon contribution to the Δ^- quadrupole moment in (5.21). For our standard parameter set of Table 1 we get $Q_{\Omega^-} = 0.022$ fm^2, a value not much different from the result $Q_{\Omega^-} = 0.028$ fm^2 obtained with configuration mixing alone [94]. Another calculation in the NRQM [120] gives $Q_{\Omega^-} = 0.057b^2 = 0.012$ fm^2 if our value $b_s = \sqrt{m_u/m_s}\, b_u = 0.475$ fm is used. In the SU(3) limit $m_s = m_u$ we obtain from (6.2) $Q_{\Omega^-} = 0.079$ fm^2, only somewhat larger than the corresponding limit taken in a relativistic bag model calculation which gives $Q_{\Omega^-} = 0.052$ fm^2 [115]. The quadrupole moment of the Ω^- provides due to the smallness of the impulse contribution and due to the absence of pionic contributions rather direct access to the effect of gluon exchange currents in baryons. A systematic study of the charge properties of the octet and decuplet hyperons remains to be done.

6.2. *Magnetic Moments of Octet Hyperons*

Table 6.1 clearly shows, that although the individual two-body current contributions are rather large,

Table 6.1. Single-quark (impulse) and exchange current contributions to the octet baryon magnetic moments. The first column μ_{imp} shows the impulse result which should be compared with our total result (μ_{tot}) (second to last column) and the experimental values(last column). The contributions of individual exchange currents are also listed using the same notation as in Table 5.4. All quantities are given in n. m. $\mu_N = e/(2M_N)$. The last line contains the transition magnetic moment for the decay $\Sigma^0 \to \Lambda$.

Octet	μ_{imp}	$\mu_{\text{gq}\bar{\text{q}}}$	μ_π	μ_{conf}	μ_σ	μ_{tot}	μ_{exp} [48]
Σ^+	2.867	0.615	0.017	–1.003	0.363	2.859	2.458 ± .010
Σ^-	–1.133	–0.361	0.017	0.444	–0.156	–1.190	–1.160 ± .025
Ξ^0	–1.467	–0.040	0.000	0.349	–0.175	–1.333	–1.250 ± .014
Ξ^-	–0.467	–0.219	0.000	0.028	–0.031	–0.689	–0.651 ± .003
Λ	–0.600	–0.018	0.000	0.116	–0.052	–0.554	–0.613 ± .004
$\Sigma^0 \to \Lambda$	1.732	0.154	0.000	–0.278	0.125	1.733	1.61 ± .08

especially the gluon and confinement part, the successful single-quark current prediction remains essentially intact. The inclusion of exchange currents generally leads to an improved agreement between theory and experiment. We stress, that no parameter is fitted to the baryon magnetic moments. All parameters were previously determined in Chapt. 3 in order to describe ground state baryon masses. After that they are fixed.

It is remarkable that the impulse approximation for the Ξ^-, which lies 28% off the experimental value $\mu_{\Xi^-} = -0.651\mu_N$, is considerably improved by the inclusion of exchange currents. In addition, the exchange currents cause that the absolute value of μ_{Ξ^-} is with $0.689\mu_N$ now bigger than the corresponding absolute value 0.554 for μ_{Λ^0} as required by experiment.

Because the isovector pion exchange currents do not couple to the strange quark, only the small isoscalar pion-pair current contributes to the charged $\Sigma^\pm$ magnetic moments. Pseudoscalar kaon exchange currents will also contribute to the hyperon magnetic moments. However, due to their larger mass and possibly due to similar cancellations between the kaon-pair current and the kaonic currents, we expect the effect of one-kaon exchange currents to be small and ignore them here. A recent estimate of the heavy pseudoscalar exchange current contribution to the magnetic moment of the Λ gives $\mu_\Lambda(\text{kaon}) \approx 0.03\mu_{\text{N}}$ [17] which seems to justfy their neglect.

Using only gluon, pion, and scalar exchange currents, we obtain again substantial cancellations between different exchange current terms. These are most pronounced for a quark core radius of $b \simeq 0.6$ fm. This value for b is also obtained from the variational principle (3.22). Our choice for $b \simeq 0.6$ fm is therefore the most consistent for the one-parameter trial wave function (3.15). This value is also the one that is required to obtain the empirical neutron charge radius according to (5.12).

Because we neglect various other effects, such as small anomalous magnetic moments of the quarks, relativistic corrections beyond the two-body currents included here, and configuration mixed wave functions, one should not expect a perfect agreement with the experimental data. The influence of these mechanisms is certainly nonneglible, as we have demonstrated in Sect. 5.3.1 and in [38] for the case of configuration mixing and in Sect. 5.3.5 for the case of relativistic corrections to the one-body current. For the magnetic moments of the nucleon we have previously shown that although configuration mixing considerably changes the relative importance of the various exchange currents, for example, gluon exchange currents are suppressed and pion exchange currents are enhanced, an almost complete cancellation is also observed if improved wave functions are used.

In summary, our main result is that gluon, pion and scalar two-body currents do not drastically modify the octet baryon magnetic moments from their additive quark model values due to cancellations between different exchange current contributions. There is one exception, the magnetic moment of the Ξ^- hyperon, which is decreased by some 40% due to the gluon-pair current and which is now in better agreement with the experimental value. We reiterate that we have employed standard vector, scalar and pseudoscalar exchange currents that satisfy the continuity equation with the corresponding exchange potentials. We use the same parameters here and in Chapt. 3 where they were used to calculate the ground state masses of the hyperons. Therefore, we think that our results provide some additional insight as to why the additive quark model is so successful in simultaneously explaining the hyperon masses and the magnetic moments of octet baryons. Although we believe that this success of the additive NRQM is not accidental, we are not certain whether this is a consequence of current conservation on the quasi-particle level. However, what these results teach us is that from the evaluation of spatial exchange currents connected with the two-body potentials one can extract important information as to the internal consistency of the chosen approach.

Table 6.2. Single-quark and exchange current contributions to the magnetic radii of octet baryons. All quantities are given in [fm^2] except for the total results, which are given in [fm].

Octet	r^2_{imp}	$r^2_{\text{gq}\bar{\text{q}}}$	r^2_{π}	r^2_{conf}	r^2_{σ}	$\sqrt{\lvert r^2_{\text{tot}}\rvert}$
Σ^+	0.702	0.116	0.003	–0.303	0.046	0.751
Σ^-	0.683	0.164	–0.008	–0.324	0.047	0.750
Ξ^0	0.706	0.015	0.000	–0.206	0.047	0.750
Ξ^-	0.370	0.162	0.000	–0.026	0.016	0.723
Λ	0.763	0.017	0.000	–0.172	0.034	0.801
$\Sigma^0 \rightarrow \Lambda$	0.704	0.048	0.000	–0.206	0.026	0.756

6.3. Magnetic Radii of Hyperons

Finally, the magnetic radii of the strange octet baryons are given in Table 6.2. With the exception of the Ξ^-, the total exchange current contribution to the magnetic radii is always negative but in absoulute magnitude quite small. As in the case of the hyperon magnetic moments we observe substantial cancellation of the various exchange currents. Due to the slightly smaller quark core radius of the strange quark, and due to the negative contribution of the exchange currents, the strange baryons have a slightly smaller magnetic size than the proton and neutron.

In this chapter only a few electromagnetic observables of hyperons have been calculated. A more complete analysis of the electromagnetic properties of the strange octet and decuplet hyperons including exchange currents has still to be done. Another important step in this direction has been recently made by studying the radiative decays of decuplet hyperons [43].

7. Electromagnetic Production of Nucleon Resonances

The reaction $\gamma + N \rightarrow N + \pi$ is next to Compton scattering $\gamma + N \rightarrow \gamma + N$ and pion-nucleon scattering $\pi + N \rightarrow \pi + N$ the most fundamental process involving the nucleon and the lightest strongly interacting particle, the pion. Because nucleons and pions are the fundamental building blocks for all of nuclear physics, it is important to have a detailed understanding of this reaction.

Electromagnetic pion production on the nucleon yields important information on the spatial and spin structure of the nucleon and its excited states and therefore on the dynamics of quarks in the non-perturbative region [121]. This information is complementary to the information coming from pion-nucleon scattering.

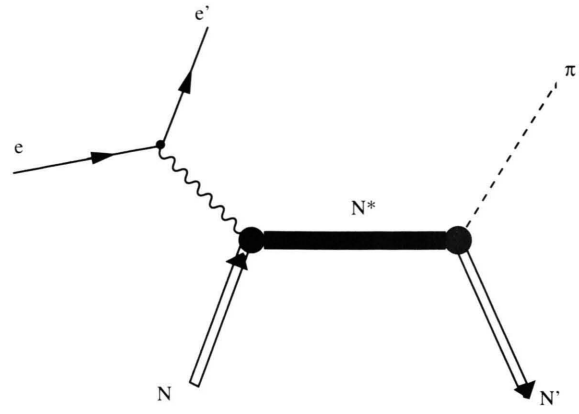

Fig. 7.1. Electromagnetic excitation of baryon resonances. The virtual photon probes the spatial and spin structure of the target and its excited states.

The most general structure of the Lorentz-invariant amplitude for this process was derived already some time ago by Chew, Goldberger, Low, and Nambu [122]. It contains eight partial amplitudes $F_1 \cdots F_8$ multiplying the eight nonrelativistic invariants for this process. These are usually referred to as CGLN amplitudes. By the requirement of gauge invariance two amplitudes can be eliminated. In the case of real photons only four amplitudes $F_1 \cdots F_4$ are needed. The partial amplitudes $F_1 \cdots F_6$ can be further decomposed into electromagnetic pionproduction multipoles [123], describing the absorption of a photon with a definite multipolarity and the emission of a pion in a definite angular momentum state. These pionproduction amplitudes are the relevant quantities that one tries to extract from the measured ineleastic electron-nucleon scattering cross section.

The inclusive inelastic electron-nucleon scattering cross section contains an incoherent sum over the different pionproduction multipoles. It is therefore extremely difficult to extract reliable information on individual small multipoles from the inclusive cross section alone. On the other hand, in exclusive experiments, where the pion is detected in coincidence with the scattered electron, the cross section involves products of different pionproduction multipoles. This allows to extract small multipoles, such as L_{1+} or S_{1+} from the data. These contain the information on the deformation of the nucleon. We will not discuss the

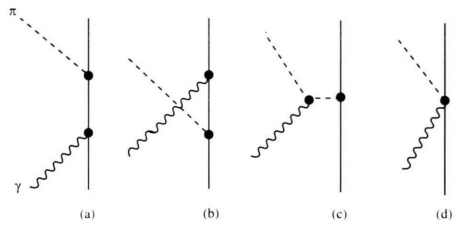

Fig. 7.2. The Born terms in photo-pionproduction (a) quark pole term, (b) crossed term, (c) pion-pole term, (d) contact term. These diagrams must be added coherently to the resonance diagram of Figure 7.1.

rather involved general structure of the coincidence cross section here and refer to a recent review [123].

Aside from the resonance amplitude of Fig. 7.1, the amplitudes for nonresonant pion production, i. e. the Born terms of Figure 7.2. should also be calculated within the same model, in order to compare directly with the experimental data. If the Born terms are simultaneously one avoids the uncertainties related to the extraction of the resonance amplitudes [124]. The Born terms have previously been investigated in the NRQM [125] near threshold but to our knowledge not yet for finite momentum transfers. In addition, the few existing calculations are solely based on the impulse approximation, i. e. pion emission and pion absorption on the same quark. A parallel calculation of the Born terms including two-body exchange currents provides an important consistency check of the model. As a first step, we calculate only the left hand vertex of Figure 7.1. The calculation of the full pionproduction cross section in the quark model remains a future challenge.

Since the early systematic analyses of the data in terms of the quark model [7], it has become customary to separate the electromagnetic resonance production part (left hand side in Fig. 7.1 from the hadronic decay part of the resonance, which is in principal known from pion-nucleon scattering. The resonance production part is most conveniently described in terms of the helicity amplitudes originally introduced in [7].

7.1. Quark Model Description

The qualitative description of photoproduction cross sections of a number of nucleon resonances constitutes one of the early successes [7], of the nonrelativistic quark model. In the NRQM, the suppression of the $A^p_{1/2}$ amplitude for the excitation of the $D_{13}(1520)$ resonance, seen in π^0 production off the proton for forward angles, could be explained by a destructive interference between the spin- and convection parts of the single-quark current.

Table 7.1. $A_{1/2}$ and $A_{3/2}$ helicity amplitudes for the electromagnetic excitation of the three lowest-lying nucleon resonances: $\gamma + N \rightarrow \Delta(1232)$, $\gamma + N \rightarrow N^*(1440)$ and $\gamma + N \rightarrow N^*(1520)$ for proton and neutron targets. The first row contains the calculations of Koniuk and Isgur [128] using a one-gluon exchange potential and a $2\hbar\omega$ configuration space to diagonalize the Hamiltonian. The second row contains the results of Capstick [126] using an enlarged configuration space ($7\hbar\omega$) as well as relativistic corrections in the one-body current. The numbers are given in the usual units [10^{-3} GeV$^{-1/2}$].

	$A^p_{1/2}$	$A^p_{3/2}$	$A^n_{1/2}$	$A^n_{3/2}$
$\Delta(1232)$	−103	−179	−103	−179
$\Delta(1232)$	−108	−186	−108	−186
Exp.	−141±5	−257±8	−141±5	−257±8
$N^*(1440)$	−24	—	16	—
$N^*(1440)$	4	—	−6	—
Exp.	−72±9	—	52±25	—
$N^*(1520)$	−23	128	−45	−122
$N^*(1520)$	−15	134	−38	−114
Exp.	−22±10	167±10	−65±13	−144± 14

For this cancellation a small quark core radius of about $b = 0.5$ fm was required. Apart from many qualitative successes of the NRQM, there are also cases where the model strikingly fails to describe the experimental data. In particular, for the excitation of the $\Delta(1232)$- and the $N^*(1440)$ resonances, large discrepancies remain that could not be removed by including relativistic corrections in the single-quark current [8, 126] (see Table 7.1).

A detailed comparison between theory and experiment is ideally performed on the level of single electromagnetic pion production multipoles [123] describing the full process of Fig. 7.1 for one particular multipolarity of the photon. On the other hand, with the help of the helicity formalism [7] one can separate the electromagnetic excitation part from the strong decay of the resonance. In this formalism [127], the inclusive cross section can be decomposed into a transversal and longitudinal part

$$\frac{\mathrm{d}^3\sigma}{\mathrm{d}\Omega_L \mathrm{d}E_L} = \Gamma_t(\sigma_T + \epsilon\sigma_L), \tag{7.1}$$

where Γ_t is the virtual photon flux and ϵ is the photon polarisation. Both quantities Γ and ϵ can be expressed

through the kinematic variables of the virtual photon [127]. The latter are external variables that can be experimentally controlled. Using the helicity amplitudes the transversal and longitudinal cross section are given as

$$\sigma_T = (C^{\mathrm{I}}_{\pi N})^2 \frac{2xM}{\Gamma_{\mathrm{tot}} W} \left(|A_{1/2}|^2 + |A_{3/2}|^2\right), \qquad \sigma_L = (C^{\mathrm{I}}_{\pi N})^2 \frac{16xM}{\Gamma_{\mathrm{tot}} W} |S_{1/2}|^2. \tag{7.2}$$

Here, $C^{\mathrm{I}}_{\pi N}$ is the Clebsch-Gordan coefficient for the coupling of the πN final state to isospin I of the intermediate resonance. The branching ratio $x = \Gamma_{\pi N}/\Gamma_{\mathrm{tot}}$ describes the fraction of pionic decay of the resonance with respect to the total decay width of the resonance. M is the mass of the nucleon, and W the center of mass energy of the photon-nucleon system. At the resonance position one has $W = M_{\mathrm{R}}$, where M_{R} is the mass of the resonance. The transversal (A) and longitudinal or scalar (S) helicity amplitudes entering in (7.2) are defined as follows

$$A_\lambda = -e\sqrt{\frac{2\pi}{\omega}} \langle N^*,\ M'_J = \lambda | \boldsymbol{\epsilon} \cdot \boldsymbol{J} | N,\ M_J = \lambda - 1 \rangle, \tag{7.3}$$

where $\lambda = 3/2(1/2)$ if the photon spin is parallel (antiparallel) to the spin of the target.

Likewise the scalar helicity amplitude is defined as

$$S_\lambda = -e\sqrt{\frac{2\pi}{\omega}} \langle N^*,\ M'_J = \lambda | \epsilon^0 J_0 | N,\ M_J = \lambda - 1 \rangle. \tag{7.4}$$

Here, $\boldsymbol{J}$ is the current and J_0 the charge operator of the interacting quark system.

In order to calculate the helicity amplitudes in the framework of the constituent quark model, the electromagnetic current operator as well as the nucleon and resonance wave functions are needed. Almost all theoretical predictions in the NRQM are based on the single-quark transition model. These impulse approximation calculations contain the interaction only in the wave function. However, this approximation, violates the continuity equation for the electromagnetic current as was pointed out at the beginning of Section 4.2. This inconsistency can be removed by including two-body exchange currents between quarks, which is particularly important for models that contain pions, where the continuity equation is already violated in lowest order if only single-quark currents are used. In view of the precise data expected from various electron accelerator facilities, it is important to go beyond the single-quark transition model. The inclusion of two-body exchange currents puts the quark model predictions on a firmer basis.

Table 7.2. The $A_{1/2}$ and $A_{3/2}$ helicity amplitudes for the process $\gamma + p \rightarrow \Delta^+(1232)$, including two-body exchange currents: i: impulse; g: gluon; $\pi q\bar{q}$: pion pair; $\gamma\pi\pi$: pionic; σ: σ-meson; c: confinement; t: total; t = i + g + π + σ + c. The helicity amplitudes for a neutron target are the same. The M1 and E2 parts of the helicity amplitudes as well as their sum are listed. The experimental helicity amplitudes are $A_{3/2} = -257 \pm 8$ and $A_{1/2} = -141 \pm 5$ [48]. A previous analysis gave $A_{1/2} = -84 \pm 5$ [129]. Our results are given at $\boldsymbol{q}^2 = 0$. All entries are given in standard units of [10^{-3} GeV$^{-1/2}$].

	A_{i}	A_{g}	$A_{\pi q\bar{q}}$	$A_{\gamma\pi\pi}$	A_σ	A_{c}	A_{t}	A_{exp}
$A^{1/2}_{p\rightarrow\Delta^+}$(M1)	−115.9	−11.5	16.7	−23.8	−11.9	45.0	−101.5	−146.5
$A^{1/2}_{p\rightarrow\Delta^+}$(E2)	0.0	7.1	3.4	0.0	0.0	0.0	10.5	5.5
$A^{1/2}_{p\rightarrow\Delta^+}$(T)	−115.9	−4.4	20.1	−23.8	−11.9	45.0	−90.9	−141.0
$A^{3/2}_{p\rightarrow\Delta^+}$(M1)	−200.7	−20.0	28.8	−41.3	−20.6	77.9	−175.8	−253.8
$A^{3/2}_{p\rightarrow\Delta^+}$(E2)	0.0	−4.1	−2.0	0.0	0.0	0.0	−6.1	−3.2
$A^{3/2}_{p\rightarrow\Delta^+}$(T)	−200.7	−24.1	26.8	−41.3	−20.6	77.9	−181.9	−257.0

7.2. $\gamma + N \rightarrow \Delta$ Helicity Amplitudes

In this section we consider the helicity amplitudes for the transition $\gamma + N \rightarrow \Delta$. The transverse helicity amplitudes are defined as

$$A_{1/2} = -e\sqrt{2\pi/\omega} \langle \Delta\, J_z = 1/2 | \boldsymbol{\epsilon} \cdot \boldsymbol{J} | N\, J_z = -1/2 \rangle, \qquad A_{3/2} = -e\sqrt{2\pi/\omega} \langle \Delta\, J_z = 3/2 | \boldsymbol{\epsilon} \cdot \boldsymbol{J} | N\, J_z = 1/2 \rangle \tag{7.5}$$

where $e^2 = 1/137$.

In Table 7.2 we show our results for the transverse helicity amplitudes. For the $N \rightarrow \Delta$ transition, only M1 and E2 multipoles contribute. In this work we calculate the E2 contribution from the charge density using Siegert's theorem, which relates the transverse electric multipoles to the Coulomb multipoles in the long wave-length limit. The advantage of using Siegert's theorem clearly outweighs the error induced by using the long wave-length limit in a situation

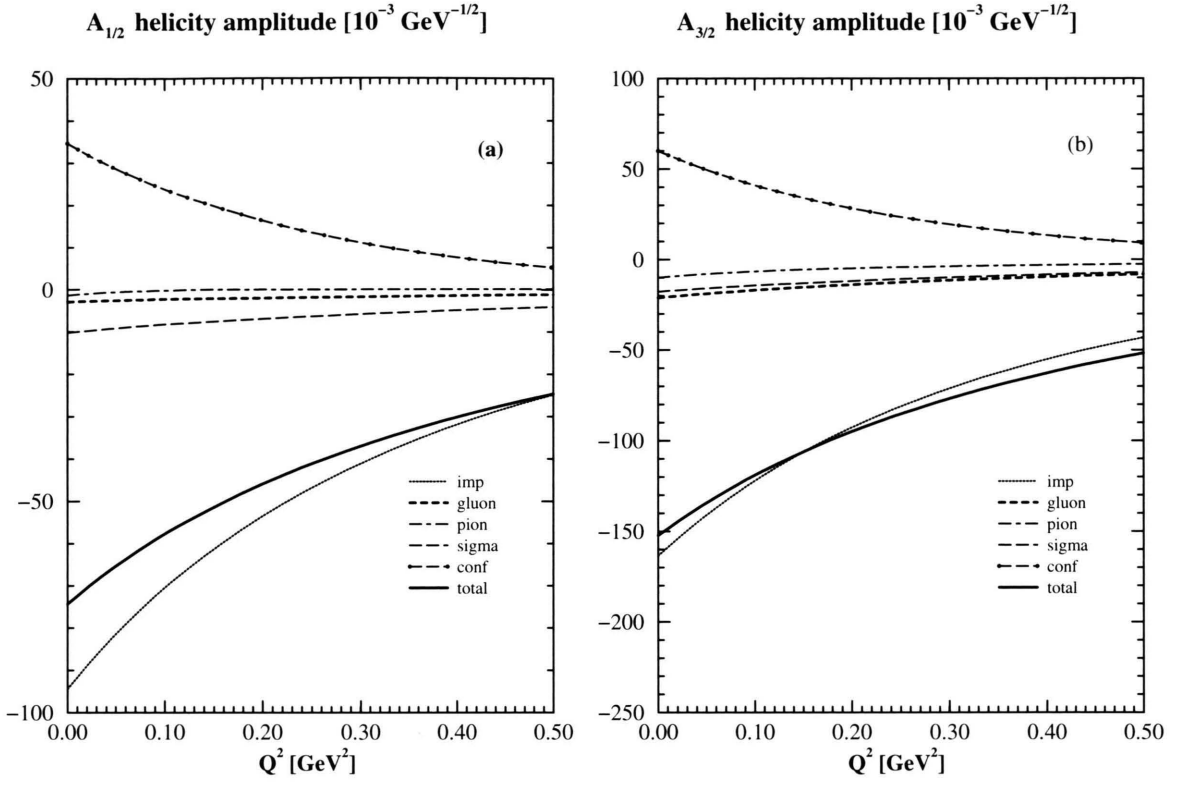

Fig. 7.3. The $A_{1/2}(Q^2)$ (a) and $A_{3/2}(Q^2)$ (b) helicity amplitudes as a function of the four-momentum transfer Q. Here, we keep $\omega_{\rm cm}$ = 258 MeV fixed and vary the three-momentum transfer $\boldsymbol{q}$. The individual two-body exchange current contributions are shown separately.

which involves a substantial momentum transfer of $q \approx M_\Delta - M_N$. We will come back to this point in Section 7.4.

The relation between the multipole form factors and the helicity amplitudes is in the center of mass frame [65]

$$\begin{aligned} A_{1/2}(\boldsymbol{q}^2) &= -\sqrt{\pi\omega}\left(\frac{e}{2M_N}\right) \\ &\quad \cdot \left(F_M^{N\to\Delta}(\boldsymbol{q}^2) + 3\,\frac{M_N\omega}{6}\,F_{\rm Q}^{N\to\Delta}(\boldsymbol{q}^2)\right), \\ A_{3/2}(\boldsymbol{q}^2) &= -\sqrt{3\pi\omega}\left(\frac{e}{2M_N}\right) \\ &\quad \cdot \left(F_M^{N\to\Delta}(\boldsymbol{q}^2) - \frac{M_N\omega}{6}\,F_{\rm Q}^{N\to\Delta}(\boldsymbol{q}^2)\right), \end{aligned} \tag{7.6}$$

where $F_{\rm M}^{N\to\Delta}$ and are the magnetic and $F_{\rm Q}^{N\to\Delta}$ quadrupole transition form factors, which are normalized to the magnetic (Sect. 4.4) and quadrupole (Sect. 4.2) transition moments. The relation between these standard definitions [81] for the magnetic dipole form factor $F_M^{N\to\Delta}$ and charge quadrupole form factor $F_{\rm Q}^{N\to\Delta}$, and the dimensionless $G_{\rm M1}$ and $G_{\rm E2}$ used in [65, 134] is:

$$\begin{aligned} G_{\rm M1}(\boldsymbol{q}^2) &= \left(\sqrt{6}/2\right)\,F_M^{N\to\Delta}(\boldsymbol{q}^2), \\ G_{\rm E2}(\boldsymbol{q}^2) &= -\frac{\omega M_N\sqrt{6}}{12}\,F_{\rm Q}^{N\to\Delta}(\boldsymbol{q}^2). \end{aligned} \tag{7.7}$$

Note that in the relation between the charge quadrupole transition form factor $F_{\rm Q}^{N\to\Delta}$ and the transverse electric quadrupole form factor $G_{\rm E2}$, an additional factor $\omega\sqrt{3}/(|\boldsymbol{q}|\sqrt{2})$ due to Siegert's

theorem (see Sect. 7.4) in addition to a ratio of Clebsch-Gordan coefficients [10] enters.

In Fig. 7.3, we show the four-momentum dependence of the helicity amplitudes. We observe that exchange currents contribute to the $A_{3/2}$ amplitude between 7% at $Q^2 = 0$ and 19% of the impulse result at $Q^2 = 0.5$ GeV^2. The small total exchange current effect at $Q^2 = 0$ is firstly due to cancellations of different exchange current contributions to $F_M^{N\to\Delta}$. Secondly, the exchange current contributions to $F_M^{N\to\Delta}$ and $F_Q^{N\to\Delta}$ form factors interfere destructively in the $A_{3/2}$ amplitude (see also Table 7.2). On the other hand, in the $A_{1/2}$ amplitude, the exchange current dominated $F_Q^{N\to\Delta}$ form factor enters with an additional weight factor of three and the exchange current contributions to $F_M^{N\to\Delta}$ and $F_Q^{N\to\Delta}$ form factors interfere constructively. Therefore, for small momentum transfers the $A_{1/2}$ helicity amplitude is appreciably influenced by exchange currents. For example, at $Q^2 = 0$ their contribution is 27% of the impulse result.

There have been previous calculations of two-body current contributions to the $N \to \Delta$ transition in the CQM. Ohta [31], calculates two-body currents resulting from minimal substitution in the one-gluon exchange and a scalar confinement potential as well as relativistic corrections to the single-quark current but does not consider pion exchange currents. In this early calculation, large anomalous magnetic moments for the quarks $\kappa = 1.83$ were used. This leads to an unconventional nonrelativistic impulse result $A_{3/2}(\text{NRI}) = -505\,10^{-3}$ GeV$^{-1/2}$ which is drastically reduced by large relativistic corrections to the single-quark current, $A_{3/2}(\text{RCI}) = 97\,10^{-3}$ GeV$^{-1/2}$, and an even larger contribution of the two-body currents, $A_{3/2}(\text{EXC}) = 189\,10^{-3}$ GeV$^{-1/2}$. However, large anomalous magnetic moments for the constituent quarks are in conflict with general current algebra arguments [66] and with explicit calculations in the Nambu-Jona-Lasinio model [3].

Robson [36] has included the pion pair and pionic exchange currents resulting from minimal substitution in the one-pion exchange potential but ignores gluons. He finds that the pionic current is small and neglects this contribution. In contrast, our calculation shows that the pionic current is big and negative. It completely cancels the positive pion pair-current. The total pion contribution has thus the same sign as the impulse result. This cancellation between pion pair and pionic currents is closely connected with a similar cancellation in the nucleon magnetic moments [38] (see also Table 5.4). Another difference is that in [36] the E2 contribution to the helicity amplitudes has been neglected. However, it is in the E2 amplitude where the exchange currents are most clearly seen.

[10] When expressing the transverse helicity amplitudes via the electromagnetic transition form factors one has to pay attention to the different total angular momentum projections required by both definitions. The transition form factors require according to (5.17) and (5.35) maximal projections $M_J = J = 1/2$ and $M_J' = J' = 3/2$, while the $A_{1/2}$ and $A_{3/2}$ helicity amplitudes of (7.5) require different projections [101].

7.3. *The E2/M1 Ratio and the Deformation of the Nucleon*

Unlike, the quadrupole moment of the $\Delta(1232)$ and the $N \to \Delta(1232)$ transition quadrupole moment, the E2/M1 ratio has the advantage that possible experimental uncertainties related to the unknown background cancel in the ratio. From the experimental point of view, the E2/M1 ratio seems to be the quantity that is best suited to extract information on the deformation of the nucleon. Using the E2/M1 ratio as defined by Kumano [130] we obtain

$$\frac{\text{E2}}{\text{M1}} = \frac{1}{3}\frac{A_{1/2}(\text{E2})}{A_{1/2}(\text{M1})} = \frac{\omega M_N}{6}\frac{Q_{N\to\Delta}}{\mu_{N\to\Delta}} = -0.035. \tag{7.8}$$

Our predicted E2/M1 ratio is somewhat larger than the recent experimental value $(\text{E2/M1})_{\text{exp}} = -0.025 \pm 0.002$ [131] extracted from recent photopionproduction data taken at the Mainz Microtron (MAMI). The recent data from the Laser Electron Beam Gamma Source (LEGS) collaboration at Brookhaven seem to favor a larger value $(\text{E2/M1})_{\text{exp}} = -0.030 \pm 0.005$ [100].

Comparing with other theoretical predictions, our result agrees well with Skyrme model results, $\text{E2/M1} \simeq -(0.02 - 0.05)$ [101] and $\text{E2/M1} = -0.037$ [132] and dynamical models for photopionproduction $\text{E2/M1} = -0.031$ [133]. Note that our E2 amplitude $G_{\text{E2}}(0) = -\frac{\omega M_N \sqrt{6}}{12} Q_{N\to\Delta} = 0.105$ compares reasonably well with the phenomenological analysis of Devenish et al. [98], which gives $G_{\text{E2}}(0) = 0.02 G_{\text{M1}}(0) \approx 0.1$ [65]. Our prediction is based on the parameter-free result (5.29) which relates the transition quadrupole moment to the neutron charge radius.

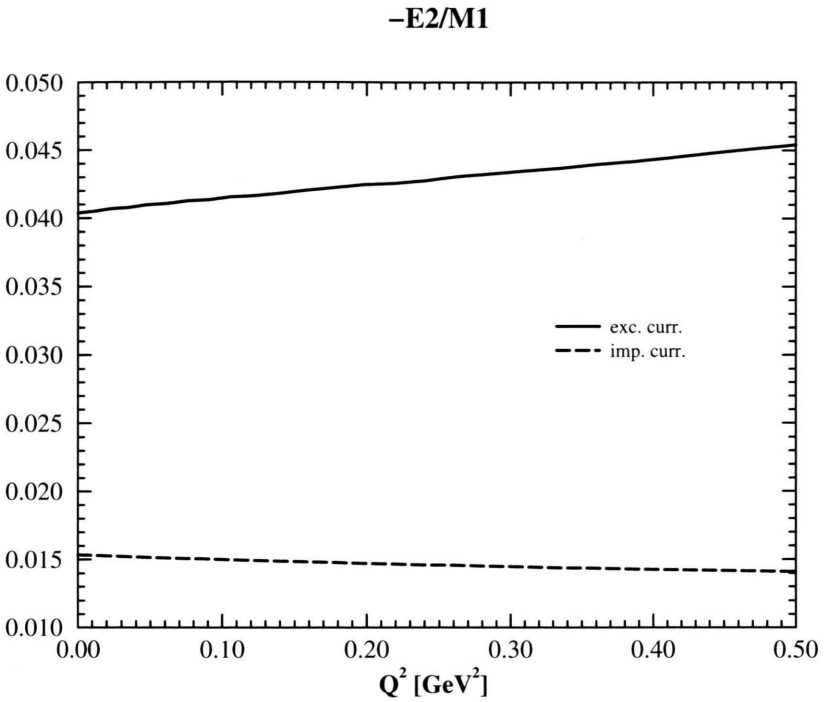

Fig. 7.4. The E2/M1 ratio for finite momentum transfers. The E2 amplitude is calculated from the total charge density according to Siegert's theorem. This approximation becomes unreliable beyond $Q^2 \geq 0.2$ GeV^2. An impulse calculation using the admixture coefficients of Giannini [65] is also shown.

Table 7.3. Various model predictions for the E2/M1 ratio (in percent) in the $\gamma + N \rightarrow \Delta$ transition. The most recent experimental value extracted from photo-pionproduction data at MAMI in Mainz is E2/M1 = $-2.5(2)\%$ [131], while the measurement of the LEGS collaboration at the Brookhaven National Laboratory gives E2/M1 = $-3.0(5)\%$ [100].

Model	E2/M1
Cloudy Bag [135]	–1.8
Skyrme [101]	–(2 - 5)
Skyrme [132]	–3.7
Lattice [110]	+(3 ± 8)
eff. Lagr. [136]	–1.5
eff. Ham. [133]	–3.1
NRQM [96]	–0.4
NRQM [134]	–2.0
NRQM [41]	–3.5
Disp. Relation [99]	–3.5

Figure 7.4 shows the calculated E2/M1 ratio as function of the four momentum transfer squared Q^2.

Very recently, there has been a new determination of the E2/M1 ratio, applying the speed plot technique to fixed-t dispersion relations for the photo-pionproduction amplitudes. The authors include new photo-pionproduction data from the continuous electron beam facilities in Mainz and Bonn. They obtain for the pure resonance part E2/M1 = -0.035 [99] in excellent agreement with our quark model prediction including exchange currents. However, several caveats are in order here. First, the inclusion of configuration mixing would certainly modify the numerical value for this ratio. We expect the modification to be less than some 20%. This estimate is based on our discussions in Sect. 4.1 and 4.2. Second, we underestimate the empirical $N \rightarrow \Delta$ transition magnetic moment. Third, the extraction of a $\gamma N \rightarrow \Delta$ photocoupling from the photo-pionproduction data is not model-independent and it would be much safer to calculate the complete photo pionproduction multipoles before comparing with experiment [124]. Nevertheless, our prediction of a relatively *large* E2/M1 ratio emphasizes the important role of nonvalence quark degrees of freedom, in the transition quadrupole moment irrespective of whether one refers to them as pion cloud of the nucleon, sea-quark degrees of freedom, or exchange currents. Establishing this interpre-

tation in the framework of the NRQM is one of the main results of this work.

7.4. *Siegert's Theorem and Gauge Invariance*

Already some time ago it was pointed out [134] that a calculation of the E2 multipole in the $N \rightarrow \Delta$ transition via the one-body charge density gives results that substantially differ from the corresponding results using the transverse current density. This constitutes a violation of the gauge invariance condition

$$q_\mu J^\mu = \omega\rho - \boldsymbol{q} \cdot \boldsymbol{J} = 0, \tag{7.9}$$

according to which both calculations should give the same answer at the unphysical pseudothreshold (Siegert limit) $q_\mu^2 = (M_\Delta - M_N)^2$ [123] where the Δ is produced at rest $|\boldsymbol{q}| = 0$.

Numerically, the violation of gauge invariance is not small leading to vastly different E2/M1 ratios depending on whether the charge or the current operator is used. For example, compare the result of [96] based on the one-body current density with the result of [134] based on the one-body charge density (Table 7.3). In fact, a calculation based on the one-body spatial current density and the admixture coefficients of [128] yields using the expression given in [134] an E2 transition moment $G_{\mathrm{E2}}^{\mathrm{imp}}(\mathrm{current}) = 0.0023$. This differs by an order of magnitude from the corresponding result based on the one-body charge density $G_{\mathrm{E2}}^{\mathrm{imp}}(\mathrm{charge}) = 0.025$, as was first observed by Drechsel and Giannini [134]. The reason for this discrepancy which constitutes a severe violation of gauge invariance is analyzed in this section.

The authors of [134] state that a calculation of the E2 transition strength via the one-body charge density is to be preferred, because it is less sensitive to a truncation of configuration space. In actual quark model calculations, the harmonic oscillator configuration space usually includes only two ($N = 2$) major shells involving at most $2\hbar\omega$ excitations with respect to the ground state. According to [134] this truncation of configuration space at $2\hbar\omega$ excitations induces a severe error in a calculation based on the transverse current density while it constitutes a reasonable approximation for a calculation based on the one-body charge density. The different sensitivity of the transition matrix elements of the charge and current operator with respect to a truncation of the model space is attributed to the different behavior of the charge and current operators under hermitean conjugation and time reversal. Furthermore, it is stated that in a sufficiently large configuration space both calculations should give the same answer.

The main findings of [134] concerning the different answers obtained from a calculation using the charge and current density were corroborated by Bourdeau and Mukhopadhyay [137]. These authors also find that a calculation based on the one-body charge density is to be preferred because it is less sensitive to a truncation of the model space. Similar conclusions were reached in [30] were it was shown that the violation of gauge invariance with one-gluon exchange alone amounts to a factor 2 - 3 depending on the admixture coefficients while it is more severe if both gluons *and pions* are included. Later Capstick and Karl [138] enlarged the model space to test the conclusions of [134, 137]. They pointed out that the truncation of configuration space may not be the only reason for the observed strong violation of current conservation. Following a suggestion of Close and Li, they argue that one should consider relativistic corrections to the quark transition operator consistently up to order $\mathcal{O}(m_{\mathrm{q}}^{-2})$. While there is general agreement that the truncation of configuration space of typical shell model calculations is partly repsonsible for the observed violation of gauge invariance an explicit evaluation of the spatial exchange currents implicitly included by the calculation of G_{E2} via the one-body charge density has never been done.

We will show that the main reason for the large difference between a calculation based on the one-body charge density and one based on the one-body current density is that the former includes the dominant spatial exchange current corrections by virtue of Siegert's theorem [139]. Before we explain this in greater detail let us briefly recall the content of Siegert's theorem.

Siegert's theorem states that the matrix elements of the transverse electric multipole operators ($T^{\mathrm{E}\,J}$) as derived from the spatial current density, can in the low-momentum transfer limit be calculated from the corresponding matrix elements of the Coulomb multipole ($T^{\mathrm{C}\,J}$) operators that are based on the charge density:

$$\begin{aligned}\langle f|T^{\mathrm{E}\,J}(|\boldsymbol{q}| \rightarrow 0)|i\rangle = &- \frac{\omega}{|\boldsymbol{q}|}\sqrt{\frac{J+1}{J}} \\ &\cdot \langle f|T^{\mathrm{C}\,J}(|\boldsymbol{q}| \rightarrow 0)|i\rangle\,,\end{aligned} \tag{7.10}$$

where ω is the energy difference between initial and final states and equals the energy transfer of the photon. J is the total angular momentum of the photon. We will not rederive Siegert's theorem here but state the necessary prerequisites for its derivation [140]:

- The continuity equation for the electromagnetic current (4.14), which relates the total charge density ρ, the total current density $\boldsymbol{J}$ and the total Hamiltonian of the system.
- The use of exact eigenstates $|i\rangle$ and $|f\rangle$ of the Hamiltonian H.
- The low-momentum transfer limit $\boldsymbol{q} \to 0$.

In actual quark model calculations of the $N \to \Delta$ quadrupole transition each of these requirements for Siegert's theorem is violated to some extent. First, the low-momentum transfer limit cannot be reached in reality because $\omega = |\boldsymbol{q}|$ and $\omega \approx 300$ MeV in the photoproduction and $q_\mu^2 < 0$ in electroproduction of the Δ. Second, in most calculations, the true eigenstates of the Hamiltonian are rarely obtained in shell-model calculations using a finite basis of trial wave functions. At best one has approximate eigenstates. The use of approximate eigenfunctions of the Hamiltonian H violates Siegert's theorem and leads to different results for a calculation based on the charge density compared to one employing the current density. However, we will show that, the most important reason why Siegert's theorem is violated is the severe violation of the continuity equation (4.14) for the electromagnetic current, if only the spatial one-body current density is used on the left hand side of (7.10).

The continuity equation for the electromagnetic current involves the total charge, the total current and the total Hamiltonian of the interacting quark system. In many applications of Siegert's theorem the continuity equation is used to express the divergence of the spatial *one-body* current density through the commutator of the *total* Hamiltonian with the one-body charge density. Thereby one has implicitly included spatial two-body currents, because in leading order one has according to (4.14)

$$\begin{aligned} &\left[H, \rho_{[1]}(\boldsymbol{r}_i, \boldsymbol{q}) + \rho_{[1]}(\boldsymbol{r}_j, \boldsymbol{q})\right] \qquad (7.11)\\ &= \boldsymbol{q} \cdot \left(\boldsymbol{J}_{[1]}(\boldsymbol{q}, \boldsymbol{r}_i) + \boldsymbol{J}_{[1]}(\boldsymbol{q}, \boldsymbol{r}_j) + \boldsymbol{J}_{[2]}(\boldsymbol{q}, \boldsymbol{r}_i, \boldsymbol{r}_j)\right) . \end{aligned}$$

Taking matrix elements on both sides of (7.11) and using that the states $|i\rangle$ and $|f\rangle$ are exact eigenstates of H with eigenvalues E_i and E_f respectively gives

$$\begin{aligned} &\langle f| \left[H, \rho_{[1]}(\boldsymbol{r}_i, \boldsymbol{q}) + \rho_{[1]}(\boldsymbol{r}_j, \boldsymbol{q})\right] |i\rangle \qquad (7.12)\\ &= \boldsymbol{q} \cdot \langle f| \left(\boldsymbol{J}_{[1]}(\boldsymbol{q}, \boldsymbol{r}_i) + \boldsymbol{J}_{[1]}(\boldsymbol{q}, \boldsymbol{r}_j) + \boldsymbol{J}_{[2]}(\boldsymbol{q}, \boldsymbol{r}_i, \boldsymbol{r}_j)\right) |i\rangle\\ &= (E_f - E_i) \langle f|\rho_{[1]}(\boldsymbol{r}_i, \boldsymbol{q}) + \rho_{[1]}(\boldsymbol{r}_j, \boldsymbol{q})|i\rangle . \end{aligned}$$

Obviously, although one is evaluating matrix elements of the one-body charge density operator $\rho_{[1]}$ one has implicitly included spatial two-body currents according to (7.12). This fact has long been known [21], and it is widely recognized that Siegert's theorem provides a convenient way to include the two-body exchange currents connected with the two-body potentials according to (4.19) in electric multipole transitions.

We would like to add the following comment pertaining to the use of (7.10) when calculating the E2 part of the electromagnetic $N \to \Delta$ transition. It is well known that the color-magnetic and tensor interactions are mainly responsible for respectively the $N - \Delta$ mass splitting and the D-states in the nucleon and Δ. The effect of spin-orbit forces on ground state mass-splittings and on the D-state admixtures is negligible. Furthermore, one observes that the tensor force and the color-magnetic interaction in V^{OGEP} of (3.2) commute with the one-body charge density in (7.11). It would however be dangerous to conclude that there is no corresponding exchange current in (7.12) connected with V^{OGEP}. In fact, the spin-orbit terms in (3.2) give rise to a spatial two-body gluon exchange current [11]. Although the contribution of spin-orbit terms to the $N - \Delta$ mass splitting or the excited D-state admixtures is negligible, the corresponding exchange currents are important and are implicitly included via (7.12).

From Table 7.4 it is evident that the implicit inclusion of spatial two-body gluon and pion exchange currents by virtue of Siegert's theorem explains the difference of the results between the two different ways of calculating the E2 amplitude. The remaining discrepancy must be attributed to the finite momentum transfer and to the truncation of the model space resulting in only approximate eigen states. Therefore, we conclude that gauge invariance is approximately restored even in a truncated model space provided that in the spatial current density the two-body exchange currents required by (7.11) are explicitly taken into account.

[11] It was previously shown that the spin-orbit generated one-gluon exchange current is closely related to the gluon-pair current $\boldsymbol{J}_{\mathrm{gq\bar{q}}}$ [28].

Table 7.4. The transverse E2 transition form factor at $q^2 = 0$: $G_{E2}(0)$ as in (7.7) for the $\gamma + p \rightarrow \Delta^+$ transition calculated with (i) the one-body charge density $\rho_{[1]}$ and Siegert's theorem, (ii) with the spatial current density $\boldsymbol{J}_{[1]}$ for (a) the Isgur-Karl model (no π) (b) a model including one-gluon and one-pion exchange between quarks (π). The admixture coefficients are taken from [37]. The difference between the first two rows is almost completely explained by the total two-body exchange current contribution $\boldsymbol{J}_{[2]}$ (last row). According to (7.12), the spatial two-body exchange current contribution $\boldsymbol{J}_{[2]}$ is implicitly included in the calculation based on $\rho_{[1]}$ and Siegert's theorem. The experimental range for the E2 transition form factor at $\mathbf{q}^2 = 0$ is: $G_{E2} = 0.055(51)$ [48], $G_{E2} = 0.095(16)$ [80, 98], $G_{E2} = 0.108$ [99]. The recent Mainz measurement gives $G_{E2} = 0.12(2)$ [131], while the LEGS data give $G_{E2} = 0.133(20)$ [100]. Note that both calculations severely underestimate the empirical result for $G_{E2}(0)$.

	no π	π
$\rho_{[1]}$	0.0153	0.0165
$\boldsymbol{J}_{[1]}$	0.0090	0.0058
difference	0.0063	0.0107
$\boldsymbol{J}_{gq\bar{q}}$	0.0059	0.0039
$\boldsymbol{J}_{\pi q\bar{q}}$	0.0000	0.0103
$\boldsymbol{J}_{\gamma\pi\pi}$	0.0000	–0.0037
$\boldsymbol{J}_{[2]}$	0.0059	0.0105

This is not to say that the gauge-invariant calculation based on the one-body charge density or the total spatial current density including exchange currents is in agreement with the experimental result. In fact, even then a large discrepancy remains between the experimental of result $G_{E2}(\text{exp}) \approx 0.1$ and the model including gluons and pions remains (see Table 7.4). In Sect. 7.3, we have shown that the two-body corrections to the *charge* operator are more important here. Although they are formally of higher order in the non-relativistic expansion, these operators can due to their particular spin and isospin structure utilize the dominant S-waves in the nucleon and Δ wave functions. This is explained in greater detail in Section 5.2.

7.5. $\gamma + N \rightarrow N^*(1440)$ *Helicity Amplitudes*

With respect to the helicity amplitudes of other resonances, we have calculated their effect for the M1 excitation of the Roper resonance [40, 42]. In this case, the inclusion of exchange currents leads for both the proton and neutron to an improved agreement with the empirical values for the $A_{1/2}$ amplitudes in comparison with the impulse approximation. This is encouraging. More work is needed to systematically study the effect of exchange currents in the photocouplings of higher resonances. Recently, we have started to calculate the photocouplings of both positive and negative parity resonances up to an excitation energy of 1.6 GeV [42].

Table 7.5. Helicity amplitudes for the $\gamma + p \rightarrow N^*(1440)$ transitions at $\boldsymbol{q}^2 = \omega^2$ including two-body exchange currents; i = impulse, g = gluon, πq$\bar{\text{q}}$= pion pair, $\gamma\pi\pi$ = pionic, σ = σ-meson, c = confinement. All entries are in $[10^{-3}\text{GeV}^{-1/2}]$.

	A_i	A_g	$A_{\pi q\bar{q}}$	$A_{\gamma\pi\pi}$	A_σ	A_c	A_{total}	exp. [48]
$A^p_{1/2}$	–29	–15	+4	–13	–14	–15	–82	–72±9
$A^n_{1/2}$	+19	+5	–8	+13	+10	+10	+49	+52±25

8. Axial Coupling Constant of the Nucleon

The ratio of weak axial coupling and weak vector coupling constants of the nucleon determines the strength of the neutron β-decay vertex and therefore the life time of the neutron. Experimentally, $(g_A/g_V)_{(\text{exp})} = 1.2573(28)$. According to the conserved vector current hypothesis (CVC) the weak vector current can be obtained from the isovector part of the electromagnetic current by the replacement

$$e\boldsymbol{\tau}_3 \rightarrow g_V(0)\boldsymbol{\tau}_\pm. \tag{8.1}$$

Weak vector current conservation also implies that $g_V(q^2)$ is not renormalized by the strong interaction and given by the isovector electromagnetic form factor of the nucleon, in particular one has $g_V(0) = 1$.

Several attempts have been made to reconcile the NRQM prediction for the nucleon axial vector coupling constant

$$g_A = \frac{5}{3} \tag{8.2}$$

with the experimental value. This 25 % deviation from the experimental contrasts sharply with the successful NRQM predictions of the anomalous magnetic moments of the nucleon.

In 1979 Glashow [141] suggested that a deformation of the valence quark distribution in the nucleon could reduce the classical NRQM result while leaving the successful NRQM prediction for the nucleon magnetic moments intact:

$$g_A = \frac{5}{3}\left(1 - \frac{6}{5}\epsilon^2\right), \tag{8.3}$$

where $\epsilon^2 = 0.21$ is the admixture probability of D-waves in the nucleon. This corresponds to a huge deformation of the nucleon.

There is an analogy to this suggestion in nuclear physics. In impulse approximation, the axial form factor of triton at zero momentum transfers is given in terms of the free neutron axial coupling constant as follows [142]: $G_A(0) = -g_A(P_S - 1/3P_{S'} + 1/3P_D)$, where P_S, $P_{S'}$, and P_D are the symmetric S-wave and the mixed symmetric S- and D-wave probabilities, respectively, which satisfy $P_S + P_{S'} + P_D = 1$. The deviation of the triton wave function from a pure S-state leads to some reduction of the axial coupling of ^{3}H with respect to g_A of the free neutron.

A different solution to the problem of the NRQM to predict g_A is given by relativistic bag model calculations. In the bag model one obtains [143]

$$g_A = \frac{5}{3}\left(1 - \frac{4}{3\langle\kappa\rangle}\int_0^\infty \mathrm{d}r\kappa(r)f^2(r)\right), \quad (8.4)$$

where $\langle\kappa\rangle = \int_0^\infty \mathrm{d}rK(r)(g^2(r)+f^2(r))$ approximately takes the center of mass correction into account. Here, g and f are the radial wave functions in the upper and lower component of the Dirac spinor of the quarks. The lower component $f(r)$ of the Dirac spinor is responsible for a considerable reduction of the NRQM result. Including recoil corrections a value of $g_A = 1.20$ has been obtained. Furthermore, these bag-model calculations show that the axial vector coupling constant is completely determined by the quark core, pion cloud effects turned out to be zero or extremely small. Therefore, the problem could be successfully resolved by the relativistic corrections in the single-quark current.

Similarly, in the NRQM, relativistic corrections in the one-body axial current considerably reduce g_A [118]. However, the corresponding next-to-leading order terms in the one-body electromagnetic current completely spoil the good agreement for baryon magnetic moments, as we have pointed out in Section 5.3.5. One should recall, that in lowest nonrelativistic order both, the magnetic moment operator and the Gamow-Teller operator, have the same spin structure $\boldsymbol{\sigma}$. The question why in the NRQM relativistic corrections lead to a satisfactory description for the axial coupling of the nucleon, but intolerably large corrections for the magnetic moments has not been answered satisfactorily [12]. In the case of the magnetic moments, the success of the NRQM is in some sense related to the cancellation of various two-body currents guaranteed by a proper choice of additive quark masses, the quark core radius b, *and* the residual interactions. We recall here that, if only gluons were included, one would obtain a fairly large correction $\mu^{\mathrm{p}}_{\mathrm{gq\bar{q}}} = 0.88\mu_N$ to the proton magnetic moments.

Before one can draw any conclusion concerning the failure of the NRQM to accurately predict g_A we must investigate the extent to which axial exchange currents affect the NRQM prediction (8.2). The contribution of exchange currents to the axial form factor of the nucleon is largely unexplored, despite of the fact that *axial exchange currents* provide sizeable corrections to the axial properties of nuclei, e. g. in the triton β-decay [142].

8.1. One-body Axial Currents

In this section, we list the axial current $A_\mu = (A^0, -\boldsymbol{A})$. Analogous to the electromagnetic current, one calls the time component A^0 axial charge density and the spatial components $\boldsymbol{A}$ axial current density. We begin with the standard nonrelativistic one-body axial charge and current operators of point-like constituent quarks (see Figure 8.1a).

$$\begin{aligned} A^0_{\mathrm{imp}}(\boldsymbol{r}_i, \boldsymbol{q}) &= g_A^{\mathrm{quark}} \boldsymbol{\tau}_i^{\pm}\left\{\frac{\boldsymbol{\sigma}_i \cdot \boldsymbol{p}_i}{2m_q}, e^{i\boldsymbol{q}\cdot\boldsymbol{r}_i}\right\}, \\ \boldsymbol{A}_{\mathrm{imp}}(\boldsymbol{r}_i, \boldsymbol{q}) &= g_A^{\mathrm{quark}} \frac{\boldsymbol{\tau}_i^{\pm}}{2}\boldsymbol{\sigma}_i e^{i\boldsymbol{q}\cdot\boldsymbol{r}_i} \end{aligned} \quad (8.5)$$

where g_A^{quark} is the axial coupling constant of the constituent quarks and $\boldsymbol{\tau}^{\pm}$ are the spherical components of the isospin of a single quark defined as

$$\begin{aligned} \boldsymbol{\tau}^+ &= -\frac{1}{\sqrt{2}}\left(\boldsymbol{\tau}_x + i\boldsymbol{\tau}_y\right), \\ \boldsymbol{\tau}^- &= \frac{1}{\sqrt{2}}\left(\boldsymbol{\tau}_x - i\boldsymbol{\tau}_y\right). \end{aligned} \quad (8.6)$$

The three-momentum transfer to the gauge boson $W_\pm$ is denoted by $\boldsymbol{q}$.

[12] Dannbom et al. argue that a simultaneous description is possible in the framework of the NRQM, provided that relativistic corrections in both the one-body electromagnetic current and the one-body axial current are taken into account [118].

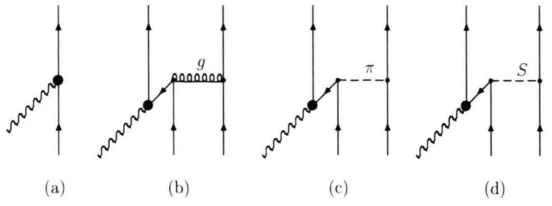

Fig. 8.1. Axial currents between quarks: (a) one-body, (b) gluon-pair, (c) pion-pair, (d) scalar pair. The large shaded circles indicate the axial form factor of the constituent quark.

8.2. *Two-body Axial Currents*

As in the electromagnetic case, the total axial current has been usually approximated by the sum of the single-quark currents (8.5)

$$A^{\mu} \approx \sum_{i=1}^{3} A^{\mu}_{\text{imp}}(i). \tag{8.7}$$

Here, we go beyond the impulse approximation and calculate the leading order weak axial exchange currents connected with the quark-pair diagrams, keeping only the local terms similar to the electromagnetic case. Instead of listing the full current operators, we consider only the Gamow-Teller operators. These are obtained by taking the low-momentum transfer limit $\boldsymbol{q} \to 0$ of the axial current operators. In order to calculate the axial coupling constant of the nucleon, only the Gamow-Teller operators are needed.

$$\begin{aligned} A^0_{\text{gq}\bar{\text{q}}}(\boldsymbol{r}_i, \boldsymbol{r}_j, \boldsymbol{q}=0) &= -ig_{\text{A}}^{\text{quark}} \frac{\alpha_{\text{s}}}{4m_{\text{q}}^2}\, \boldsymbol{\lambda}_i \cdot \boldsymbol{\lambda}_j \\ &\quad \cdot \left\{\boldsymbol{\tau}_i^{\pm}(\boldsymbol{\sigma}_i \times \boldsymbol{\sigma}_j) \cdot \nabla_r + (i \leftrightarrow j)\right\} \frac{1}{r}, \\ \boldsymbol{A}_{\text{gq}\bar{\text{q}}}(\boldsymbol{r}_i, \boldsymbol{r}_j, \boldsymbol{q}=0) &= -g_{\text{A}}^{\text{quark}} \frac{\alpha_{\text{s}}}{32m_{\text{q}}^3}\, \boldsymbol{\lambda}_i \cdot \boldsymbol{\lambda}_j \\ \cdot \Big\{ \boldsymbol{\tau}_i^{\pm} \Big(\frac{3}{4}\boldsymbol{\sigma}_i \nabla_r^2 &- (\boldsymbol{\sigma}_i + \boldsymbol{\sigma}_j) \cdot \nabla_r \nabla_r \Big) + (i \leftrightarrow j) \Big\} \frac{1}{r}. \end{aligned} \tag{8.8}$$

These coordinate space expressions for the axial gluon-exchange current have been derived using a nonrelativistic expansion of the Feynman diagram of Figure 8.1b. They describe a quark-antiquark pair creation process connected with the emission or absorption of the gauge boson $\boldsymbol{W}$. Because the gluon does not carry any isospin the axial gluon-pair current has the same isospin structure as the one-body axial current. The axial gluon-pair currents are of relativistic origin as is reflected in the higher powers of $(1/m_{\text{q}})$ as compared to the nonrelativistic one-body axial current (8.5).

Axial pion-pair exchange currents (see Fig. 8.1c) resulting from pseudoscalar pion-quark coupling are discussed next. Due to the isospin $T = 1$ of the pion, the isospin structure of these operators is more complicated than that of the one-body, gluon, and scalar exchange currents.

$$\begin{aligned} A^0_{\pi\text{q}\bar{\text{q}}}(\boldsymbol{r}_i, \boldsymbol{r}_j, \boldsymbol{q}=0) &= g_{\text{A}}^{\text{quark}} \frac{g^2_{\pi\text{q}}}{4\pi(4m_{\text{q}}^2)} \frac{\Lambda^2}{\Lambda^2 - \mu^2} \\ \cdot \left\{(\boldsymbol{\tau}_i \times \boldsymbol{\tau}_j)^{\pm} \boldsymbol{\sigma}_j \cdot \nabla_r + (i \leftrightarrow j)\right\} &\left(\frac{e^{-\mu r}}{r} - \frac{e^{-\Lambda r}}{r}\right), \\ \boldsymbol{A}_{\pi\text{q}\bar{\text{q}}}(\boldsymbol{r}_i, \boldsymbol{r}_j, \boldsymbol{q}=0) &= g_{\text{A}}^{\text{quark}} \frac{g^2_{\pi\text{q}}}{4\pi\,(8m_{\text{q}}^3)} \frac{\Lambda^2}{\Lambda^2 - \mu^2} \\ \cdot \left\{(\boldsymbol{\tau}_i \times \boldsymbol{\tau}_j)^{\pm} (\boldsymbol{\sigma}_i \times \nabla_r \boldsymbol{\sigma}_j \cdot \nabla_{\mathbf{r}} &+ (i \leftrightarrow j)\right\} \\ \cdot \left(\frac{e^{-\mu r}}{r} - \frac{e^{-\Lambda r}}{r}\right)&. \end{aligned} \tag{8.9}$$

Finally, the axial scalar pair current corresponding to a Lorentz scalar interaction reads:

$$A^0_{\text{S}}(\boldsymbol{r}_i, \boldsymbol{r}_j, \boldsymbol{q}=0) \approx 0 \tag{8.10}$$

$$\begin{aligned} &\boldsymbol{A}_{\text{S}}(\boldsymbol{r}_i, \boldsymbol{r}_j, \boldsymbol{q}=0) \\ &= g_{\text{A}}^{\text{quark}} \frac{1}{32m_{\text{q}}^3} \left\{ \boldsymbol{\tau}_i^{\pm} \boldsymbol{\sigma}_i \nabla^2 \text{V}^{\text{S}}(\boldsymbol{r}_i, \boldsymbol{r}_j) + (i \leftrightarrow j) \right\}. \end{aligned} \tag{8.11}$$

Equation (8.11) is used to calculate both the axial confinement and axial σ-meson exchange currents.

The total axial charge operator consists of the usual one-body axial charge operator and the two-body axial charge operators due to the interaction between the quarks

$$\begin{aligned} A^0(\boldsymbol{q}=0) &= \sum_{i=1}^{3} A^0_{\text{imp}}(\boldsymbol{r}_i, \boldsymbol{q}=0) \\ &+ \sum_{i<j}^{3} \Big(A^0_{\text{gq}\bar{\text{q}}}(\boldsymbol{r}_i, \boldsymbol{r}_j, \boldsymbol{q}=0) + A^0_{\pi\text{q}\bar{\text{q}}}(\boldsymbol{r}_i, \boldsymbol{r}_j, \boldsymbol{q}=0) \\ &\qquad + A^0_{\sigma\text{q}\bar{\text{q}}}(\boldsymbol{r}_i, \boldsymbol{r}_j, \boldsymbol{q}=0) + A^0_{\text{conf}}(\boldsymbol{r}_i, \boldsymbol{r}_j, \boldsymbol{q}=0) \Big). \end{aligned} \tag{8.12}$$

Likewise, the total Gamow-Teller operator consists of

the standard one-body term and the two-body corrections

$$\begin{aligned}\boldsymbol{A}(\boldsymbol{q}=0) &= \sum_{i=1}^{3} \boldsymbol{A}_{\mathrm{imp}}(\boldsymbol{r}_i, \boldsymbol{q}=0) \\ &+ \sum_{i<j}^{3} \Big(\boldsymbol{A}_{\mathrm{gq\bar{q}}}(\boldsymbol{r}_i, \boldsymbol{r}_j, \boldsymbol{q}=0) + \boldsymbol{A}_{\sigma \mathrm{q\bar{q}}}(\boldsymbol{r}_i, \boldsymbol{r}_j, \boldsymbol{q}=0) \\ &\quad + \boldsymbol{A}_{\pi \mathrm{q\bar{q}}}(\boldsymbol{r}_i, \boldsymbol{r}_j, \boldsymbol{q}=0) + \boldsymbol{A}_{\mathrm{conf}}(\boldsymbol{r}_i, \boldsymbol{r}_j, \boldsymbol{q}=0) \Big).\end{aligned} \tag{8.13}$$

8.3. PCAC

Although the axial current is not conserved exactly, the partial conservation of the axial current (PCAC), which can be formulated as [142]

$$\boldsymbol{q} \cdot \boldsymbol{A} = \left[H, A^0(\boldsymbol{q})\right] + i f_\pi M^\pi(\boldsymbol{q}) \tag{8.14}$$

provides a connection between the two-body potentials and the two-body axial currents. Here, $M_\pi(\boldsymbol{q})$ is the pion absorption operator, describing the pion-quark coupling. Its one-body piece is given by the familiar pion-quark vertex

$$M^\pi_{[1]}(\boldsymbol{q}) = \tau_i^{\pm} \frac{\boldsymbol{\sigma}_i \cdot \boldsymbol{q}}{2m_{\mathrm{q}}}.$$

We have not yet considered the additional constraints implied by (8.14). Therefore, the present calculation, which is based on the quark-pair diagrams, can only be considered as indicative for the size of various exchange current corrections.

Using the ground-state wave functions (3.15) we obtain for the impulse, pion, gluon and scalar contributions to axial vector coupling constant of the nucleon the following expression

$$\begin{aligned}g_{\mathrm{A}} = g_{\mathrm{A}}^{\mathrm{quark}} \Big(&\frac{5}{3} - \frac{17}{24} \frac{\delta_{\mathrm{g}}(b)}{M_N} + \frac{\delta_\pi(b)}{M_N} \\ &- \frac{5}{72} \frac{1}{m_{\mathrm{q}}^3} \left(m_\sigma^2 V_\sigma^\sigma(b) - m_\Lambda^2 V_\Lambda^\sigma(b) \right) \\ &- \frac{5}{36} \frac{1}{m_{\mathrm{q}}^3} V^{\mathrm{conf}}(b)/b^2 \Big).\end{aligned} \tag{8.15}$$

As is evident from Table 8.1, the axial pair current contributions to the axial coupling constant are quite small and cannot explain the difference between the additive quark model result and experiment. However, one should take these numbers only as a qualitative estimate for the following reason. The axial exchange currents were derived from the corresponding quark-antiquark pair diagrams in analogy to the electromagnetic pair currents. In the case of electromagnetic currents, we have shown that the pair currents, together with the pionic current are indeed those required by gauge invariance. The corresponding check for the axial currents has still to be done. It may very well be, that the axial quark pair currents of Fig. 8.1 are not the most important axial two-body currents. In fact, PCAC suggests that the two-body currents connected with the *positive* frequency part of the intermediate quark propagation provide the leading order terms in $1/m_{\mathrm{q}}$ [142]. More work is required to construct and systematically investigate the appropriate axial two-body operators that satisfy the PCAC condition in the NRQM.

Table 8.1. Contribution of the various axial quark currents to the axial coupling constant of the nucleon. An unrenormalized $g_{\mathrm{A}}^{\mathrm{quark}} = 1$ is assumed.

$g_{\mathrm{A}}^{\mathrm{imp}}$	$g_{\mathrm{A}}^{\mathrm{g}}$	g_{A}^{π}	g_{A}^{σ}	$g_{\mathrm{A}}^{\mathrm{c}}$	$g_{\mathrm{A}}^{\mathrm{t}}$	$(g_{\mathrm{A}}/g_{\mathrm{V}})^{\mathrm{exp}}$
1.666	–0.149	0.101	0.045	–0.085	1.578	1.2573(28)

We close this Section with some remarks concerning a possible solution of the g_{A} problem in the NRQM. So far, we have made the tacit assumption that $g_{\mathrm{A}}^{\mathrm{quark}} = 1$. Suppose that the cancellation of different exchange current contributions, found for the case of the axial pair currents is confirmed in a more complete calculation applying the constraints (8.14). In that case, the most natural implication for the NRQM would be to assign a renormalized axial coupling constant to the constituent quarks. If a $g_{\mathrm{A}}^{\mathrm{quark}} \approx 0.8$ is used, the axial coupling constant of the nucleon would be reproduced in NRQM.

Weinberg [66, 144] has shown that while constituent quarks have no anomalous magnetic moments, their axial coupling of the quark may be considerably renormalized by the strong interaction. In fact, explicit calculation shows

$$g_{\mathrm{A}}^2(\mathrm{quark}) = 1 - \frac{m_{\mathrm{q}}^2}{2\pi^2 F_\pi^2},$$

where $F_\pi \approx 190$ MeV is the pion decay constant used in [144]. This leads to a 10% reduction of $g_{\mathrm{A}}^{\mathrm{quark}}$. Weinberg's arguments have recently been reinvestigated. Using Witten's large N_{C} counting rules, it has

been shown that, in contrast to the magnetic moments of the quarks, corrections to g_A^{quark} appear already in order N_c^0 [145].

Additional evidence for a g_A^{quark} different from unity comes from the Goldberger Treiman relation [13] for the constituent quarks, from which

$$m_q g_A^{quark} = g_{\pi q} f_\pi$$

using the phenomenological pion-quark coupling and the empirical pion decay constant, a $g_A^{quark} \approx 0.78$ is deduced. Further investigation of the constituent quark structure in the NJL model shows that

$$g_A^{quark} \approx \left(1 + \frac{1}{3}\frac{g_V^2(\text{quark})}{4\pi}\right)^{-1},$$

and $g_A^{quark} \approx 0.75$. Here, $g_V^2(\text{quark})/4\pi$ is the ρ-meson quark coupling constant.

Therefore, in the framework of the NRQM model, it is natural to employ a renormalized axial coupling of the constituent quark. While the electromagnetic couplings of the quark are protected by electromagnetic current conservation and are not renormalized in the transition from current to constituent quarks (no anomalous magnetic moments are acquired) the axial current is only partially conserved. Consequently, the axial coupling of the constituent quark should be renormalized in comparison to the axial coupling of the nearly massless current quarks. We understand that the origin of this renormalization is the spontaneous breaking of chiral symmetry in QCD [146].

We have seen that large relativistic corrections of one-body nature are not required to solve the g_A problem in the framework of the NRQM. Also, this seems to fit with our results concerning the cancellation of two-body currents in the axial properties. In addition, it shows that the NRQM using $m_q \approx M_N/3$ already incorporates some relativistic corrections as we have discussed in Section 5.3.5. An improved exchange current calculation emphasizing the PCAC condition is needed to substantiate our finding that exchange currents do not contribute significantly to g_A and to make the above arguments more quantitative.

[13] This relation holds in the chiral constituent quark model [11].

9. Summary and Outlook

This work presents a review of the recent progress made towards the formulation of a gauge invariant current operator for constituent quarks and its application to baryon electromagnetic properties. After discussing the basic idea of spontaneous chiral symmetry breaking (Chapt. 2), which is responsible for the constituent quark mass generation and the quasiparticle interpretation of constituent quarks, we formulate a chiral potential model that reflects the symmetries and main properties of QCD at low energies (Chapt. 3).

In Chapt. 4 we go beyond the usual single-quark impulse approximation by including various two-body exchange currents. We discuss that a model built on free quark currents is incomplete because it violates the fundamental requirement of current conservation (gauge invariance). Current conservation establishes a link between the potentials used to calculate the baryonic excitation spectrum and the corresponding currents needed to calculate the electromagnetic properties of baryons. In most previous calculations of baryon electromagnetic properties this well known fact has not been sufficiently appreciated.

In Chapt. 5 we calculate the complete set of electromagnetic form factors of the $N - \Delta$ system. In particular, we investigate the low-energy behavior of these form factors, i. e. the electromagnetic moments and radii including the lowest nonvanishing order two-body exchange charges and currents. Our main purpose is to study the extent to which the theoretical predictions for various low-energy observables are modified by the inclusion of these corrections of *two-body nature*. All observables are calculated with a single set of parameters in order to see how the different two-body currents affect various observables. In order to isolate and emphasize the contribution of exchange currents we use unmixed wave functions for the N and Δ in this work. We expect this to be a good approximation to the total exchange current contribution.

In this approximation, we show that the inclusion of exchange currents leads to a number of interesting relations between baryon mass splittings and electromagnetic observables. In particular, we find that the neutron charge radius is closely connected to the empirical $\Delta - N$ mass splitting and the quark core radius b via

$$r_n^2 M_N = -b^2(M_\Delta - M_N). \tag{9.1}$$

This relation is satisfied to within 4%, if the canonical choice $b = 1/m_q = 0.63$ fm is made. This value for the quark core radius b is significantly smaller than the unphysically large value $b \approx 1$ fm, that has previously been employed to describe the negative neutron charge radius using only single-quark currents and mixed wave functions. Although relation (9.1) was derived with pure ground state $(0s)^3$ wave functions, it remains approximately valid in a more complete calculation, using mixed wave functions. We have previously shown [37] that a more consistent calculation including both configuration mixing and exchange currents leads to deviations of some $10 - 20\%$ between the prediction (9.1) and the total result including configuration mixing. Thus, the inclusion of exchange corrections in the charge density operator of the quarks allows a simultaneous description of the neutron charge radius and of the positive parity excitation spectrum of the nucleon with the same set of parameters. This is one of our main results. Furthermore, we find that the charge radius of the charged Δ states is given by the simple relation

$$r_\Delta^2 = r_p^2 - r_n^2. \tag{9.2}$$

Equation (9.2) indicates that the charge radius of the $\Delta(1232)$ is slightly larger than the proton charge radius.

For the quadrupole moments of the Δ and the $N \to \Delta$ transition quadrupole moment, we show that even if there is no D-state admixture in the nucleon and Δ wave function, i. e. if there is no deformation of the valence quark distribution, one nevertheless obtains nonvanishing quadrupole moments, due to two-body pion and gluon pair terms in the charge operator. This is depicted in Fig. 5.6 where a C2 photon is absorbed on an interacting pair of quarks. Without two-body exchange currents, the C2 amplitude would be exactly zero in the present approximation, which neglects configuration mixing. Excited D-state admixtures alone are too small to explain the empirical C2 amplitude if a realistic quark core radius of $\simeq 0.6$ fm is chosen. We find that the C2 transition to the Δ is mainly a *two-body* transition involving the simultaneous spin-flip of two quarks.

Based on the exchange current diagrams of Fig. 4.2, we derive new relations [41] between the Δ quadrupole moment Q_Δ, the $N \to \Delta$ transition quadrupole moment, $Q_{N\to\Delta}$, and the neutron charge radius, r_n^2:

$$Q_\Delta = r_n^2 e_\Delta,\ Q_{N\to\Delta} = \frac{1}{\sqrt{2}} r_n^2. \tag{9.3}$$

These relations are useful for the following reasons. First, the theoretical predictions based on them, e. g. for the neutron charge radius are in excellent agreement with experiment. Although there is no experimental information on the Δ quadrupole moment, previous and very recent extractions of the transition quadrupole moment from pionproduction data indicate a value consistent with the prediction (9.3). Second, they seem to correctly describe the underlying physics common to these three observables: r_n^2, Q_Δ and $Q_{N\to\Delta}$ are dominated by nonvalence quark degrees of freedom, that is in our language, exchange currents. Third, relations (9.1) - (9.3) clearly show that the charge properties of the first excited state are intimately related to those of the ground state. Moreover, via (9.1) the underlying connection between the excitation spectrum of the nucleon (potentials) and electromagnetic properties (two-body currents) is made explicit. It is conceivable that the above relations have a more general validity than our derivation of them as matrix elements of the Feynman diagrams of Figs. 4.2a, b suggests.

With respect to the magnetic moments, we find that individual exchange current corrections can be quite large. For example, we have shown that the one-gluon exchange current, which is consistent with the one-gluon exchange potential gives an undesirably big correction to the nucleon and Δ magnetic moments. If only these contributions were included the success of the single valence quark model would be completely spoiled [14]. The scalar two-body currents connected with the σ-meson-exchange and confinement potentials yield important corrections which largely cancel the one-gluon exchange contribution. In addition, we find that the inclusion of pions gives generally better results for the magnetic properties of the nucleon compared to a calculation without pions. The total effect of the pion is small due to substantial

[14] We recall here that a model with effective one-gluon exchange predicts a large spin-orbit splitting between the $D_{13}(1520)$ and the $S_{11}(1535)$ excitation of the nucleon, which is not observed [15]. With the corresponding one-gluon-exchange current only, we would have obtained untolerably large corrections for the magnetic moments.

cancellations between the pion-pair and pionic current. In this context, it is important to include the δ-function term in the one-pion exchange potential, otherwise the cancellation between the pion-pair and pionic current in the nucleon magnetic moments disappears [38]. In a model that uses only a one-pion exchange interaction between quarks, the omission of the δ-function would lead to disastrous results for the magnetic moments of the nucleon. Thus, a major result of this work is that although individual two-body currents provide large corrections, the total exchange current contribution is typically less than 15% (in most cases less than 10%) of the additive quark model result leaving the additive quark model prediction essentially intact. We point out that, for the $N \rightarrow \Delta$ transition magnetic moment, a large discrepancy between our prediction and the experimental result is left unexplained even after inclusion of exchange currents.

This conclusion remains firm in a recent SU(3) extension of the model [39]. We found that the cancellations observed for the nucleon and Δ magnetic moments also occur for other members of the baryon octet, provided that the hyperon masses are reproduced, and that the quark core radius b for the light quarks is consistent with the one suggested by (9.1). In the case of the magnetic moment of the Ξ^- hyperon, the inclusion of exchange currents leads to a substantial increase of its absolute value, in agreement with experiment [39].

In Chapt. 7 we return to the question of the deformation of the nucleon and Δ, as observed in recent electro- and photo pionproduction experiments. Theoretical predictions and experimental results are usually compared and analyzed for the E2/M1 or C2/M1 ratio, which measures the deformation of the nucleon. Our prediction for the E2/M1 ratio, which is based on our analytic expressions for $Q_{N\rightarrow\Delta}$ and $\mu_{N\rightarrow\Delta}$ and the use of Siegert's theorem, results in E2/M1 = -0.035. This value is significantly larger than the value given by the Particle Data Group [48] but it is consistent with a recent reanalysis of photo-pionproduction data from several experiments [99].

In this work, we calculate the E2 strength in the $N \rightarrow \Delta$ transition in two different ways. First, we evaluate the *total* spatial current density, between mixed wave functions in a $2\hbar\omega$ configuration space. Second, using Siegert's theorem, we calculated the E2 amplitude with the help of the one-body charge density and mixed wave functions. We found that both calculations agree remarkably well. In [139] it is shown that this conclusion is independent of the particular model considered. Thus, we have explicitly shown that the strong violation of gauge invariance, found in Refs. [30, 134, 137, 138] is mainly due to the omission of *explicit* spatial two-body currents in previous comparisons. We consider this result as compelling evidence for the dominant role of two-body exchange currents in the electric quadrupole form factor of the $N \rightarrow \Delta$ transition.

Based on these results we conclude that the deformation of the nucleon comes mainly from the residual pion and gluon degrees of freedom in the electromagnetic charge and current operator (exchange currents). This is one of our main results. We believe that this result is not an artefact of the model used and the approximations made. Similar conclusions concerning the importance of nonvalence degrees of freedom have been obtained in quite different models [91, 130, 147] recently.

In this work we also study how the gluon, pion and scalar pair currents affect the axial coupling constant of the nucleon, which is overestimated in the NRQM. As in the case of the magnetic moments, we find substantial cancellations between different axial pair current contributions. Unlike the spatial electromagnetic current, for which we have checked the continuity equation, the corresponding PCAC constraint for axial currents has not yet been taken into account. If the observed cancellations between various two-body operators is confirmed in an improved calculation taking PCAC into account, the reduction of the axial coupling of the constituent quark by some 20% is the most natural way to resolve the g_{A} problem in the framework of the NRQM. As in the case of the electromagnetic one-body current, relativistic corrections are largely incorporated in the leading order one-body axial current.

In summary, we have seen that the same degrees of freedom which produce the $\Delta - N$ mass splitting and are responsible for the structure in the excited baryon spectrum, affect the electromagnetic properties of baryons in the form of gluon- and pion-, and scalar exchange currents. Exchange currents describe the coupling of the photon to the residual gluon, pion and scalar exchange degrees of freedom, which are not yet included in the mass, size, and wave function of the constituent quarks. We have argued that it is sometimes more important to include exchange

currents in the NRQM than to use improved wave functions (configuration mixing).

Clearly, there are a number of other effects, that should be included in a more detailed analysis. Nevertheless, the residual spin-dependent interactions manifest themselves not only in excited state admixtures to ground state wave functions but also in the form of two-body exchange currents between quarks. Exchange currents must be included in the theoretical interpretation of experimental results before one can draw conclusions about details of the quark-quark interaction. For example, unlike the standard explanation of the $N \rightarrow \Delta$ quadrupole transition based on the single-quark currents and deformed valence quark orbits, we find that the E2-amplitude, in photopionproduction is predominantly a *two-quark spin-flip transition* induced by the presence of gluon and pion degrees of freedom. Hence, the experimental confirmation of a large E2-amplitude in the $N \rightarrow \Delta$ transition must be considered as evidence for exchange currents in the nucleon.

One could ask why we did not include vector and pseudovector mesons (ρ and a_1) in our chiral potential model. Having included pions and heavy scalar mesons, there seems to be no good reason to exclude heavy vector and pseudovector mesons. Vector mesons provide a natural explanation of the electromagnetic size of constituent quarks. The inclusion of residual ρ and a_1 meson exchange potentials between constituent quarks will lead to a reduction of the importance of one-gluon exchange in the NRQM. This could have interesting consequences for excited baryon spectra and the electromagnetic properties of baryons. The task of finding the most appropriate non-valence degrees of freedom (gluons, pions, instantons, vector mesons) which determine the structure of baryons on the confinement scale is far from being completed.

With the new generation of continuous electron beam accelerators we are in the position to study the electromagnetic properties of the nucleon and its excited states with an unprecedented precision. From the theoretical side, one has to go beyond the impulse approximation and include exchange currents. We expect that, similar to nuclear few-body systems, where the study of exchange currents has led to many important insights and results, exchange currents will play an equally important role in understanding the structure of baryons.

I would like to thank Amand Faessler, E. Hernández, Uli Meyer, Georg Wagner, and K. Yazaki for their collaboration on the results reported here.

Appendix

Next, we give the expressions for the integrals in (5.37). The function $I_{\mathrm{gq\bar{q}}}(q)$ entering the gluon pair current is

$$I_{\mathrm{gq\bar{q}}}(q) = 4\pi(\frac{1}{2\pi b^2})^{3/2} \int_0^\infty \mathrm{d}\rho e^{-\rho^2/(2b^2)} j_1(\frac{q\rho}{2}). \tag{.1}$$

The integrals $I^{(ii)}_{\pi\mathrm{q\bar{q}}}(q)$ needed in the pion pair current are defined as follows

$$I^{(ii)}_{\pi\mathrm{q\bar{q}}}(q) = 4\pi(\frac{1}{2\pi b^2})^{3/2} \frac{\Lambda^2}{\Lambda^2-\mu^2}\mu^2 \int_0^\infty \mathrm{d}\rho\rho^2 e^{-\rho^2/(2b^2)} j_i(\frac{q\rho}{2})(\mu Y_i(\mu\rho) - \Lambda\frac{\Lambda^2}{\mu^2} Y_i(\Lambda\rho)), \tag{.2}$$

with $i = 0$ and $i = 2$ for the isoscalar part and

$$I^{(11)}_{\pi\mathrm{q\bar{q}}}(q) = 4\pi(\frac{1}{2\pi b^2})^{3/2} \frac{\Lambda^2}{\Lambda^2-\mu^2}\mu^2 \int_0^\infty \mathrm{d}\rho\rho^2 e^{-\rho^2/(2b^2)} j_1(\frac{q\rho}{2})(Y_1(\mu\rho) - \frac{\Lambda^2}{\mu^2} Y_1(\Lambda\rho)), \tag{.3}$$

for the isovector pion-pair current. Here, the functions $Y_i(x)$ are defined as

$$Y_0(x) = \frac{e^{-x}}{x}, \quad Y_1(x) = \frac{e^{-x}}{x}(1+\frac{1}{x}), \quad Y_2(x) = \frac{e^{-x}}{x}(1+\frac{3}{x}+\frac{3}{x^2}). \tag{.4}$$

The integral $I_{\gamma\pi\pi}(q)$ needed in pionic (pion in flight) current is

$$I_{\gamma\pi\pi}(q) = 4\pi(\frac{1}{2\pi b^2})^{3/2}\frac{\Lambda^2}{\Lambda^2-\mu^2}\int_0^\infty \mathrm{d}\rho\rho^2 e^{-\rho^2/b^2}(I_\mathrm{v}(q,\rho,\mu) - I_\mathrm{v}(q,\rho,\Lambda)), \tag{.5}$$

where the function $I_\mathrm{v}(q,\rho,m)$ is defined as

$$I_\mathrm{v}(q,\rho,m) = \int_{-1/2}^{1/2}\mathrm{d}v(j_0(q\rho v)g_0(q,\rho,v,m) + j_2(q\rho v)g_2(q,\rho,v,m)), \tag{.6}$$

with the abbreviations

$$g_0 = L_m\exp(-L_\mathrm{m}\rho)\Big(1-\frac{2}{L_m\rho}\Big),\ g_2 = L_m\exp(-L_\mathrm{m}\rho)\Big(1+\frac{1}{L_m\rho}\Big),\ \text{and}\ L_m = (\frac{1}{4}q^2(1-4v^2)+m^2)^{1/2}. \tag{.7}$$

Finally, the integrals I_S^C and I_S^M for the scalar currents are given by

$$\begin{aligned} I_\mathrm{S}^\mathrm{C}(q) &= 4\pi\big(\frac{1}{2\pi b^2}\big)^{3/2}\int_0^\infty \mathrm{d}\rho\rho^2 e^{-\rho^2/(2b^2)} \\ &\quad\cdot\Big[j_0(\frac{q\rho}{2})\Big(3q^2V_{1,2}^\mathrm{S}(\rho) + \frac{2}{\rho}\frac{\mathrm{d}}{\mathrm{d}\rho}V_{1,2}^\mathrm{S}(\rho) + \frac{\mathrm{d}^2}{\mathrm{d}\rho^2}V_{1,2}^\mathrm{S}(\rho)\Big) + 2qj_1(\frac{q\rho}{2})\frac{\mathrm{d}}{\mathrm{d}\rho}V_{1,2}^\mathrm{S}(\rho)\Big], \end{aligned} \tag{.8}$$

$$I_\mathrm{S}^\mathrm{M}(q) = 4\pi(\frac{1}{2\pi b^2})^{3/2}\int_0^\infty \mathrm{d}\rho\rho^2 e^{-\rho^2/(2b^2)}j_0(\frac{q\rho}{2})V_{1,2}^\mathrm{S}(\rho).$$

[1] R. K. Bhaduri, Models of the nucleon, Lecture notes and supplements in physics: 22, ed. Davis Pines, Addison-Wesley, Redwood City, California 1988.

[2] A. W. Thomas, Adv. Nucl. Phys. **13**, 1 (1983).

[3] U. Vogl and W. Weise, Prog. Part. Nucl. Phys. **27**, 195 (1991).

[4] R. F. Alvarez-Estrada, F. Fernandez, J. L. Sanchez-Gomez, and V. Vento, Lecture Notes in Physics **259**, Springer, Berlin, 1986; W. Lucha, F. F. Schöberl, and D. Gromes, Phys. Rep. **200**, 127 (1991); J. M. Richard, Phys. Rep. **212**, 1 (1992).

[5] M. A. B. Beg, B. W. Lee, and A. Pais, Phys. Rev. Lett. **13**, 514 (1964).

[6] G. Karl, Int. J. Mod. Phys. **E1**, 491 (1992).

[7] L. A. Copley, G. Karl, and E. Obryk, Nucl. Phys. **B13**, 303 (1969).

[8] F. E. Close and Zhenping Li, Phys. Rev. **D42**, 2194 (1990).

[9] E. Shuryak, Phys. Rep. **115**, 151 (1984).

[10] D. Diakonov, Progr. Part. Nucl. Phys. **36**, 1 (1996).

[11] A. Manohar and H. Georgi, Nucl. Phys. **B234**, 189 (1984).

[12] B. H. J. McKellar, M. D. Scadron, and R. C. Warner, Int. J. Mod. Phys. **A3**, 20 (1988).

[13] G. Morpurgo, Phys. Rev. **D40** (1989) 3111; Phys. Rev. **D41**, 2865 (1990).

[14] A. De Rujula, Howard Georgi, and S. L. Glashow, Phys. Rev. **D12**, 147 (1975).

[15] N. Isgur and G. Karl, Phys. Rev. **D18**, 4187 (1978); Phys. Rev. **D19** (1979) 2653; Phys. Rev. **D21**, 3175 (1980); N. Isgur, G. Karl, and R. Koniuk, Phys. Rev. Lett. **41**, 1269 (1978); N. Isgur, G. Karl, and D. W. L. Sprung, Phys. Rev. **D23**, 163 (1981).

[16] B. Metsch, Habilitation thesis, University of Bonn, 1993

[17] L. Ya. Glozman and D. O. Riska, Phys. Rep.**268**, 263 (1996).

[18] Progr. Part. Nucl. Phys. **34**, 1, ed. Amand Faessler, Pergamon Press, Oxford 1995.

[19] Frank Kalleicher et al., Z. Phys. **A359**, 201 (1997).

[20] J. L. Friar in Mesons in Nuclei, Vol. II, pg. 597, eds. M. Rho and D. Wilkinson, North-Holland, New York 1979.

[21] A. J. F. Siegert, Phys. Rev. **52**, 787 (1937).

[22] H. Arenhövel, Czech. J. Phys. **43**, 207 (1993).

[23] S. J. Brodsky, Comm. Nucl. Part. Phys. **12**, 213 (1984).

[24] M. Beyer, D. Drechsel, and M. M. Giannini, Phys. Lett **B122**, 1 (1983).

[25] D. Drechsel and M. M. Giannini, J. Phys. **G12**, 1165 (1986).

[26] D. Drechsel, Nuovo Cim. **76A**, 388 (1983).

[27] A. Buchmann, Y. Yamauchi, H. Ito, and A. Faessler, J. Phys. **G14** 1037 (1988); Y. Yamauchi, A. Buchmann, and A. Faessler, Nucl. Phys. **A494**, 401 (1989).
[28] A. Buchmann, Y. Yamauchi, and A. Faessler, Nucl. Phys. **A496**, 621 (1989); Phys. Lett. **B225**, 301 (1989); Progr. Part. Nucl. Phys. **24**, 333, ed. A. Faessler, Pergamon Press, Oxford 1990.
[29] D. Robson, Phys. Rev. **D35**, 1029 (1985).
[30] M. Weyrauch and H. J. Weber, Phys. Lett. **B171**, 13 (1986).
[31] K. Ohta, Phys. Rev. Lett. **43**, 1201 (1979).
[32] G. E. Brown, M. Rho, V. and Vento, Phys. Lett. **B97**, 423 (1980).
[33] M. I. Krivoruchenko, JETP Lett. **38**, 173 (1983).
[34] R. Mignani and D. Prosperi, Nuovo Cim. **A75**, 221 (1983).
[35] H. J. Weber and M. Weyrauch, Phys. Rev. **C32**, 1342 (1985).
[36] D. Robson, Nucl. Phys. **A560**, 389 (1993).
[37] A. Buchmann, E. Hernandez, and K. Yazaki, Phys. Lett. **B269**, 35 (1991).
[38] A. Buchmann, E. Hernandez, and K. Yazaki, Nucl. Phys. **A569**, 661 (1994).
[39] Georg Wagner, A. J. Buchmann, and Amand Faessler, Phys. Lett. **B359**, 288 (1995).
[40] A. J. Buchmann, U. Meyer, E. Hernández, Amand Faessler, Acta Phys. Pol. **B27**, 3161 (1996).
[41] A. J. Buchmann, E. Hernandez, and Amand Faessler, Phys. Rev. **C55**, 448 (1997).
[42] U. Meyer, A. J. Buchmann, and Amand Faessler, Phys. Lett. **B408**, 19 (1997).
[43] Georg Wagner, A. J. Buchmann, and Amand Faessler, Phys. Lett. **B** (1997) submitted
[44] C. N. Yang and R. L. Mills, Phys. Rev. **96**, 191 (1954).
[45] F. J. Yndurain, Quantum Chromodynamics, Springer-Verlag, New York 1983.
[46] P. Becher, M. Böhm, and H. Joos, Eichtheorien, B. G. Teubner, Stuttgart 1981.
[47] F. Halzen, and A. D. Martin, Quarks and Leptons, John Wiley, New York 1984.
[48] L. Montanet et al., Phys. Rev. **D50**, 1173 (1994).
[49] A. Szczurek, A. J. Buchmann, and Amand Faessler, J. Phys. **G22**, 1741 (1996).
[50] M. Kirchbach, Czech. J. Phys. **43**, 319 (1993).
[51] Y. Nambu and G. Jona-Lasinio, Phys. Rev. **122**, 345 (1960).
[52] D. Ebert, H. Reinhardt, and M. K. Volkov, in Progr. Part. Nucl. Phys. **33**, ed. Amand Faessler, Pergamon Press, Oxford 1994.
[53] A. Akhiezer and V. B. Beretstetski, Quantum Electrodynamics, John Wiley, New York 1963.
[54] Ya. B. Zeldovich and A. D. Sakharov, Sov. J. Nucl. Phys. **4**, 283 (1964).
[55] K. Shimizu, Phys. Lett. **B148**, 418 (1984).
[56] K. Maltman, Nucl. Phys. **A446**, 623 (1985).
[57] F. Fernandez and E. Oset, Nucl. Phys. **A455**, 720 (1986).
[58] J. R. Bergervoet et al., Phys. Rev. **C41**, 1435 (1990).
[59] I. T. Obukhovsky and A. M. Kusainov, Phys. Lett. **B238**, 142 (1990).
[60] F. Fernandez, A. Valcarce, U. Straub, and A. Faessler, J. Phys. **G19**, 2013 (1993).
[61] F. E. Close, An introduction to Quarks and Partons, Academic Press, London 1979.
[62] Amand Faessler, A. Buchmann, and Y. Yamauchi, Int. J. Mod. Phys.**E2**, 39 (1993).
[63] L. J. Reinders and K. Stam, Phys. Lett. **B180**, 125 (1986).
[64] J. M. Namyslowski, Phys. Lett. **B192**, 170 (1987).
[65] M. M. Giannini, Rep. Prog. Phys. **54**, 453 (1990).
[66] Steven Weinberg, Phys. Rev. Lett. **65**, 1181 (1990).
[67] M. Chemtob and M. Rho, Nucl. Phys. **A163**, 1 (1971).
[68] J. L. Friar, Ann. Phys. **104**, 380 (1977).
[69] S. Ichii, W. Bentz, and A. Arima, Nucl. Phys. **A464**, 575 (1987);
P.G. Blunden, Nucl. Phys. **A464**, 525 (1987).
[70] V. A. Petrunkin, Sov. J. Part. Nucl. **12**, 278 (1981).
[71] D. P. Stanley and D. Robson, Phys. Rev. **D26**, 223 (1982).
[72] P. Stichel and E. Werner, Nucl. Phys. **A145**, 257 (1970).
[73] H. Arenhövel, Nukleonika **24**, 274 (1979).
[74] A. Buchmann, W. Leidemannn, and H. Arenhövel, Nucl. Phys. **A443**, 726, (1985).
[75] D. Drechsel and H. J. Weber, Nucl. Phys. **A256**, 317 (1975).
[76] A. D. Jackson, A. Lande, and D. O. Riska, Phys. Lett. **B55**, 23 (1975).
[77] H. Henning, J. Adam, P. U. Sauer, and A. Stadler, Phys. Rev. **C52**, R471 (1995).
[78] A. J. Buchmann, H. Henning, and P. U. Sauer, Few-Body Systems **21**, 149 (1996).
[79] H. J. Weber, and H. Arenhövel, Phys. Rep. **36**, 277 (1978).
[80] H. F. Jones and M. D. Scadron, Ann. Phys. **81**, 1 (1973).
[81] M. Gari and H. Hyuga, Nucl. Phys. **A264**, 409 (1976).
[82] G. G. Simon, F. Borkowski, Ch. Schmitt, and V. H. Walther, Z. Naturforsch. **35a**, 1 (1980).
[83] S. Platchkov et al., Nucl. Phys. **A510**, 470 (1990).
[84] F. Klein, Invited paper at the PANIC 1996 International Conference, Williamsburg, May 1996.
[85] M. Meyerhoff et al., Phys. Lett. **B327**, 201 (1994).
[86] C. E. Jones et al., Phys. Rev. **C44**, R571 (1991).
[87] A. K. Thompson et al., Phys. Rev. Lett. **68**, 2901 (1992).
[88] T. Eden et al., Phys. Rev. **C50**, 1749 (1994).
[89] Y. Yamauchi, A. J. Buchmann, Amand Faessler, and Akito Arima, Nucl. Phys. **A526**, 495 (1991).
[90] R. D. Carlitz, S. D. Ellis, and R. Savit, Phys. Lett. **B68**, 443 (1977).
[91] Chr. V. Christov et al., Progr. Part. Nucl. Phys. **37**, 91 (1996).
[92] C. Gobbi, S. Boffi, and D. O. Riska, Nucl. Phys. **A547**, 633 (1992).
[93] S. J. Brodsky and F. Schlumpf, Progr. Part. Nucl. Phys. **34**, 69 (1995).
[94] M. I. Krivoruchenko and M. M. Giannini, Phys. Rev. **C43**, 3763 (1991).

[95] S. S. Gershtein and G. V. Dzhikiya, Sov. J. Nuc. Phys. **34**, 870 (1982).
[96] N. Isgur, G. Karl, and R. Koniuk, Phys. Rev. **D25**, 2394 (1982).
[97] C. Becchi and G. Morpurgo, Phys. Lett. **17**, 352 (1965).
[98] R. C. E. Devenish, T. S. Eisenschitz, and J. G. Körner, Phys. Rev. **D14**, 3063 (1976).
[99] O. Hanstein, D. Drechsel, and L. Tiator, Phys. Lett. **385**, 45 (1996); see also: nucl-th/9709067.
[100] G. Blanpied et al., Phys. Rev. Lett. **79**, 4337 (1997).
[101] A. Wirzba and W. Weise, Phys. Lett. **B188**, 6 (1987).
[102] H. Anklin et al., Phys. Lett. **336**, 313 (1994).
[103] J. Franklin, AIP Conf. Proc. No. **187**, 384 (1989).
[104] A. Arima and H. Horie, Progr. Theor. Phys. **12**, 623 (1954).
[105] A. Arima, K. Shimizu, W. Bentz, and H. Hyuga, Adv. Nucl. Phys. **18**, 1 (1987).
[106] E. B. Hughes, T. A. Griffy, M. R. Yearian, and R. Hofstadter, Phys. Rev. **139**, B458 (1965).
[107] P. Markowitz et al., Phys. Rev. **C48**, R5 (1993).
[108] E. E. W. Bruins et al., Phys. Rev. Lett. **75**, 21 (1995).
[109] W-Y. P. Hwang, Z. Phys. **C16**, 331 (1983).
[110] D. B. Leinweber, T. Draper, and R. M. Woloshyn, Phys. Rev. **D46**, 3067 (1992).
[111] G. Dillon and G. Morpurgo, Z. Phys. **C62**, 31 (1994).
[112] B. M. K. Nefkens, Phys. Rev. **D18**, 3911 (1978).
[113] A. Bosshard et al., Phys. Rev. **D44**, 1962 (1991).
[114] R. H. Dalitz and D. G. Sutherland, Phys. Rev. **146**, 1180 (1966).
[115] M. I. Krivoruchenko, Sov. J. Nucl. Phys. **45**, 109 (1987).
[116] Z. Y. Zhang, Y. W. Yu, P. N. Shen, and Y. B. Dong, Nucl. Phys. **A561**, 595 (1993).
[117] W. Lucha and F. F. Schöberl, hep-ph/9501278
[118] K. Dannbom, L. Ya. Glozman, C. Helminen, and D. O. Riska, Nucl. Phys. **A616**, 555 (1997).
[119] R. M. Sternheimer and M. Goldhaber, Phys. Rev. **A8**, 2207 (1973).
[120] S. S. Gershtein and Yu. M. Zinov'ev, Sov. J. Nucl. Phys. **33**, 772 (1981).
[121] V. D. Burkert, Czech. J. Phys. **46**, 627 (1996).
[122] G. F. Chew, M. L. Goldberger, F. E. Low, and Y. Nambu, Phys. Rev. **106**, 1345 (1957).
[123] D. Drechsel and L. Tiator, J. Phys. **G18**, 449 (1992).
[124] P. Wilhelm, Th. Wilbois, and H. Arenhövel, Phys. Rev. **C54**, 1423 (1996).
[125] D. Drechsel and L. Tiator, Phys. Lett. **B148**, 413 (1984).
[126] S. Capstick, Phys. Rev. **D46**, 2864 (1992).
[127] M. Warns, H. Schröder, W. Pfeil, and H. Rollnik, Z. Phys. **C45**, 627 (1990).
[128] R. Koniuk and N. Isgur, Phys. Rev. **D21**, 1868 (1980).
[129] H. Tanabe and K. Ohta, Phys. Rev. **C31**, 1876 (1985).
[130] S. Kumano, Phys. Lett. **B214**, 13 (1988).
[131] G. Beck, H. P. Krahn, Phys. Rev. Lett. **71**, 606 (1997).
[132] A. Abada, H. Weigel, and Hugo Reinhardt, Phys. Lett. **366**, 26 (1996).
[133] S. Nozawa, B. Blankleider, and T.-S.H. Lee, Nucl. Phys. **A513**, 459 (1990).
[134] D. Drechsel and M. M. Giannini, Phys. Lett. **B143**, 329 (1984).
[135] K. Bermuth, D. Drechsel, L. Tiator, and J. B. Seaborn, Phys. Rev. **D37**, 89 (1988); I. Guiasu and R. Koniuk, Phys. Rev. **D36**, 2757 (1987); M. Weyrauch, Phys. Rev. **D35**, 1574 (1987).
[136] R. M. Davidson, N. C. Mukhopadhyay, and R. S. Wittman, Phys. Rev. **D43**, 71 (1991).
[137] M. Bourdeau and N. C. Mukhopadhyay, Phys. Rev. Lett. **58**, 976 (1987).
[138] S. Capstick and G. Karl, Phys. Rev. **D41**, 2767 (1990).
[139] A. J. Buchmann, E. Hernandez, U. Meyer, and Amand Faessler, Phys. Rev. **C** (1997) submitted.
[140] T. de Forest and J. D. Walecka, Adv. in Physics **15**, 1 (1966); C. Ciofi degli Atti, Prog. Part. Nucl. Phys. **3**, 163 (1980).
[141] S. L. Glashow, Physica **96 A**, 27 (1979).
[142] J. Adam, Ch. Hajduk, H. Henning, P. U. Sauer, and E. Truhlik, Nucl. Phys. **A531**, 623 (1991).
[143] R. Tegen and W. Weise, Z. Phys. **A314**, 357 (1983).
[144] Steven Weinberg, Phys. Rev. Lett. **67** (1991) 3473
[145] W. Broniowski, M. Lutz, and A. Steiner, Phys. Rev. Lett. **71**, 1787 (1993).
[146] E. M. Henley, W.-Y. P. Hwang, and L. S. Kisslinger, Phys. Rev. **D46**, 431 (1992).
[147] M. Fiolhais, B. Golli, and S. Sirca, Phys. Lett. **B373**, 229 (1996).